THE PENNSYLVANIA STATE UNIVERSITY
SCHREYER HONORS COLLEGE

DEPARTMENT OF ASTRONOMY AND ASTROPHYSICS

THE SEARCH FOR MICROQUASARS IN M33 FROM THE PHATTER-VIRUS SURVEY

JOEL HODGES
SPRING 2024

A thesis
submitted in partial fulfillment
of the requirements
for baccalaureate degrees
in Computer Science and Astronomy and Astrophysics
with honors in Astronomy and Astrophysics

Reviewed and approved* by the following:

Donald P. Schneider
Distinguised Professor of Astronomy and Astrophysics
Thesis Supervisor

Steinn Sigurdsson
Professor of Astronomy and Astrophysics
Honors Adviser

*Signatures are on file in the Schreyer Honors College.

Abstract

We describe an optical survey for microquasars in the nearby galaxy M33. These objects, thought to be stellar mass black holes accreting material from a nearby companion star, are exceedingly rare, with only a dozen known in our galaxy. The brightest optical microquasar, SS 433, has spectacular emission lines in its spectra, which display extraordinarily large velocities, up to an appreciable fraction of the speed of light.

Our survey was undertaken using the Visible Integral-field Replicable Unit Spectrograph (VIRUS) of the Hobby-Eberly Telescope (HET). VIRUS can simultaneously obtain over 30,000 spectra covering 3500-5500Å. We have acquired VIRUS observations covering a large fraction of M33 and have examined a set of 432 locations based on a microquasar candidate list presented by Calzetti et al. (1995). Each Calzetti target object is cross-referenced with known surveys of radio sources, X-ray sources, SNRs, HII regions, and Wolf-Rayet stars, as well as the Hubble Space Telescope's PHATTER F475W imaging. Based on their emission features at Hβ, [O III]λ5007, CIII/NIIIλ4645, and Heλ4686, or other notable spectral features, a total of 40 candidates were selected for further review. Each of these 40 objects were classified as one of six types of objects. None of the candidates meet the requirements to be considered an SS 433-like object. It seems unlikely at this time that an SS 433 analog exists in M33.

Table of Contents

List of Figures

List of Tables

Acknowledgements

I would like to thank everyone who has supported my education and my goals over the last four years.

To Kacie and Clay Hodges, without which none of this would have been possible.

To Elijah Hodges, who was a model of academic excellence for my entire childhood.

To Gregory Zeimann, who was instrumental as an advisor and co-author throughout the writing of this thesis.

To Professor Donald Schneider, for advising me and helping me find research I enjoyed working on for much of my time at Penn State.

Chapter 1

Introduction

1.1 Microquasars

Quasars were first recognized as luminous, distant objects six decades ago [Schmidt, 1963]. They are supermassive black holes with masses on the order of millions to billions of solar masses located at the center of a galaxy. Gas and dust from the surrounding galaxy fall into the black hole, and due to the extreme gravitational forces, become luminous. These objects are among the most luminous sources in the universe, often emitting thousands of times more light than the entire Milky Way galaxy, and doing so in a volume comparable to the scale of the solar system. While these are interesting objects, the extreme distances at which they are found and the large timescales on which they evolve makes them challenging objects to study in detail.

Microquasars deal with a very similar phenomenon, but on a far smaller scale. Currently, microquasars are understood to be stellar mass ($\sim$10-40 $M_{\odot}$) black holes, orbiting as a binary around a companion star, with the star transferring mass to the black hole [Mirabel and Rodríguez, 1999]. The presence of the companion star allows the microquasar to form an accretion disk, similar to those found around quasars. As microquasars are scaled down by many orders of magnitude from typical quasars, observing a microquasar on a fairly short timescale (even days or minutes) provides insights that would take thousands of years to observe from a quasar.

Microquasars are unique sources due to their emissions in both the radio and x-ray bands. The accretion disks described in Mirabel and Rodríguez (1999) are incredibly luminous in x-ray wavelengths. This property has led to studies of other ultraluminous X-ray sources (ULXs) in the galaxy, which have been hypothesized to be microquasars [Poutanen et al., 2007]. In addition to the extremely x-ray luminous accretion disks, microquasars are observed to have double-sided radio jets [Spencer, 1979, Mirabel et al., 1992]. These jets produce relativistic ($v \geq 0.1c$) synchrotron emission, with the ejecta from some microquasars reaching speeds up to $0.98c$ [Mirabel and Rodríguez, 1999].

Stephenson-Sanduleak 433 (SS 433; Stephenson and Sanduleak, 1977) was the first discovered microquasar, and has proven to be an interesting object, even among other microquasars. Its high luminosity in the optical band has made it easier to study than other microquasars, which typically have very low optical luminosity [Margon, 1984]. The optical spectrum of SS 433 contains many unusual emission lines, including a very strong and broad Hα line and He I lines, which appear in various components - one with a large redshift and another with a large blueshift [Liebert et al., 1979, Margon et al., 1979]. These spectral features change in wavelength on a time scale of days, and the variability in Doppler shift reaches magnitudes up to 50,000 km s^{-1} in redshift and 30,000 km s^{-1} in blueshift [Margon, 1984].

1.2 Discovery of SS 433: The First Microquasar

SS 433 was discovered in 1975 in a radio survey designed to detect and classify supernova remnants (SNRs) [Clark et al., 1975a]. The survey labeled what is known today as SS 433 as the source G39.7-2.0, and associated it with the SNR W50. At the 408 MHz waveband used in the survey, SS 433 was described as having low surface brightness, making it difficult to estimate the flux density. However, the authors supported the classification of G39.7-2.0 as an SNR.

The following year, the X-ray Astronomy Group at the University of Leicester published results detailing ten new X-ray sources [Seward et al., 1976]. Their survey identified the X-ray source A1909+04 and associated it with SNR W50 from Clark and Caswell's catalogue. The authors labeled A1909+04 as the most interesting object in their survey, as the X-ray observations appeared as a variable point source, indicating that it could be a remnant of the original star, rather than a source associated with the ejecta from the supernova.

The first documentation of SS 433 in the optical band was in 1977, when Stephenson and Sanduleak [Stephenson and Sanduleak, 1977] published a catalog of stars with H-alpha emissions in the plane of the Milky Way. The catalog details observations of 455 sources, including positions on the sky and magnitude. SS 433 was one of many stars in the catalog noted to have a very strong H alpha emission line, but there was no other feature of note in their data.

One of the first papers to note that all three observations were from the same source in the sky was published by Clark and Murdin (1978). The authors compared SS 433 to a similar radio/X-ray/optical source, Circinus X-1, which had been associated with the SNR G321.9-0.3, and hypothesized that these objects may represent a subclass of stellar remnants of supernovae. Each source had a very broad H-alpha line and three Helium emission lines at 5,876, 6,678, and 7,065 Angstroms. As Cir X-1 had been modeled as a binary system containing an X-ray emitter orbiting a massive early type star [Clark et al., 1975b], the authors suggested that SS 433 may be the same type of object. Subsequent research suggested that while both objects are interesting, SS 433 far was more exotic than Cir X-1 [Margon et al., 1979]. Currently, SS 433 has been classified as a microquasar.

1.3 Neighborhood Search for Microquasars

Despite other Galactic examples of similar phenomenon, SS 433 remains unique. Finding another source like SS 433 in a less extinct and different environment would add to our understanding of the jet phenomenon, creation mechanisms, and influence of such systems on their surroundings.

SS 433 is intrinsically luminous ($M_V \approx -7$), which means it is feasible to find similar objects in the Local Group of galaxies, i.e., M31 and M33. Since SS 433 is a Population I object associated with a supernova remnant [Calzetti et al., 1995] (hereafter C95), it is important to search for analogs in a galaxy which has active star formation. M33 is such a galaxy, and it is a face-on system, which means there is less extinction along the majority of the lines of sight to the galaxy when compared to M31. Additionally, M33 has been recently covered by a Hubble Space Telescope (HST) treasury survey, PHATTER [Williams et al., 2021], allowing one to photmetrically resolve complex populations in M33 (see §2.2).

There have been many efforts to identify SS 433 analogs in M33; of particular interest is that of C95. The team compiled a list of 432 candidate SS 433 stars based on a list of criteria.

C95 lists 432 potential optical candidates of microquasars in M33. The candidates were identified from an imaging survey of M33 using the Kitt Peak 4m telescope covering the Hα region and a narrow band continuum around 6100Å [Long et al., 1990]. This survey covered the central

$15'$ of M33, accounting for about 70% of the most active star-forming region.

Images were obtained in two observing runs, one in September 1986 and one in November 1987, and covered 19 fields. The 800×800 pixel TI-2 CCD on the Kitt Peak telescope has a field of view of $3.86'$ on each side, and the centers of each observation were separated by $3.5'$, giving an overlap of about $30''$ between each region. More information on these observations can be found in Long et al. (1990).

In each of the 19 fields, SS 433 candidates were identified using two sets of criteria. Objects which appeared brighter in the Hα images than the 6100Å continuum images were flagged as being Hα emitters, a characteristic which is expected of SS 433-like objects. A total of 153 of these "emission line candidates" were found by C95, which are reproduced in Table A.1.

The other group of candidates defined by C95 are sources which appeared as point-like objects in the 6100Å continuum images, and are projected onto extended nebulosity in the Hα images. These sources are likely to be associated with extended Hα emission, and are labeled as "embedded candidates"; 279 of these sources were identified, which are reproduced in Table A.2.

1.4 Project Goals

We aim to cover the list of candidate SS 433 objects, along with the wider PHATTER survey, using the VIRUS IFU spectrograph to provide the highest spatial resolution integral field unit dataset on a nearby galaxy to date. With the VIRUS data, we can examine the spectra of each target and their surrounding environment to assess if they are a good microquasar candidate star.

While the project may not definitively answer the question if there are microquasars in our galactic neighborhood, the results of this survey will have important impacts. If a microquasar (or multiple) is found, it could provide unique insight to where these objects come from and how they form. If, however, a microquasar is not found, this result will place strong constraints on the cosmic frequency of microquasars in M33, and presumably, all galaxies of similar type.

Chapter 2

Observations

2.1 VIRUS

Our study of M33 and the PHATTER survey region (see §2.2) was carried out on the 10-m Hobby-Eberly Telescope (HET; Ramsey et al., 1998). The data were obtained by VIRUS (Visible Integral-field Replicable Unit Spectrograph; Hill et al., 2021) is a massively replicated, fiber-fed spectrograph consisting of 78 integral field units (IFUs), each comprised of 448 1.5″ diameter fibers covering a 50″ x 50″ field of view. Each IFU feeds two low-resolution (R ∼800) spectrographs that cover the wavelength region of $3500 < \lambda < 5500$Å.

The fibers within each IFU have roughly a one-third fill factor of the IFU. To account for these gaps, observations of a given field are taken in a 3-point dither pattern. The M33 pointings use a minimum exposure time of 360 seconds per dither, for a total exposure time of 18 minutes per observation. In the case of non-optimal observing conditions, the exposure time is adjusted using real-time estimates of seeing conditions and the sky brightness background to achieve a more consistent signal-to-noise ratio per exposure [Gebhardt et al., 2021].

There are six missing IFUs at the center of the VIRUS FoV for other fiber-fed instruments at the HET. Each VIRUS IFU is separated from its nearest neighbor by 100″, leaving a gap of 50″ between each fiber bundle. Pointings were manually chosen to fill in the gaps between IFUs and sufficiently cover the center of the galaxy. M33 was observed both in December 2022 - January 2023 and in December 2023 - January 2024. In the 2022-23 observing period, the goal was to obtain 13 shots that efficiently covered the PHATTER region of M33 completely while including enough overlap of IFU observations for self-consistent relative calibration. In the 2023-24 season, the coverage was extended to larger radii of M33 with 16 additional pointings placing an emphasis on star-forming regions as well as more uniformly covering the PHATTER footprint and filling in gaps where poor IFU data from the VIRUS instrument left blank regions.

While the HET can point at any azimuth, it is a fixed altitude telescope, and only observes at an elevation of 55°. At the declination of M33, there are two possible observing times: once when the galaxy is rising through the HET's line of sight to the east, and once when it is setting through the line of sight to the west. Due to conflicts with the Hobby Eberly Telescope Dark Energy Experiment (HETDEX; Gebhardt et al., 2021), M33 was always observed on the western track. This constraint provided a common position angle of the VIRUS field of view for all exposures. The VIRUS coverage of M33 can be seen in Figure 2.1.

2.2 PHATTER Survey

The Panchromatic Hubble Andromeda Treasury: Triangulum Extended Region (PHATTER) survey is a dataset of resolved stellar photometry over 6 wavebands, providing data for 22 million stars in M33 [Williams et al., 2021]. The survey covers ∼14 square kpc and extends to 14′ from the center of M33.

Observations were taken on the Hubble Space Telescope (HST) using the Advanced Camera for Surveys (ACS) for optical band exposures and the Wide Field Camera 3 (WFC3) for near-ultraviolet and near-infrared exposures. The survey area was broken into 3 'bricks', each of which

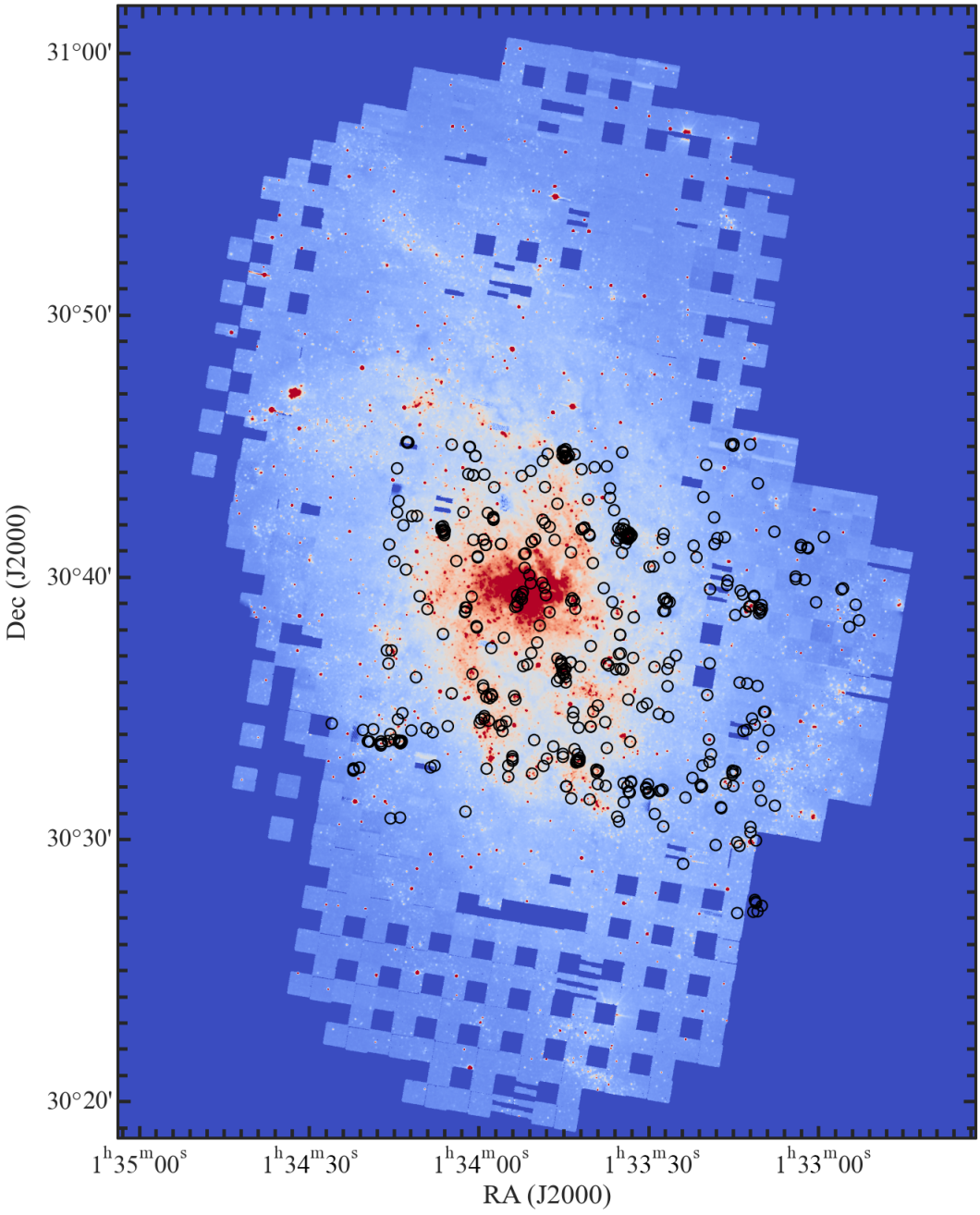

Figure 2.1: VIRUS coverage of M33. Covered regions are overlaid with F473W imagery from the PHATTER survey while uncovered regions are blue. C95 SS 433 candidates are shown as black circles. The nine candidates which have no VIRUS coverage can be seen in the lower right corner of the image.

has a total area of 3×6 WFC3 footprints. Each brick was divided into 18 fields, with one half brick (9 fields) being observed at a time. WFC3 and ACS observed in parallel - while WFC3 observed one half of a brick, ACS observed the other. Exposures for the other half of the brick were taken ∼6 months later, after HST had rotated $180°$.

The most relevant waveband covered by the PHATTER survey for this paper is the F475W data, which provides good coverage around 5000Å, within the VIRUS range. In this band, PHATTER provides imagery to a depth of ~ 28.5 in the lowest surface density regions of M33, and ~ 26.5 in the most crowded regions near the center of M33. ACS provides $\sim 0.05''$ spatial resolution for this waveband.

These data will be used in this project to better resolve the bright stars responsible for spectroscopic features seen in either the VIRUS data or the C95 candidate list. The PHATTER survey covers 343 out of the 432 SS 433 candidates, giving much deeper and more highly resolved images for most of the candidate set.

2.3 JVLA Radio Survey of M33

Radio data in this paper is from a survey conducted from 2012-2013 with the Jansky Very Large Array (JVLA; White et al., 2019). Observations were taken in JVLA's 1.4 GHz and 5 GHz bands, which span 1-2 GHz and 4-6 GHz, respectively. The 1.4 GHz exposures were captured with seven unique pointings. The 5 GHz exposures, which have a smaller field of view, required 41 pointings. The survey covers the central region of M33 with full sky coverage of all 432 Calzetti SS 433 candidates.

SS 433 was discovered in an SNR with radio emission, so it is reasonable to assume that an analog may be found in a similar environment. The JVLA survey has a limiting depth of 20 μJy and a resolution of $5.9''$(FWHM). While radio emission from a microquasar may be fainter than this survey could detect, collecting known radio sources in M33 and matching them with the Calzetti catalog may still provide insights into the origins of some of the more interesting objects found in M33.

2.4 MMT Spectroscopy in M33

Previous surveys from the Multiple Mirror Telescope (MMT) have obtained optical spectra in M33, with the primary goal of investigating candidate lists for various objects. These surveys are applicable to the search for microquasars in M33, as they provide additional spectroscopy over the C95 candidates.

In the case of a microquasar candidate, these additional spectra could provide evidence of a moving emission lines typical of an actively accreting disk. These MMT surveys can also provide insight into potential classifications for interesting objects in M33 that are not microquasars.

Each MMT survey used the 270 line mm^{-1} grating, which covers 3700-9000Å, thus overlapping all but the bluest wavelength range in VIRUS. The MMT observations included four general

classes of objects: Supernova Remnants, HII Regions, Wolf-Rayet Stars, and Luminous Blue Variables/Supergiant Stars.

Supernova remnants have been linked to the formation of microquasars, as SS 433 was found in a known supernova remnant. Therefore, it may be useful to compare each C95 target with known SNRs in M33. A 2018 MMT survey [Long et al., 2018] provides spectroscopic observations of SNR candidates proposed by Long et al. (2010) and Lee & Lee (2014). This survey covered 197 SNR candidates, and provided first-time spectroscopy of 120 of the candidates.

HII regions are extended environments of ionized hydrogen in which star formation can take place. These objects are important in the search for microquasars because microquasars are expected to be Population I objects, i.e., they likely will be in a region of star formation. Specifically for this search, HII regions may also be important because they have strong Hα emission lines, which could cause an HII region to make it on to the C95 candidate list. A 2017 survey (Lin et al., 2017) provides spectroscopic follow up for HII region candidates proposed by Hoopes et al. (2001). The survey covers 413 HII region candidates. Table 1 from Lin et al. (2017) is used in this paper to cross reference C95 candidates with HII regions.

Wolf-Rayet (WR) stars are the final stage of a high mass star's evolution before it erupts into a Type Ibc supernova. These stars are characterized by high mass loss rates, and the resulting stellar winds create the broad emission lines found in a WR star's spectrum. These objects are important to this search because many of their spectral features coincide with those expected of a microquasar, which can cause them to be flagged as microquasar candidates. A 2011 survey (Neugent and Massey, 2011) provides spectroscopic observations of WR star candidates found in narrow-band images of the critical WR emission features NIIIλ4650 and HeIIλ4686. The survey covers 206 WR star candidates. Table 5 from Neugent and Massey (2011) is used in this paper to cross reference Calzetti candidates with known WR stars.

Supergiant stars commonly possess strong hydrogen emission in their spectra, which would cause them to be included in the C95 candidate list. Luminous blue variables (LBVs) are a subset of supergiant stars which show photometric variations, but are also extremely luminous and have strong hydrogen emission lines. Any of these objects that have already been classified can be removed from the C95 candidate list. A 2014 and 2017 survey (Humphreys et al., 2014, Humphreys et al., 2017) provides spectroscopic observations of luminous blue variable stars, FeII emission line stars, and other supergiants. The survey covers a total of 214 luminous and variable stars in M31 and M33. Table 1 from Humphreys et al. (2014) and Table 7 from Humphreys et al. (2017) were merged and used in this paper to cross reference Calzetti candidates with known luminous variable stars.

2.5 Chandra Observations of M33

The data used from the Chandra X-ray Observatory in this paper was produced by the Chandra ACIS Survey of M33 (ChASeM33; Plucinsky et al., 2008). Exposures of seven different fields were taken to cover the central region of M33 at a resolution of 5″ to resolve source confusion in the inner galaxy and increase the reliability of association between X-ray sources and sources

at other wavelengths. Each field was observed twice during the period from September 2005 - November 2006, with most exposures having an integration time of 100 ks, but some being shorter due to scheduling constraints [Tüllmann et al., 2011].

ChASeM33 detected 662 X-ray sources, at least 100 of which were identified to be within M33 [Tüllmann et al., 2011]. Of the 662 sources, classifications were suggested for 183, of which 45 are likely some form of SNR.

Chapter 3

Data Processing

The initial processing of the VIRUS observations were performed by the software package `Remedy`[1] (Zeimann et al. 2024, submitted). The reductions included bias subtraction, gain multiplication, error propogation, pixel masking, fiber trace, wavelength calibration, scattered light subtraction, spectral extraction, and fiber normalization. The astrometric calibration was calculated through a comparison with Pan-STARRS1 photometric catalogs (Chambers et al., 2019) as described in Zeimann et al. (2024, submitted). Due to the large presence of M33 continuum and line emission throughout our VIRUS frames, we opted for a new sky subtraction and flux calibration method than was done for more "blank" fields in Gebhardt et al. (2021) and Zeimann et al. (2024, submitted).

The HET is a fixed-altitude telescope with a wide-field corrector and a focal plane situated on a moving tracker. The total mirror illumination and the mirror segments that are illuminated changes as a function of tracker position. As the mirror illumination changes so does the flat-field of the focal plane. The offsets of the flat-field from center track to the edge of a track is most dramatic for IFUs on the edge of the focal plane; this effect is well-modeled by a first order 2D polynomial. For "blank" observations (i.e., where most of the fibers do not contain an object), a local sky subtraction for each IFU can correct this flat-field effect. However, we cannot perform a local sky subtraction because the VIRUS exposures of M33 have fewer fibers that include only sky emission. To effectively handle this issue, we require an imaging survey of M33 that overlaps with the VIRUS wavelength coverage, has good flux calibration, and has a wide enough field of view that background subtraction is not an issue. We chose the B-band imaging from the Local Group Survey (Massey et al. 2006), as it is well situated in the VIRUS wavelength coverage and it is from a dedicated program to provide UBVRI photometry obtained from the Mosaic camera of M31 and M33 using the Kitt Peak 4-m telescope.

For each VIRUS exposure, we synthesized a B-band image for the total flux in each fiber (sky + science) and performed aperture photometry using the fiber radius on the Massey et al. (2006) B-band imaging. By comparing the VIRUS measurements to the imaging, we can fit a line whose intercept indicates the sky intensity of the B-band and whose slope indicates residual flux calibration offset. Using a median sky from neighboring "blank" observations and scaling that sky by our B-band sky intercept, we constructed an initial sky model for sky subtraction. Since the initial sky model comes from a separate observation and the sky (especially in the blue) can change over the different timescales involved ($\sim$1-2 hours), we modified the initial sky using a principal component analysis (PCA). We combined all of the neighboring sky observations to create a five component PCA vector basis, and for each exposure we solved for the five eigenvalues to adjust our initial sky spectrum. This task was performed by computing a median spectrum after initial sky subtraction, using `PPXF` (Cappellari & Emsellem 2004; Cappellari 2017; Cappellari 2023) to model the stellar and gas emission along with solving for the five eigenvalues in an iterative fashion. This process was iterated three times before convergence. The PCA additions to the initial sky are mostly minor and are highly correlated to sky line intensities and the blue continuum of the sky. Our final sky estimate includes this PCA component.

We also examined the flux calibration factors as function of focal plane position. The differential illumination over the field of view requires a first order 2D polynomial to account for the

[1] https://github.com/grzeimann/Remedy

fiber normalization of each exposure. We also took an average of all of the offsets for individual amplifiers over all of our exposures to account for gain multiplication errors in the data frame headers (usually a 1-2% effect). The final comparison between the imaging and the VIRUS synthetic values suggests a flux calibration on the order of $\sim$5%.

After our sky subtraction and flux normalization steps, a combined data cube over our VIRUS coverage was created. We constructed a 32.8′ x 43.2′ grid with 1″ pixels; for each exposure we identified the closest pixel to each fiber. This process had to be performed at each wavelength separately to account for differential atmospheric refraction. All of the light for a given fiber is placed into its closest pixel, conserving flux by accounting for the fiber area compared to the pixel area. After this correction is made for each exposure, we create the median image to account for fibers contributing multiple times from different exposures to a single pixel (i.e., overlapping exposures). A flux conserving Gaussian filter is then used to spread out the light using a seeing kernel of 1.8″. This process is flux conserving and is one approach to move from an irregular layout of fibers from many exposures to a uniform grid with minimal interpolation and loss of signal-to-noise ratio. Our data cube was primarily used for image creation and visual examination.

Despite extensive efforts, data processing issues remain in both our fiber spectra and our data cube. The most common problem related to this program is an incorrect wavelength solution for an amplifier not flagged by our automated quality control. This error led to artifacts that mimic real emission at incorrect wavelengths. Because of this feature, we visually inspected of all of our candidates and re-inspected of the processed fiber data to verify truly interesting objects.

3.1 Extraction of the Object Spectra

The sky positions from C95 were in B1950 coordinates so they were converted to the J2000 coordinate system of our VIRUS observations. For each target, we calculated the mean spectrum for all of the fibers within 3.5″. Since this extraction region contains light from our target source as well as emission from the underlying M33 population, we also calculated the median spectrum of fibers from between 12″ and 15″ to form our background spectrum. We subtracted the median of the background fibers from our mean central aperture spectrum, then scaled the result by the area ratio of the extraction aperture divided by the area of a single fiber. This method produces a background-subtracted total spectrum of our target.

In total, good spectra were obtained for 408 of the 432 C95 candidates, which are used for further analysis. A list of the 24 candidates that do not have good spectra can be found in Table 4.1.

Chapter 4

Classification of Spectra of Microquasar Candidates

In this section, all C95 candidates will be referred to by their ID number, which can be found in the second column of the tables in Appendix A. IDs ending in e come from Table A.1, and IDs ending in b come from Table A.2.

4.1 Analysis of VIRUS Spectroscopy of Microquasar Candidates

Prior to searching for microquasars in the C95 candidate list, several classes of objects were removed from the list. The first group of objects removed from the list are those which are not well covered by VIRUS. Nine of the original 432 C95 candidates were not included in the VIRUS observations. Another 15 objects were removed from consideration either because they have bad amplifiers due to wavelength solution issues, or because they are so close to the edge of the coverage that the data are compromised. A full list of these objects is in Table 4.1.

The second group of objects removed from the dataset is those that have previously been catalogued as Wolf-Rayet stars. Wolf-Rayet stars share many of the emission lines expected of a microquasar, including a strong Hα line (explaining their inclusion in the C95 candidate list), as well as strong CIII/NIIIλ4645 and Heλ4686 emission. A total of 47 of the C95 candidates coincided (within 3.5″) of Wolf-Rayet stars catalogued by Nuegent and Massey (2011). A list of objects can be found in Table 4.2. After removing candidates not well covered by VIRUS and those coincident with WR stars, 361 remained to be analyzed.

Fabrika et al. (1995) compiled a list of criteria for microquasars. Within the VIRUS spectra themselves, we expect to have broad emission lines with significant velocity offset from known emission lines. This would imply a high velocity collimated jet at fractions of the speed of light, likely associated with Balmer emission, and characteristic of microquasars. If there are multiple exposures of the source, they can be compared for changes in the spectra, which could add additional evidence of a high-speed jet and therefore a microquasar. We also expect to see broad Heλ4686 and the blended CIII,NIII lines at 4640-50Å; these lines are typical in Wolf-Rayet stars with strong winds.

The C95 candidate list was compiled essentially on the criterion that an object be associated with Hα emission (either through its own emission of Hα, or through extended Hα emission). However, this feature alone is not sufficient to make a source a good microquasar candidate. In order to effectively isolate potential microquasar candidates from the 423 VIRUS spectra, we have two additional selection criteria.

The first selection criterion arises from the known emission lines associated with SS 433. The strongest features in SS 433 are strong stationary hydrogen lines. With VIRUS spectroscopy, we expect to have good coverage of the Hγ and Hβ emission lines at 4340Å and 4861Å. Additionally, SS 433 is associated with strong emission lines at HeIIλ4686 and CIII/NIIIλ4645 (Fabrika and Sholukhova, 1995), which are also well covered by VIRUS. Another emission line is [O III]λ5007; this line is a key diagnostic because it separates SS 433 from other objects, such as SNRs, HII regions, and Wolf-Rayet stars, which all have strong [O III]λ5007 emission, while a microquasar is not expected to show strong [O III] emission. Any source displaying strong emission lines in Hβ,

HeIIλ4686 and CIII/NIIIλ4645, but weak or no emission in [O III]λ5007 were selected for further analysis. Sources with strong emission in Hβ, HeIIλ4686 and CIII/NIIIλ4645, and emission in [O III] were also selected for additional study, since it is possible that a microquasar could have weak [O III] emission or potentially a doppler-shifted line around 5007Å.

The second criterion is based on the jet phenomenon of SS 433. Since microquasars have high velocity doppler shifts, it is expected that broad emission lines or emission lines at unknown wavelengths will be present. For this reason, the spectra of the 423 objects were visually examined for spectral features that fell into these two categories. These objects were also selected for further analysis, regardless of emission in the wavebands discussed for the first criterion.

For each candidate, we created an inspection figure that includes 6 images and two spectra. Starting from the VIRUS data cube described in §3, we created a synthetic continuum image by collapsing the wavelengths of the data cube from 4870Å to 5070Å in a 40″ x 40″ region centered on the candidate. To examine the emission features of Hβ, [O III]λ5007, CIII/NIIIλ4645, and Heλ4686, we used a moving median (window $\approx$ 100Å) to subtract the continuum of each pixel in the cube and sum the light within $\pm$6Å of the target emission. Cutouts (40″ x 40″) of the same region of the F475W imaging from the PHATTER survey allowed us to resolve the stellar population well below the typical seeing of our VIRUS observations ($\sim$1.8″). An example of the inspection format is presented in Figure 4.1. These inspection diagrams allowed us to easily identify key features of each object, especially emission in each of the four important wavelengths for a potential microquasar.

Using these inspection figures, the remaining 361 candidates were visually inspected for the presence of broad emission lines, emission lines at unknown wavelengths, or strong emission lines in Hβ, HeIIλ4686 and CIII/NIIIλ4645. A total of 40 candidates met at least one of these criteria and were selected for further analysis. A list of these candidates can be found in Table 4.3.

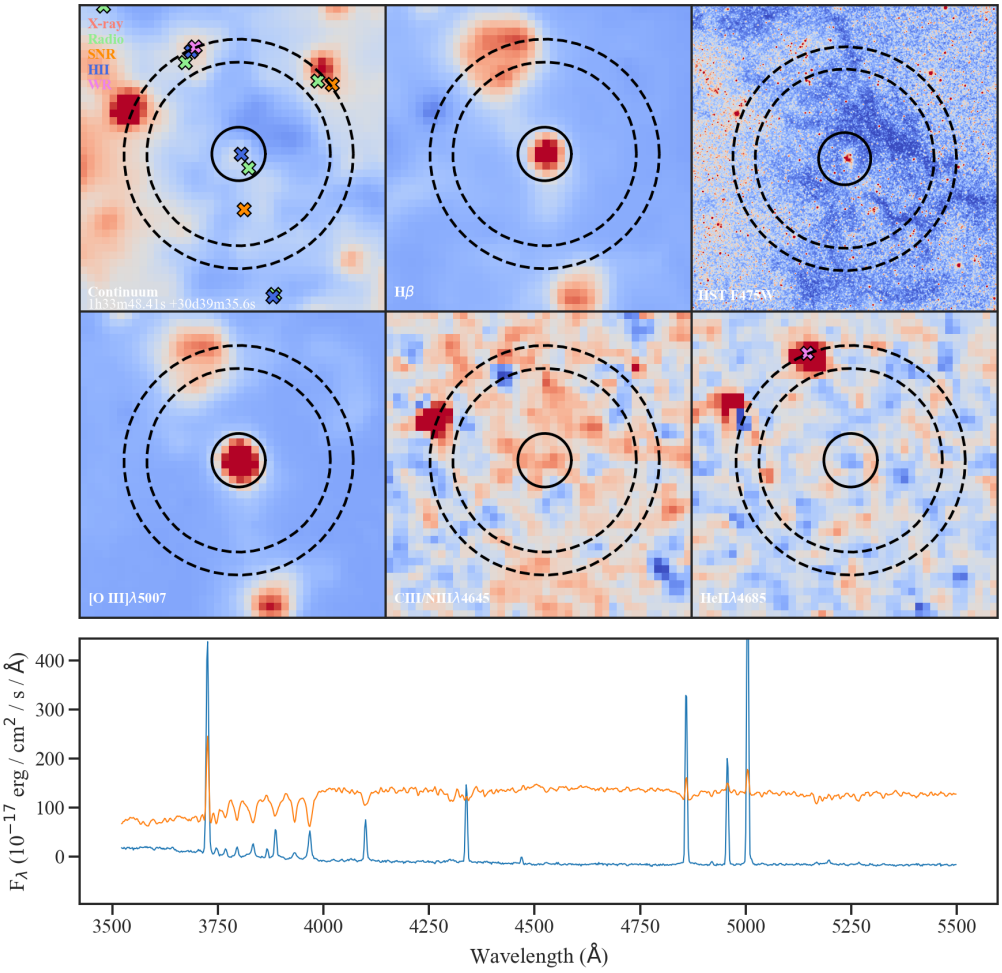

Figure 4.1: Example Inspection Diagram; this is the information for object 1 in Table A.1 (ID 95e). The top left image in the grid shows the synthetic VIRUS continuum image from 4780Å to 5070Å, as well as markings representing known sources, with red marks representing X-ray sources, green marks representing radio sources, orange marks representing SNRs, blue marks representing HII regions, and pink marks representing Wolf-Rayet stars. The top right image is PHATTER survey F475W imaging. The top middle, bottom left, bottom middle, and bottom right images are the VIRUS data of the source in the Hβ, [O III]λ5007, CIII/NIIIλ4645, and HeIIλ4686 wavebands, respectively. The bottom of the panel displays VIRUS spectroscopy, with the orange line representing the median spectra of pixels between the inner dashed annulus ($>12''$) and the outer dashed annulus ($<15''$). The orange line was scaled from the area of a single fiber to the extraction annulus aperture ($3.5''$). The blue line represents the background-subtracted spectrum of pixels within the solid annulus ($<3.5''$).

Table 4.1: Candidates Lacking Quality VIRUS Spectra

ID[a]	RA (J2000)	Dec (J2000)	Reason
26e	1:33:15.92	30:39:51.9	Not covered
25e	1:33:15.33	30:45:03.6	Bad amplifier
27e	1:33:16.03	30:39:41.4	Edge of Coverage
16e	1:33:10.71	30:27:14.8	Not covered
37e	1:33:19.71	30:44:16.8	Bad amplifier
18e	1:33:11.46	30:27:13.7	Not covered
133e	1:34:08.60	30:32:44.4	Not covered
131e	1:34:07.89	30:32:48.4	Edge of coverage
18b	1:33:10.97	30:27:33.5	Not covered
19b	1:33:10.97	30:29:56.9	Edge of coverage
38b	1:33:14.92	30:45:00.4	Bad amplifier
98b	1:33:34.38	30:42:01.2	Bad amplifier
15b	1:33:09.96	30:27:27.5	Not covered
47b	1:33:19.06	30:39:32.3	Not covered
21b	1:33:11.20	30:27:40.9	Not covered
20b	1:33:11.09	30:27:36.6	Not covered
101b	1:33:34.53	30:41:50.8	Bad amplifier
37b	1:33:14.86	30:45:04.4	Bad amplifier
256b	1:34:12.77	30:45:07.4	Edge of coverage
52b	1:33:22.20	30:32:20.4	Bad amplifier
123b	1:33:40.67	30:42:57.8	Bad amplifier
255b	1:34:12.59	30:45:07.9	Edge of coverage
29b	1:33:12.61	30:34:10.1	Edge of coverage
257b	1:34:12.90	30:45:09.5	Edge of coverage

[a] As given in C95 (see §A.1)

Table 4.2: Known Wolf-Rayet Stars in Calzetti Candidate List

ID[a]	RA (J2000)[b]	Dec (J2000)[b]	Spectral Type[c]	ID[c]	Ang. Sep (″)[d]
68e	1:33:36.80	30:43:01.5	WN4+O		1.98
45e	1:33:26.61	30:35:50.3	WN6		0.11
25e	1:33:15.32	30:45:03.6	WN3, WN/CE	MC 20	0.21
22e	1:33:14.31	30:29:52.8	WN	MJ E6	2.52
107e	1:33:52.46	30:43:51.8	WN8	MCA 12	0.37
144e	1:34:15.75	30:34:00.5	WNL	AM 27	0.32
146e	1:34:16.09	30:36:42.0	Ofpe/WN9		0.23
108e	1:33:54.84	30:32:23.0	WN9-10	OB 6-5	0.25
112e	1:33:58.29	30:34:31.2	WNL	AM 18	2.88
114e	1:33:58.72	30:35:26.1	B1 Ia+WNE	OB 2-4	0.54
148e	1:34:18.76	30:34:11.6	Ofpe/WN9	UIT 349	0.30
137b	1:33:43.18	30:39:06.5	WN 7+abs	W91 129	0.33
221b	1:33:58.71	30:35:26.0	B1 Ia+WNE	OB 2-4	0.52
92b	1:33:33.79	30:41:32.2	WNLx2?	MC 31	1.83
25b	1:33:11.88	30:38:53.6	WNL	MC 17	0.96
84b	1:33:33.50	30:41:33.0	WNL?	MC 30	0.37
209b	1:33:55.86	30:34:07.5	WC4-5	AM 15	1.08
83b	1:33:33.49	30:41:31.8	WNL?	MC 30	1.57
203b	1:33:53.80	30:35:27.7	WNE	MJ G34	1.01
202b	1:33:53.61	30:38:51.6	Ofpe/WN9	MJ X15	0.14
213b	1:33:56.42	30:34:20.6	WN3		1.19
184b	1:33:48.81	30:39:47.1	WN	MJ X4	2.60
60b	1:33:27.28	30:39:09.5	Ofpe/WN9	MJ C7	0.45
74b	1:33:32.97	30:41:35.9	WNL	AM 4	0.26
133b	1:33:42.56	30:33:14.5	WC4-5	MC 44	0.37
179b	1:33:46.86	30:33:32.6	WN6/C4	MC 48	2.07
63b	1:33:27.76	30:31:50.8	WN	MC 27	0.15
97b	1:33:34.30	30:41:30.1	WN8	AM 7	0.33
23b	1:33:11.26	30:39:14.6	WN3+abs		2.83
193b	1:33:51.92	30:40:21.2	WC4+abs	MC 56	2.58
90b	1:33:33.74	30:41:36.2	WNLx2?	MC 31	2.22
96b	1:33:34.04	30:41:16.9	WN	MCA 4	0.27
178b	1:33:46.18	30:36:01.9	WN4b	MC 46	2.61
274b	1:34:17.40	30:33:34.6	WN3+neb		2.43
86b	1:33:33.59	30:41:35.1	WNL?	MC 30	2.12
277b	1:34:19.54	30:33:43.8	WN3-4+ne		2.04
278b	1:34:19.73	30:33:44.0	WN3-4+ne		1.17
110b	1:33:35.73	30:36:28.9	WC	MC 34	0.16
81b	1:33:33.47	30:41:29.4	WC6	AM 5	2.01
93b	1:33:33.80	30:41:29.5	WN7	N595-WR9	0.23
91b	1:33:33.74	30:41:33.8	WNLx2?	MC 31	0.27
232b	1:34:00.49	30:38:07.7	WN?	MJ X16	1.89
271b	1:34:16.38	30:37:12.3	WN7	UIT 343	0.29
87b	1:33:33.63	30:41:31.8	WNL?	MC 30	2.34
88b	1:33:33.65	30:41:29.6	WN7	N595-WR9	2.14
22b	1:33:11.23	30:39:17.0	WN3+abs		1.20
228b	1:33:59.65	30:34:35.0	WN5		0.78

[a] As given in C95 (see §A.1)
[b] J2000 coordinates of the C95 target
[c] As given in Table 5 of Neugent and Massey (2011)
[d] Angular separation between C95 target and WR star

4.2 Results

All 361 candidates were evaluated following the criteria set in §4.1; 40 were chosen for further study, which are given in Table 4.3. The objects in this table were further analyzed to see if they could actually be microquasars, and were assigned into various groups based on their proposed classification. For each group, one example inspection diagram is shown. All other inspection diagrams for objects in Table 4.3 can be found in Appendix B.

Table 4.3: Potential SS 433 Candidates

ID	RA (J2000)	Dec (J2000)	Hβ^a	$O_3{}^a$	$C_3/N_3{}^a$	$He_2{}^a$	Section^b
100e	1:33:50.11	30:41:26.4	y	n	n	n	4.2.3
101e	1:33:50.12	30:41:26.4	y	n	n	n	4.2.3
130e	1:34:06.66	30:41:47.5	y	y	n	n	4.2.3
48e	1:33:27.39	30:30:29.3	y	n	y	y	4.2.4
99e	1:33:49.25	30:38:09.2	y	y	n	y	4.2.6
80e	1:33:40.41	30:31:31.2	y	y	y	y	4.2.1
147e	1:34:16.13	30:33:44.7	y	n	y	y	4.2.3
122e	1:34:01.19	30:36:18.2	y	y	y	y	4.2.2
177b	1:33:46.13	30:36:53.6	y	y	y	y	4.2.5
28b	1:33:12.09	30:38:52.2	y	y	y	y	4.2.1
165b	1:33:45.15	30:36:19.9	y	n	y	y	4.2.6
113b	1:33:37.05	30:36:37.5	y	n	y	y	4.2.4
65b	1:33:29.09	30:40:24.2	y	y	y	y	4.2.2
199b	1:33:53.23	30:38:53.7	y	y	n	n	4.2.1
139b	1:33:43.70	30:39:05.3	y	y	n	n	4.2.5
251b	1:34:06.74	30:41:54.2	y	y	y	y	4.2.2
155b	1:33:44.72	30:44:37.0	y	y	y	y	4.2.2
99b	1:33:34.39	30:32:08.2	y	y	n	y	4.2.2
62b	1:33:27.50	30:31:53.6	y	y	y	y	4.2.1
116b	1:33:38.98	30:32:06.4	y	y	n	n	4.2.2
58b	1:33:26.96	30:39:11.2	y	y	y	y	4.2.1
55b	1:33:26.27	30:40:44.9	y	y	n	y	4.2.4
49b	1:33:20.53	30:32:01.5	y	y	n	n	4.2.5
85b	1:33:33.56	30:41:27.0	y	y	y	y	4.2.1
76b	1:33:33.12	30:41:32.6	y	y	y	y	4.2.1
94b	1:33:34.00	30:41:35.6	y	y	y	y	4.2.1
250b	1:34:06.53	30:41:48.6	y	y	y	y	4.2.3
276b	1:34:19.38	30:33:43.3	y	y	y	y	4.2.1
67b	1:33:29.89	30:31:47.3	y	y	y	y	4.2.2
64b	1:33:28.07	30:31:50.5	y	y	y	y	4.2.1
171b	1:33:45.26	30:36:26.4	y	n	n	n	4.2.4
164b	1:33:44.96	30:36:16.8	y	y	n	n	4.2.5
148b	1:33:44.55	30:44:32.5	y	y	n	n	4.2.5
146b	1:33:44.42	30:44:35.2	y	y	y	y	4.2.2
154b	1:33:44.70	30:44:36.9	y	y	y	y	4.2.2
30b	1:33:12.73	30:38:40.9	y	y	y	y	4.2.4
168b	1:33:45.16	30:44:47.2	y	y	y	y	4.2.2
147b	1:33:44.43	30:44:35.1	y	y	y	y	4.2.2
163b	1:33:44.92	30:44:48.9	y	y	y	y	4.2.2
161b	1:33:44.90	30:44:48.8	y	y	y	y	4.2.2

[a] Indicates if the object has emission in the given waveband
[b] Section in which the object is classified

4.2.1 Objects Near Wolf-Rayet Stars

This class of objects contains pointings which are outside of the angular separation range ($<3.5''$) considered to be coincident with a known Wolf-Rayet star, but close enough that a known Wolf-Rayet star may contaminate the spectroscopy for the object of interest. These objects typically display strong Hβ and [O III] lines, with weak CIII/NIII and HeII emission, all of which are typical of Wolf-Rayet stars. The proximity to the known W-R stars and the lack of broad, unknown emission lines make it unlikely for these objects to be SS 433 candidates.

The ten C95 objects which fall into this category are 80e, 28b, 199b, 62b, 58b, 85b, 76b, 94b, 276b, and 64b (also noted in Table 4.3). Figure 4.2 shows the inspection diagram for object 62b as an example of this class of objects. The rest of the inspection diagrams can be found in Appendix B.1.

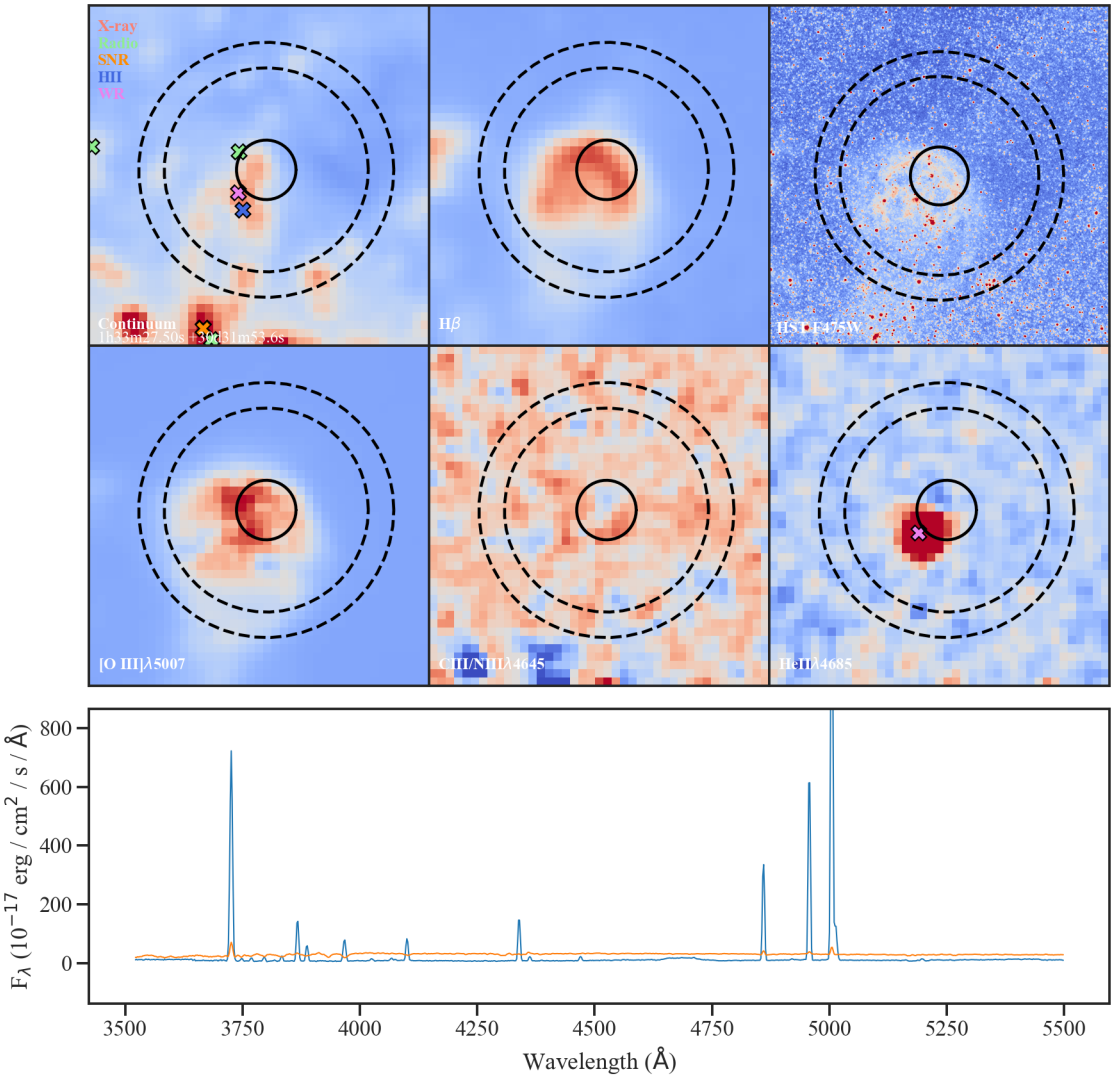

Figure 4.2: Inspection diagram for object 62b. The diagram shows the strong Hβ and [O III] lines and weak CIII/NIII and HeII lines. A W-R star is just outside the inner $3.5''$ annulus, and is likely contaminating the spectrum.

4.2.2 New Wolf-Rayet Stars

This class of objects contains pointings which are neither coincident with a known Wolf-Rayet star nor close enough to be contaminated by one. These objects typically display strong Hβ and [O III] lines, with weak CIII/NIII and HeII emission, all of which are typical of Wolf-Rayet stars. The lack of proximity to the known W-R stars, the presence of W-R emission lines, and the lack of broad, unknown emission lines make it likely that these are new Wolf-Rayet stars, and not microquasars.

The twelve C95 objects which fall into this category are 122e, 65b, 251b, 155b, 99b, 116b, 67b, 146b, 154b, 168b, 147b, and 161b/163b[1] (also noted in Table 4.3). Figure 4.3 shows the inspection diagram for object 154b as an example of this class of objects. The rest of the inspection diagrams can be found in Appendix B.2.

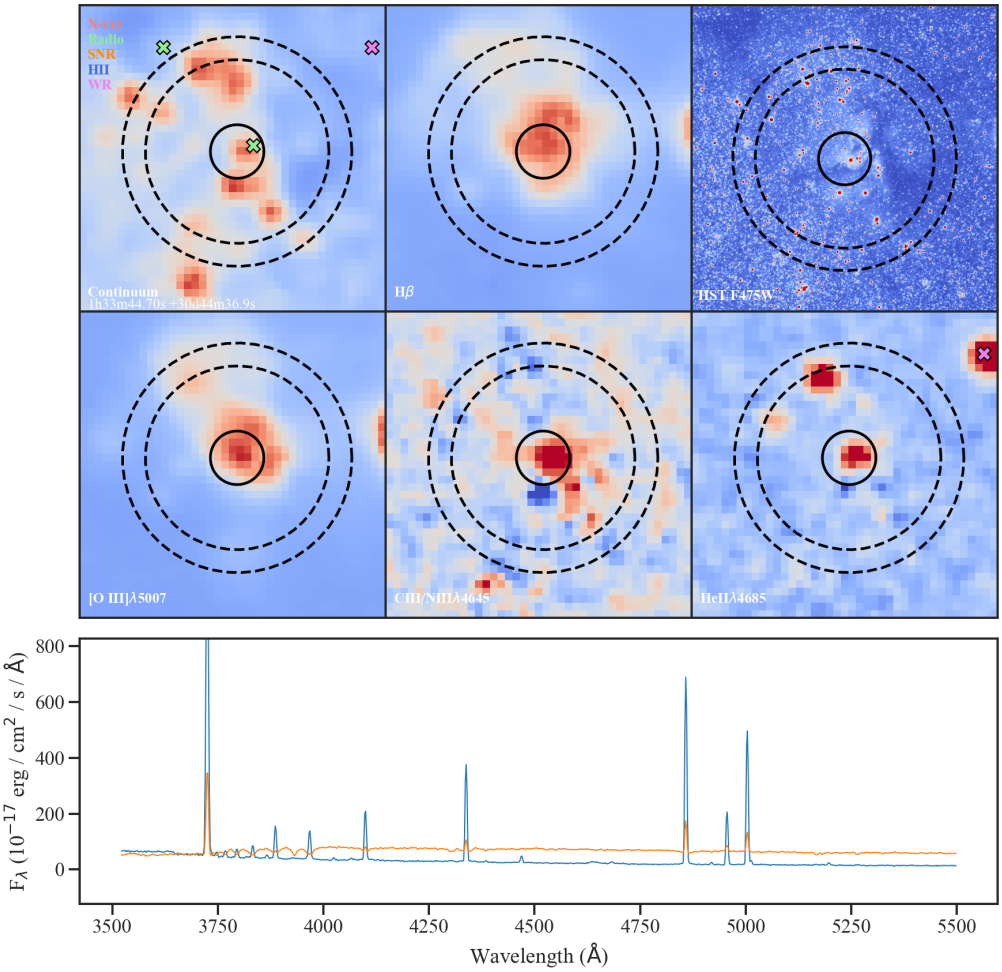

Figure 4.3: Inspection diagram for object 154b. The diagram shows the strong Hβ and [O III] lines, and the weak CIII/NIII and HeII lines. No known W-R stars are sufficiently near ($<3.5''$) to contaminate the spectrum.

[1]Objects 161b and 163b are likely the same object, with pointings only separated by $\sim 0.03''$.

4.2.3 Known Supergiant Stars

These objects are supergiant stars, each of which have been previously classified in the literature. These stars are known to have strong Balmer emission lines, so they would be included in the C95 candidate set since they possess strong Hα features, and are included in this set because they are strong in Hβ and often have emission at forbidden lines, which is expected of a microquasar. The five C95 candidates which fall into this category and their classifications are:

- Object 100e/101e[2] is a supergiant B[e] star [Kraus, 2019].
- Object 147e (Figure 4.4) is known as B526 and is a B2.5 Ia star [Humphreys et al., 2014].
- Object 130e/250b[3] is known as B416 and is a luminous blue variable with spectral type B[e] [Shemmer et al., 2000].

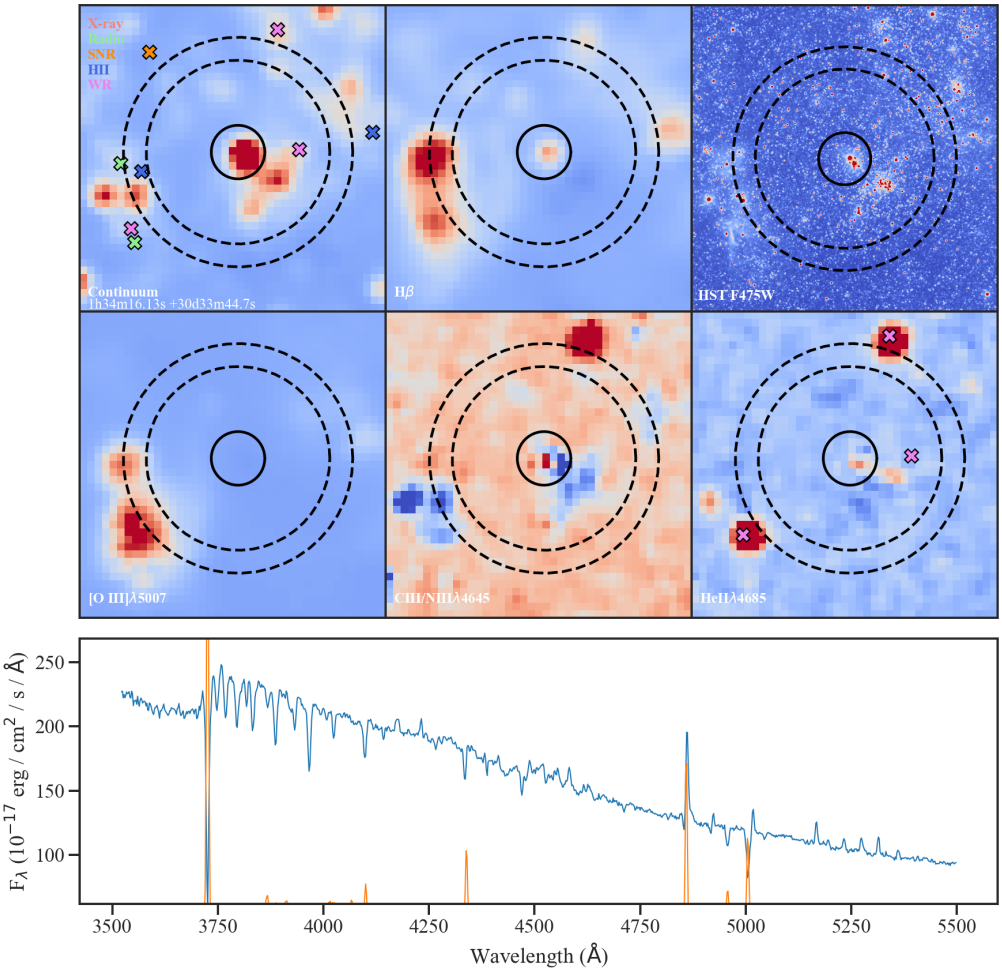

Figure 4.4: Inspection diagram for object 147e. The diagram shows the strong Hβ emission line, as well as numerous other spectral features including FeII emission that are typical of a B-type supergiant.

[2]Objects 100e and 101e are likely the same object, with pointings only separated by $\sim$0.01″.
[3]Objects 130e and 250b are likely the same object, with pointings only separated by $\sim$1.1″.

4.2.4 Bright Star Spectra

These objects were flagged for further consideration because their spectra potentially contained emission at all of the critical wavelengths. Their spectra, however, are dominated by bright stars; for this reason, they cannot be confidently classified from their spectroscopy as a microquasar or otherwise. While broad emission cannot easily be discounted from these spectra, it is unlikely that any of these sources are microquasars, as they are not coincident with X-ray sources or SNRs, both of which SS 433 is associated.

The five C95 candidates which fall into this category are 48e, 113b[4], 55b, 174b, and 30b (also noted in Table 4.3). Figure 4.5 shows the inspection diagram for object 174b as an example of this class of objects. The rest of the inspection diagrams can be found in Appendix B.4.

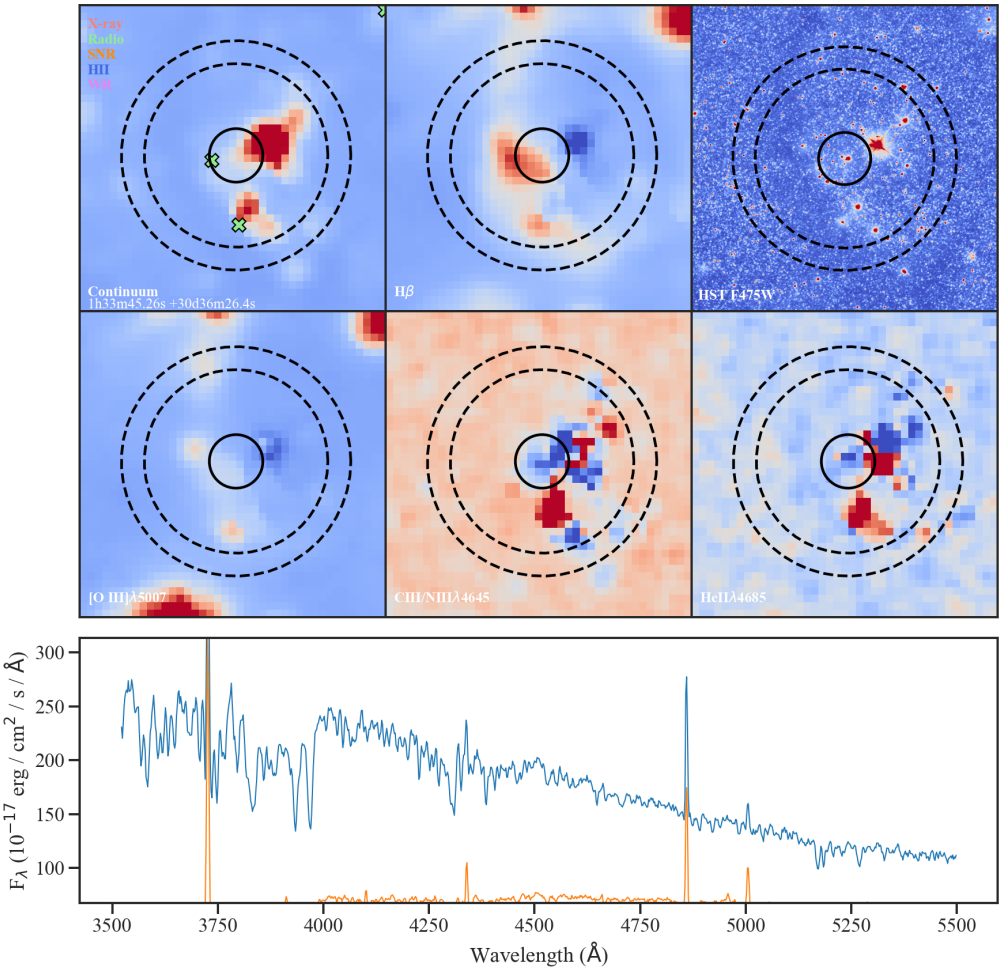

Figure 4.5: Inspection diagram for object 174b, which shows a spectrum dominated by a bright star.

[4]Object 113b is listed in Humphreys et al. (2014) as an intermediate type F5-F8 Ia star.

4.2.5 Narrow Emission Spectra

Objects in this group were flagged because they have emission at critical wavelengths; however, these objects only show narrow emission, with no broad emission at unknown wavelengths. This result makes it extremely unlikely that they are microquasars, since such an object should show broad emission due to the jet phenomenon. Additionally, these sources are not coincident with know X-ray sources or SNRs.

The five C95 candidates which fall into this category are 177b, 139b, 49b, 164b, and 148b (also noted in Table 4.3). Figure 4.6 shows the inspection diagram for object 148b as an example of this class of objects. The rest of the inspection diagrams can be found in Appendix B.5.

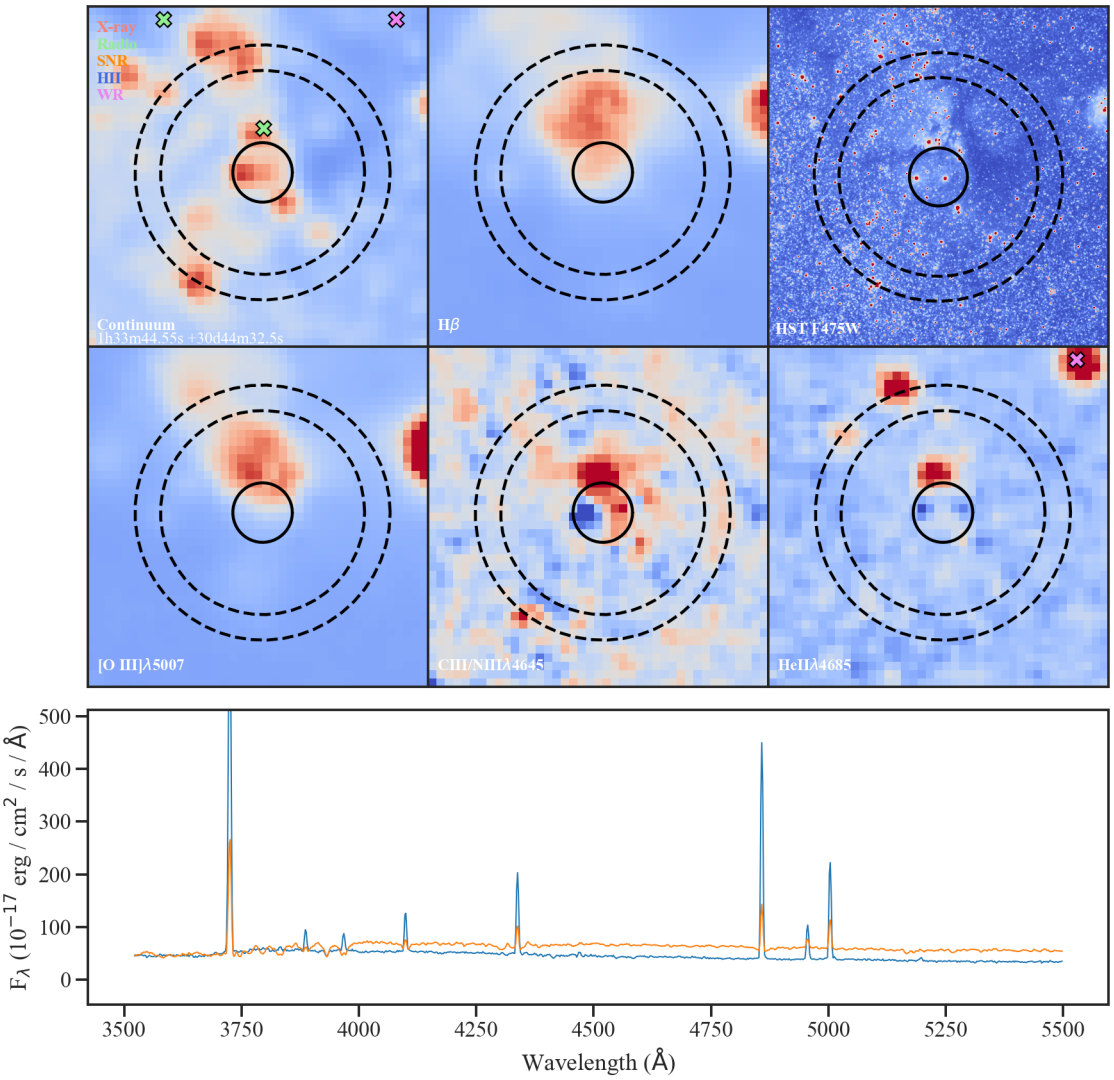

Figure 4.6: Inspection diagram for object 148b. The diagram shows clear emission lines at Hβ and [O III], with weaker emission at CIII/NIII and HeII. However, there are no broad spectral features.

4.2.6 Other Objects

The last two objects in the sample do not fall neatly into the other categories.

Object 165b

Object 165b shows emission in all critical wavebands. It appears to be a normal HII region, with a bright star (seen clearly in the PHATTER F475W image in Figure 4.7) affecting the continuum estimate and masking the emission lines. Although there is a star spectrum in the data, this is likely just a typical HII region, and therefore not a microquasar candidate.

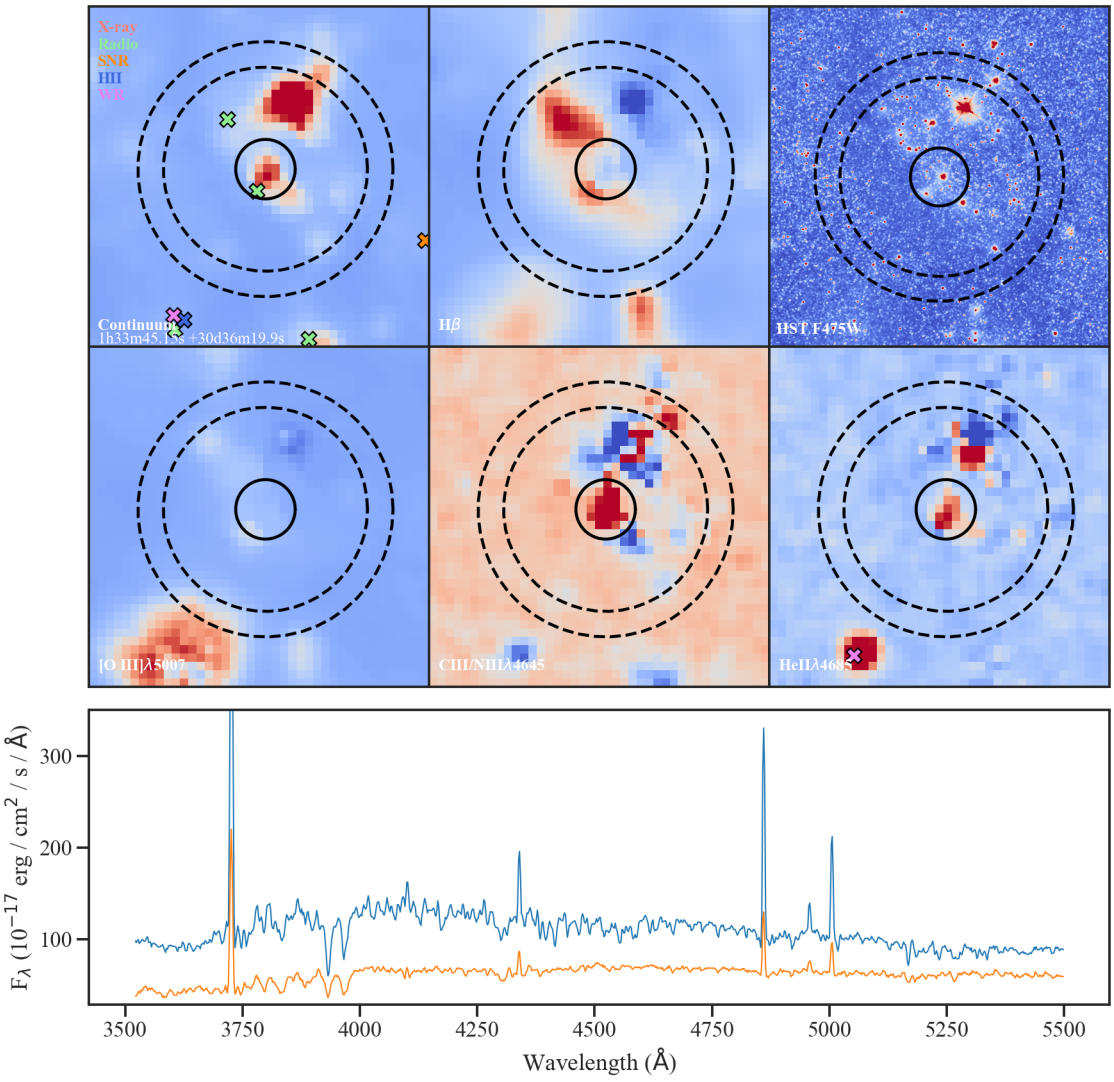

Figure 4.7: Inspection diagram for object 165b. The diagram shows the emission lines characteristic of a Wolf-Rayet star. An extremely luminous source can be seen in the upper right of the second annulus, which likely affects the continuum estimate.

Object 99e

Object 99e is Variable B, originally discovered and named by Hubble and Sandage in 1953. It is an extremely luminous star with spectral type B0-B2 [Humphreys et al., 2014], and not a microquasar candidate. The inspection diagram with VIRUS spectroscopy for Var B is shown in Figure 4.8.

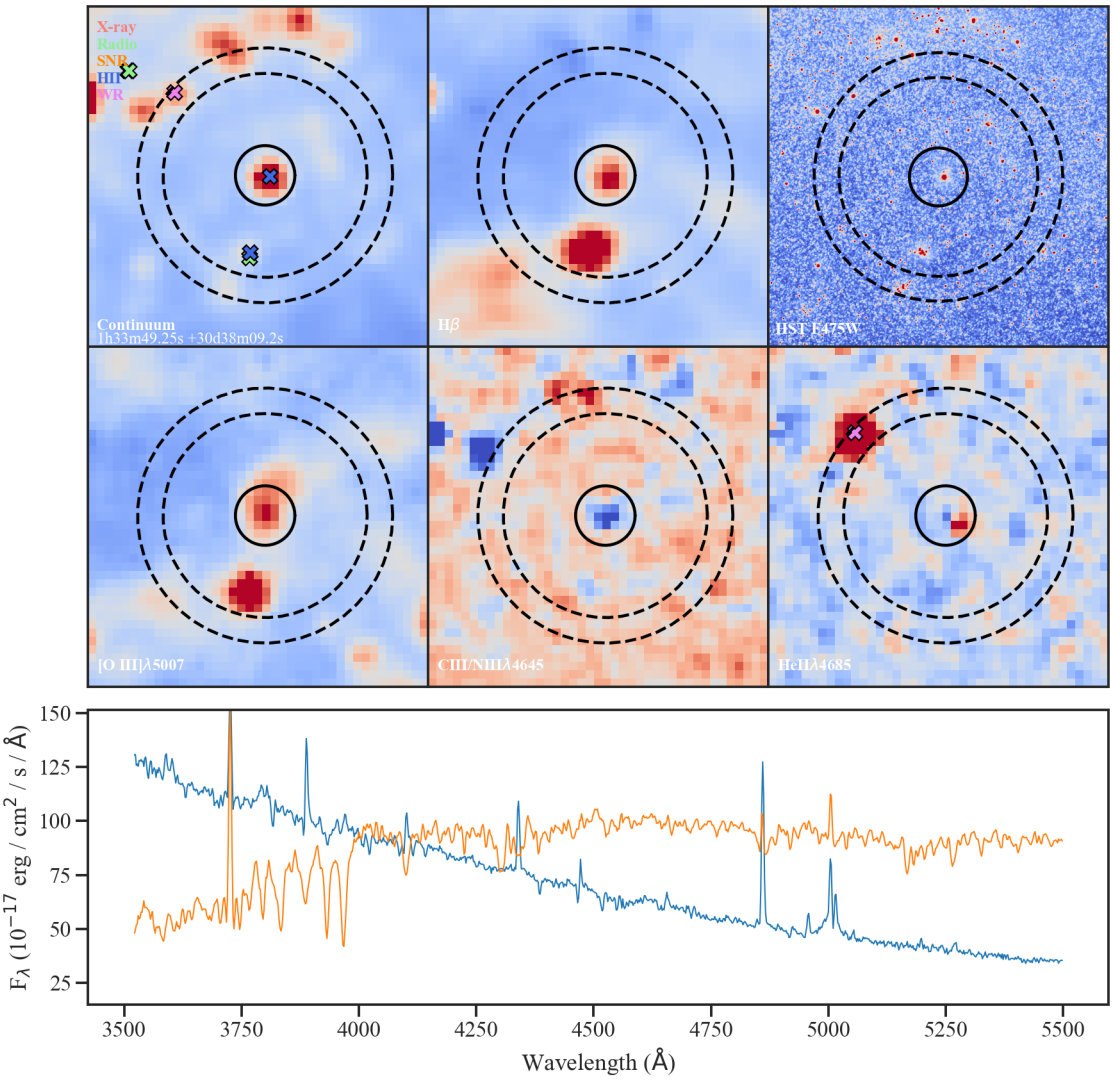

Figure 4.8: Inspection diagram for object 99e (Var B).

4.3 Summary

This paper has provided spectroscopic observations for the microquasar candidate object list presented by C95. VIRUS spectroscopy taken during December 2022-January 2023 and December 2023-January 2024 provides the highest resolution IFU dataset of a nearby galaxy to date. Processing of the VIRUS observations were done using `Remedy`, and object spectra were extracted and background-subtracted. Spectra 408 of the 432 C95 sources were acquired by VIRUS spectroscopy.

Each C95 target object was cross-referenced with known surveys of radio sources, X-ray sources, SNRs, HII regions, and Wolf-Rayet stars, as well as PHATTER F475W imaging. These surveys provide the context in which each C95 source should be examined, and what the nature of each object was.

Objects were selected for further examination depending on their spectral features. A total of 40 out of the 408 well-covered objects were selected, with 27 objects being selected for their emission features in Hβ, [O III], CIII/NIII, and HeII, and another 13 objects being selected for interesting features in their spectra that may indicate a dopper-shifted line typical of a microquasar. These 40 candidates were broken broadly into 6 different classifications: objects near Wolf-Rayet stars (10 targets), new Wolf-Rayet stars (13 targets), supergiant stars (5 targets), noisy spectra (5 targets), narrow band spectra (5 targets), and other objects (2 targets).

Of these groups, the one particularly of note is the proposed set of 13 new Wolf-Rayet stars. Neugent and Massey (2011) give a list of 206 Wolf-Rayet stars in M33, a value they estimate is complete to within 5%. If this estimate is correct, the new Wolf-Rayet stars found in this paper nearly represents the remainder of the W-R population in M33.

VIRUS spectroscopy does not support the existence of an SS 433-like object within the 408 well-covered objects in the C95 candidate list. Since the list was constructed of the most luminous Hα sources in M33, and we expect a microquasar to possess a strong Hα line, this result limits the potential presence of a microquasar in M33 to $\sim 5\%$ of the Hα emitters in the galaxy. While possible, we expect that it is not likely for a microquasar to be present in the 24 Hα sources not covered by this survey. Our failure to identify any microquasars in our M33 data indicates that it is unlikely that any microquasars with luminosities near the prototype, SS 433, exist in this galaxy.

Bibliography

[Calzetti et al., 1995] Calzetti, D., Kinney, A. L., Ford, H., Doggett, J., and Long, K. S. (1995). An Atlas of H(alpha) Emitting Regions in M33: A Systematic Search for SS433 Star Candidates. *The Astronomical Journal*, 110:2739.

[Chambers et al., 2019] Chambers, K. C., Magnier, E. A., Metcalfe, N., Flewelling, H. A., Huber, M. E., Waters, C. Z., Denneau, L., Draper, P. W., Farrow, D., Finkbeiner, D. P., Holmberg, C., Koppenhoefer, J., Price, P. A., Rest, A., Saglia, R. P., Schlafly, E. F., Smartt, S. J., Sweeney, W., Wainscoat, R. J., Burgett, W. S., Chastel, S., Grav, T., Heasley, J. N., Hodapp, K. W., Jedicke, R., Kaiser, N., Kudritzki, R. P., Luppino, G. A., Lupton, R. H., Monet, D. G., Morgan, J. S., Onaka, P. M., Shiao, B., Stubbs, C. W., Tonry, J. L., White, R., Bañados, E., Bell, E. F., Bender, R., Bernard, E. J., Boegner, M., Boffi, F., Botticella, M. T., Calamida, A., Casertano, S., Chen, W. P., Chen, X., Cole, S., Deacon, N., Frenk, C., Fitzsimmons, A., Gezari, S., Gibbs, V., Goessl, C., Goggia, T., Gourgue, R., Goldman, B., Grant, P., Grebel, E. K., Hambly, N. C., Hasinger, G., Heavens, A. F., Heckman, T. M., Henderson, R., Henning, T., Holman, M., Hopp, U., Ip, W. H., Isani, S., Jackson, M., Keyes, C. D., Koekemoer, A. M., Kotak, R., Le, D., Liska, D., Long, K. S., Lucey, J. R., Liu, M., Martin, N. F., Masci, G., McLean, B., Mindel, E., Misra, P., Morganson, E., Murphy, D. N. A., Obaika, A., Narayan, G., Nieto-Santisteban, M. A., Norberg, P., Peacock, J. A., Pier, E. A., Postman, M., Primak, N., Rae, C., Rai, A., Riess, A., Riffeser, A., Rix, H. W., Röser, S., Russel, R., Rutz, L., Schilbach, E., Schultz, A. S. B., Scolnic, D., Strolger, L., Szalay, A., Seitz, S., Small, E., Smith, K. W., Soderblom, D. R., Taylor, P., Thomson, R., Taylor, A. N., Thakar, A. R., Thiel, J., Thilker, D., Unger, D., Urata, Y., Valenti, J., Wagner, J., Walder, T., Walter, F., Watters, S. P., Werner, S., Wood-Vasey, W. M., and Wyse, R. (2019). The pan-starrs1 surveys.

[Clark et al., 1975a] Clark, D. H., Green, A. J., and Caswell, J. L. (1975a). Improved 408 MHz Observations of Some Galactic Supernova Remnants. *Australian Journal of Physics Astrophysical Supplement*, 37:75–86.

[Clark and Murdin, 1978] Clark, D. H. and Murdin, P. (1978). An unusual emission-line star/X-ray source radio star, possibly associated with an SNR. *Nature*, 276:44–45.

[Clark et al., 1975b] Clark, D. H., Parkinson, J. H., and Caswell, J. L. (1975b). Is CIR X-1 a runaway binary. *Nature*, 254:674–676.

[Fabrika and Sholukhova, 1995] Fabrika, S. and Sholukhova, O. (1995). A Search for Unique

Objects in Nearby Galaxies. *Astrophysics and Space Science*, 226(2):229–244.

[Gebhardt et al., 2021] Gebhardt, K., Mentuch Cooper, E., Ciardullo, R., Acquaviva, V., Bender, R., Bowman, W. P., Castanheira, B. G., Dalton, G., Davis, D., de Jong, R. S., DePoy, D. L., Devarakonda, Y., Dongsheng, S., Drory, N., Fabricius, M., Farrow, D. J., Feldmeier, J., Finkelstein, S. L., Froning, C. S., Gawiser, E., Gronwall, C., Herold, L., Hill, G. J., Hopp, U., House, L. R., Janowiecki, S., Jarvis, M., Jeong, D., Jogee, S., Kakuma, R., Kelz, A., Kollatschny, W., Komatsu, E., Krumpe, M., Landriau, M., Liu, C., Niemeyer, M. L., MacQueen, P., Marshall, J., Mawatari, K., McLinden, E. M., Mukae, S., Nagaraj, G., Ono, Y., Ouchi, M., Papovich, C., Sakai, N., Saito, S., Schneider, D. P., Schulze, A., Shanmugasundararaj, K., Shetrone, M., Sneden, C., Snigula, J., Steinmetz, M., Thomas, B. P., Thomas, B., Tuttle, S., Urrutia, T., Wisotzki, L., Wold, I., Zeimann, G., and Zhang, Y. (2021). The hobby–eberly telescope dark energy experiment (hetdex) survey design, reductions, and detections. *The Astrophysical Journal*, 923(2):217.

[Hill et al., 2021] Hill, G. J., Lee, H., MacQueen, P. J., Kelz, A., Drory, N., Vattiat, B. L., Good, J. M., Ramsey, J., Kriel, H., Peterson, T., DePoy, D. L., Gebhardt, K., Marshall, J. L., Tuttle, S. E., Bauer, S. M., Chonis, T. S., Fabricius, M. H., Froning, C., Häuser, M., Indahl, B. L., Jahn, T., Landriau, M., Leck, R., Montesano, F., Prochaska, T., Snigula, J. M., Zeimann, G., Bryant, R., Damm, G., Fowler, J. R., Janowiecki, S., Martin, J., Mrozinski, E., Odewahn, S., Rostopchin, S., Shetrone, M., Spencer, R., Mentuch Cooper, E., Armandroff, T., Bender, R., Dalton, G., Hopp, U., Komatsu, E., Nicklas, H., Ramsey, L. W., Roth, M. M., Schneider, D. P., Sneden, C., and Steinmetz, M. (2021). The HETDEX Instrumentation: Hobby-Eberly Telescope Wide-field Upgrade and VIRUS. *The Astrophysical Journal*, 162(6):298.

[Hoopes et al., 2001] Hoopes, C. G., Walterbos, R. A. M., and Bothun, G. D. (2001). Far-Ultraviolet and Hα Imaging of Nearby Spiral Galaxies: The OB Stellar Population in the Diffuse Ionized Gas. *The Astrophysical Journal*, 559(2):878–891.

[Hubble and Sandage, 1953] Hubble, E. and Sandage, A. (1953). The Brightest Variable Stars in Extragalactic Nebulae. I. M31 and M33. *The Astrophysical Journal*, 118:353.

[Humphreys et al., 2017] Humphreys, R. M., Gordon, M. S., Martin, J. C., Weis, K., and Hahn, D. (2017). Luminous and Variable Stars in M31 and M33. IV. Luminous Blue Variables, Candidate LBVs, B[e] Supergiants, and the Warm Hypergiants: How to Tell Them Apart. *The Astrophysical Journal*, 836(1):64.

[Humphreys et al., 2014] Humphreys, R. M., Weis, K., Davidson, K., Bomans, D. J., and Burggraf, B. (2014). Luminous and Variable Stars in M31 and M33. II. Luminous Blue Variables, Candidate LBVs, Fe II Emission Line Stars, and Other Supergiants. *The Astrophysical Journal*, 790(1):48.

[Kraus, 2019] Kraus, M. (2019). A Census of B[e] Supergiants. *Galaxies*, 7(4):83.

[Lee and Lee, 2014] Lee, J. H. and Lee, M. G. (2014). Properties of Optically Selected Supernova Remnant Candidates in M33. *The Astrophysical Journal*, 793(2):134.

[Liebert et al., 1979] Liebert, J., Angel, J. R. P., Hege, E. K., Martin, P. G., and Blair, W. P. (1979). The moving emission features in SS433 require a dynamical interpretation. *Nature*, 279:384–387.

[Lin et al., 2017] Lin, Z., Hu, N., Kong, X., Gao, Y., Zou, H., Wang, E., Cheng, F., Fang, G., Lin, L., and Wang, J. (2017). Spectroscopic Observation and Analysis of H II Regions in M33 with MMT: Temperatures and Oxygen Abundances. *The Astrophysical Journal*, 842(2):97.

[Long et al., 1990] Long, K. S., Blair, W. P., Kirshner, R. P., and Winkler, P. F. (1990). An Atlas of Confirmed and Candidate Supernova Remnants in M33. *The Astrophysical Journal Supplement*, 72:61.

[Long et al., 2018] Long, K. S., Blair, W. P., Milisavljevic, D., Raymond, J. C., and Winkler, P. F. (2018). MMT Spectroscopy of Supernova Remnant Candidates in M33. *The Astrophysical Journal*, 855(2):140.

[Long et al., 2010] Long, K. S., Blair, W. P., Winkler, P. F., Becker, R. H., Gaetz, T. J., Ghavamian, P., Helfand, D. J., Hughes, J. P., Kirshner, R. P., Kuntz, K. D., McNeil, E. K., Pannuti, T. G., Plucinsky, P. P., Saul, D., Tüllmann, R., and Williams, B. (2010). The Chandra ACIS Survey of M33: X-ray, Optical, and Radio Properties of the Supernova Remnants. *The Astrophysical Journal Supplement*, 187(2):495–559.

[Margon, 1984] Margon, B. (1984). Observations of SS 433. *Annual Review of Astronomy and Astrophysics*, 22:507–536.

[Margon et al., 1979] Margon, B., Ford, H. C., Katz, J. I., Kwitter, K. B., Ulrich, R. K., Stone, R. P. S., and Klemola, A. (1979). The bizarre spectrum of SS 433. *The Astrophysical Journal*, 230:L41–L45.

[Mirabel and Rodríguez, 1999] Mirabel, I. F. and Rodríguez, L. F. (1999). Sources of Relativistic Jets in the Galaxy. *Annual Review of Astronomy and Astrophysics*, 37:409–443.

[Mirabel et al., 1992] Mirabel, I. F., Rodriguez, L. F., Cordier, B., Paul, J., and Lebrun, F. (1992). A double-sided radio jet from the compact Galactic Centre annihilator 1E1740.7-2942. *Nature*, 358(6383):215–217.

[Neugent and Massey, 2011] Neugent, K. F. and Massey, P. (2011). The Wolf-Rayet Content of M33. *The Astrophysical Journal*, 733(2):123.

[Plucinsky et al., 2008] Plucinsky, P. P., Williams, B., Long, K. S., Gaetz, T. J., Sasaki, M., Pietsch, W., Tüllmann, R., Smith, R. K., Blair, W. P., Helfand, D., Hughes, J. P., Winkler, P. F., de Avillez, M., Bianchi, L., Breitschwerdt, D., Edgar, R. J., Ghavamian, P., Grindlay, J., Haberl, F., Kirshner, R., Kuntz, K., Mazeh, T., Pannuti, T. G., Shporer, A., and Thilker, D. A. (2008). Chandra ACIS Survey of M33 (ChASeM33): A First Look. *The Astrophysical Journal Supplement*, 174(2):366–378.

[Poutanen et al., 2007] Poutanen, J., Lipunova, G., Fabrika, S., Butkevich, A. G., and Abolmasov, P. (2007). Supercritically accreting stellar mass black holes as ultraluminous X-ray sources.

Monthly Notices of the Royal Astronomical Society, 377(3):1187–1194.

[Ramsey et al., 1998] Ramsey, L. W., Adams, M. T., Barnes, T. G., Booth, J. A., Cornell, M. E., Fowler, J. R., Gaffney, N. I., Glaspey, J. W., Good, J. M., Hill, G. J., Kelton, P. W., Krabbendam, V. L., Long, L., MacQueen, P. J., Ray, F. B., Ricklefs, R. L., Sage, J., Sebring, T. A., Spiesman, W. J., and Steiner, M. (1998). Early performance and present status of the Hobby-Eberly Telescope. In Stepp, L. M., editor, *Advanced Technology Optical/IR Telescopes VI*, volume 3352 of *Society of Photo-Optical Instrumentation Engineers (SPIE) Conference Series*, pages 34–42.

[Schmidt, 1963] Schmidt, M. (1963). 3C 273 : A Star-Like Object with Large Red-Shift. *Nature*, 197(4872):1040.

[Seward et al., 1976] Seward, F. D., Page, C. G., Turner, M. J. L., and Pounds, K. A. (1976). X-ray sources in the Aquila-Serpens-Scutum region. *Monthly Notices of the Royal Astronomical Society*, 175:39P–46.

[Shemmer et al., 2000] Shemmer, O., Leibowitz, E. M., and Szkody, P. (2000). Periodic microvariation of B416, a new luminous blue variable in M33. *Monthy Notices of the Royal Astronomical Society*, 311(4):698–706.

[Spencer, 1979] Spencer, R. E. (1979). A radio jet in SS433. *Nature*, 282(5738):483–484.

[Stephenson and Sanduleak, 1977] Stephenson, C. B. and Sanduleak, N. (1977). New H-alpha emission stars in the Milky Way. *The Astrophysical Journal*, 33:459–469.

[Tüllmann et al., 2011] Tüllmann, R., Gaetz, T. J., Plucinsky, P. P., Kuntz, K. D., Williams, B. F., Pietsch, W., Haberl, F., Long, K. S., Blair, W. P., Sasaki, M., Winkler, P. F., Challis, P., Pannuti, T. G., Edgar, R. J., Helfand, D. J., Hughes, J. P., Kirshner, R. P., Mazeh, T., and Shporer, A. (2011). The Chandra ACIS Survey of M33 (ChASeM33): The Final Source Catalog. *The Astrophysical Journal Supplement*, 193(2):31.

[White et al., 2019] White, R. L., Long, K. S., Becker, R. H., Blair, W. P., Helfand, D. J., and Winkler, P. F. (2019). A New, Deep JVLA Radio Survey of M33. *The Astrophysical Journal Supplement*, 241(2):37.

[Williams et al., 2021] Williams, B. F., Durbin, M. J., Dalcanton, J. J., Lang, D., Girardi, L., Smercina, A., Dolphin, A., Weisz, D. R., Choi, Y., Bell, E. F., Rosolowsky, E., Skillman, E., Koch, E. W., Lindberg, C. W., Hagen, L., Gordon, K. D., Seth, A., Gilbert, K., Guhathakurta, P., Lauer, T., and Bianchi, L. (2021). The Panchromatic Hubble Andromeda Treasury: Triangulum Extended Region (PHATTER). I. Ultraviolet to Infrared Photometry of 22 Million Stars in M33. *The Astrophysical Journal Supplement*, 253(2):53.

Appendix A

Candidate List Tables

Table A.1: Emission Line Candidates

#	ID	R.A. (J2000)	Dec. (J2000)	EW (Hα)	V[b]	Hβ	O_3	C_3/N_3	He_2	
1	95e	1:33:48.41	30:39:35.6	1763.5	19.18	y	y	n	n	
2	73e	1:33:37.91	30:39:34.7	1312.5	20.13	y	y	n	n	
3	59e	1:33:34.39	30:31:24.9	663.9	20.66	y	y	y	n	
4	68e	1:33:36.80	30:43:01.5	603.2	21.21	y	y	n	y	
5	152e	1:34:22.29	30:32:37.0	396.1	21.16	y	y	y	n	
6	20e	1:33:12.49	30:35:56.4	377.6	22.03	n	n	n	n	
7	100e	1:33:50.11	30:41:26.4	375.2	17.23	y	n	n	n	*
8	101e	1:33:50.12	30:41:26.4	285.0	17.22	y	n	n	n	*
9	90e	1:33:44.57	30:32:01.0	250.9	18.87	y	y	n	n	
10	71e	1:33:37.40	30:36:41.8	245.0	19.35	y	n	n	n	
11	89e	1:33:44.56	30:32:01.1	226.4	18.59	y	y	n	n	
12	151e	1:34:22.25	30:32:41.8	203.9	21.84	y	y	n	n	
13	149e	1:34:21.21	30:32:44.0	183.1	21.73	n	n	n	n	
14	19e	1:33:11.90	30:45:03.1	159.8	20.43	n	n	n	n	
15	96e	1:33:48.61	30:32:47.8	147.9	20.25	n	n	n	n	
16	120e	1:34:00.71	30:44:37.0	145.4	19.12	y	y	n	n	
17	153e	1:34:26.12	30:34:24.6	144.7	19.54	y	y	n	y	
18	110e	1:33:57.35	30:43:25.6	142.7	20.34	n	n	n	n	
19	26e	1:33:15.92	30:39:51.9	130.1	20.69					
20	117e	1:33:59.24	30:41:25.9	128.2	20.24	n	n	n	n	
21	81e	1:33:41.85	30:44:06.9	114.6	20.53	n	n	n	n	
22	123e	1:34:01.34	30:39:15.4	112.8	20.20	n	n	n	n	
23	45e	1:33:26.61	30:35:50.3	109.8	20.52	y	y	y	y	
24	130e	1:34:06.66	30:41:47.5	109.1	16.76	y	y	n	n	*
25	41e	1:33:23.88	30:29:03.7	104.3	20.38	y	n	n	n	
26	85e	1:33:42.80	30:32:55.9	99.0	18.76	y	n	n	n	
27	118e	1:34:00.41	30:38:04.5	97.5	20.73	y	y	n	n	
28	113e	1:33:58.68	30:32:41.6	96.6	20.75	n	n	n	n	
29	84e	1:33:42.79	30:32:56.1	91.6	18.56	y	y	n	n	
30	4e	1:33:07.60	30:31:16.6	85.7	19.50	y	y	n	n	
31	3e	1:32:54.35	30:38:05.3	85.2	20.27	n	n	n	n	
32	25e	1:33:15.32	30:45:03.6	84.9	20.30	n	n	n	n	
33	126e	1:34:04.06	30:40:36.9	83.3	19.17	n	n	n	n	
34	134e	1:34:09.18	30:38:46.7	82.4	20.74	n	n	n	n	
35	75e	1:33:39.54	30:44:11.8	80.3	20.36	y	y	n	n	
36	22e	1:33:14.31	30:29:52.8	78.0	20.28	n	n	n	y	
37	27e	1:33:16.03	30:39:41.4	71.5	20.88	n	n	n	n	
38	63e	1:33:35.02	30:37:47.9	66.2	20.68	y	n	n	n	

#	ID	R.A. (J2000)	Dec. (J2000)	EW (Hα)	V[b]	Hβ	O_3	C_3/N_3	He_2	
39	12e	1:33:10.37	30:38:36.6	64.1	19.91	y	y	n	n	
40	48e	1:33:27.39	30:30:29.3	63.2	18.45	y	n	y	y	*
41	107e	1:33:52.46	30:43:51.7	62.4	19.65	y	y	y	y	
42	144e	1:34:15.75	30:34:00.5	61.3	19.60	n	n	y	y	
43	16e	1:33:10.71	30:27:14.8	61.0	19.95					
44	138e	1:34:14.00	30:30:49.5	57.0	20.96	n	n	n	n	
45	70e	1:33:37.36	30:33:28.8	56.9	19.30	y	n	n	y	
46	109e	1:33:54.84	30:32:48.9	56.8	19.18	y	n	n	n	
47	62e	1:33:35.01	30:37:47.9	51.0	20.65	n	n	n	n	
48	143e	1:34:15.69	30:30:47.7	49.1	20.06	y	n	n	n	
49	121e	1:34:01.02	30:41:25.3	47.1	20.67	n	n	n	n	
50	57e	1:33:33.50	30:31:49.5	45.9	19.77	y	n	n	n	
51	136e	1:34:11.94	30:42:19.4	45.7	20.90	n	n	n	n	
52	119e	1:34:00.68	30:44:37.1	45.4	19.76	y	y	n	n	
53	31e	1:33:18.11	30:29:46.6	43.0	20.01	n	n	n	n	
54	78e	1:33:40.24	30:34:17.7	41.5	19.23	n	n	n	n	
55	49e	1:33:27.42	30:41:26.3	37.2	20.87	n	n	n	n	
56	37e	1:33:19.71	30:44:16.8	36.7	21.05	n	n	n	n	
57	38e	1:33:20.21	30:43:02.8	36.0	19.82	n	n	n	n	
58	14e	1:33:10.55	30:43:34.2	33.9	20.36	n	n	n	n	
59	54e	1:33:31.07	30:35:03.0	33.8	19.42	n	n	n	n	
60	53e	1:33:30.28	30:35:10.5	32.6	19.60	n	n	n	n	
61	146e	1:34:16.09	30:36:42.0	32.4	18.10	y	y	y	y	
62	69e	1:33:37.35	30:44:13.5	31.7	20.88	n	n	n	n	
63	99e	1:33:49.25	30:38:09.2	31.3	16.76	y	y	n	y	*
64	77e	1:33:39.84	30:40:32.1	31.1	19.47	n	n	n	n	
65	18e	1:33:11.46	30:27:13.7	30.3	20.47					
66	98e	1:33:48.74	30:42:11.3	30.2	20.06	n	n	n	n	
67	139e	1:34:14.23	30:33:43.2	29.7	19.35	y	y	n	n	
68	51e	1:33:28.89	30:30:57.8	29.2	19.70	n	n	n	n	
69	106e	1:33:52.43	30:39:09.6	28.3	16.33	y	y	y	n	
70	50e	1:33:28.15	30:34:46.9	27.6	20.37	n	n	n	n	
71	60e	1:33:34.63	30:44:45.4	26.9	19.76	y	y	n	n	
72	66e	1:33:35.63	30:38:36.6	25.1	18.87	n	n	n	n	
73	74e	1:33:38.98	30:35:06.1	24.6	19.89	y	n	n	n	
74	97e	1:33:48.71	30:44:25.9	24.5	19.70	n	n	n	n	
75	2e	1:32:53.23	30:38:56.1	22.5	19.82	y	n	n	n	
76	47e	1:33:27.26	30:41:39.2	22.3	21.18	n	n	n	n	
77	88e	1:33:43.36	30:34:38.0	22.1	19.32	n	n	n	n	
78	65e	1:33:35.54	30:30:51.6	21.3	19.80	y	n	n	n	

#	ID	R.A. (J2000)	Dec. (J2000)	EW (Hα)	V[b]	Hβ	O_3	C_3/N_3	He_2	
79	44e	1:33:26.53	30:34:39.9	21.1	20.18	n	n	n	n	
80	83e	1:33:42.38	30:34:15.3	21.0	19.94	y	n	n	n	
81	32e	1:33:18.31	30:42:16.5	20.9	21.04	n	n	n	n	
82	46e	1:33:26.63	30:36:29.6	20.5	20.11	n	n	n	n	
83	58e	1:33:33.56	30:35:19.9	20.5	20.18	n	n	n	n	
84	102e	1:33:50.62	30:32:30.2	20.4	18.20	y	n	n	n	
85	5e	1:33:07.62	30:41:43.5	20.2	19.11	n	n	n	n	
86	39e	1:33:21.46	30:40:45.3	20.1	19.57	n	n	n	n	
87	40e	1:33:21.96	30:41:11.9	$< 20.$	19.26	n	n	n	n	
88	82e	1:33:42.09	30:36:35.2	$< 20.$	19.91	n	n	n	n	
89	76e	1:33:39.78	30:34:52.2	$< 20.$	19.07	n	n	n	n	
90	43e	1:33:26.31	30:36:44.0	$< 20.$	20.11	n	n	n	n	
91	30e	1:33:17.74	30:41:29.1	$< 20.$	19.99	n	n	n	n	
92	87e	1:33:43.32	30:34:51.0	$< 20.$	20.02	n	n	n	n	
93	145e	1:34:15.98	30:41:14.5	$< 20.$	19.48	y	n	n	n	
94	29e	1:33:16.44	30:41:31.1	$< 20.$	19.02	n	n	n	n	
95	127e	1:34:04.87	30:35:33.8	$< 20.$	19.63	n	n	n	n	
96	42e	1:33:25.12	30:37:00.5	$< 20.$	18.13	n	n	n	n	
97	64e	1:33:35.23	30:30:40.8	$< 20.$	19.48	n	n	n	n	
98	67e	1:33:36.39	30:39:03.1	$< 20.$	20.09	n	n	n	n	
99	79e	1:33:40.24	30:34:17.6	$< 20.$	18.90	n	n	n	n	
100	80e	1:33:40.41	30:31:31.2	$< 20.$	20.23	y	y	y	y	*
101	116e	1:33:59.22	30:41:25.6	$< 20.$	19.27	n	n	n	n	
102	21e	1:33:13.84	30:35:58.5	$< 20.$	17.58	y	n	n	n	
103	93e	1:33:48.33	30:43:26.2	$< 20.$	20.19	y	y	n	n	
104	111e	1:33:57.86	30:37:17.7	$< 20.$	19.09	n	n	n	n	
105	104e	1:33:51.47	30:36:40.0	$< 20.$	19.22	y	n	n	n	
106	72e	1:33:37.66	30:34:28.3	$< 20.$	20.27	y	y	n	n	
107	115e	1:33:59.09	30:43:54.8	$< 20.$	20.11	n	n	n	n	
108	92e	1:33:47.51	30:41:54.9	$< 20.$	19.63	n	n	n	n	
109	140e	1:34:14.31	30:42:54.0	$< 20.$	19.73	n	n	n	n	
110	23e	1:33:14.59	30:38:32.9	$< 20.$	20.05	n	n	n	n	
111	137e	1:34:12.01	30:34:09.0	$< 20.$	20.00	n	n	n	n	
112	91e	1:33:46.60	30:41:25.3	$< 20.$	18.81	n	n	n	n	
113	33e	1:33:19.14	30:36:42.5	$< 20.$	18.76	n	n	n	n	
114	34e	1:33:19.19	30:32:56.9	$< 20.$	18.10	n	n	n	n	
115	108e	1:33:54.84	30:32:23.0	$< 20.$	18.12	y	y	y	y	
116	141e	1:34:14.58	30:44:08.8	$< 20.$	20.39	y	y	n	n	
117	8e	1:33:09.71	30:33:31.5	$< 20.$	17.99	n	n	n	n	
118	94e	1:33:48.35	30:42:03.9	$< 20.$	19.91	n	n	n	n	

#	ID	R.A. (J2000)	Dec. (J2000)	EW (Hα)	V[b]	Hβ	O_3	C_3/N_3	He_2	
119	124e	1:34:02.43	30:31:03.2	$< 20.$	18.90	y	y	n	n	
120	103e	1:33:50.86	30:44:03.2	$< 20.$	18.70	y	n	n	n	
121	61e	1:33:34.65	30:40:55.9	$< 20.$	18.28	y	n	n	y	
122	55e	1:33:32.59	30:38:27.7	$< 20.$	19.30	n	n	n	n	
123	105e	1:33:52.20	30:36:36.4	$< 20.$	18.31	y	y	n	n	
124	6e	1:33:08.71	30:34:09.2	$< 20.$	19.44	n	n	n	n	
125	35e	1:33:19.29	30:33:48.2	$< 20.$	15.29	n	n	n	n	
126	28e	1:33:16.30	30:32:07.3	$< 20.$	18.38	n	n	n	n	
127	135e	1:34:09.34	30:34:14.2	$< 20.$	19.10	y	y	n	n	
128	7e	1:33:09.52	30:34:51.5	$< 20.$	18.63	y	y	n	n	
129	24e	1:33:14.97	30:32:01.5	$< 20.$	18.61	y	n	n	n	
130	17e	1:33:11.16	30:34:21.8	$< 20.$	17.21	n	n	y	y	
131	13e	1:33:10.50	30:32:00.9	$< 20.$	18.43	n	n	y	y	
132	10e	1:33:10.07	30:31:28.3	$< 20.$	19.03	n	n	y	n	
133	86e	1:33:42.96	30:38:47.4	$< 20.$	18.92	y	n	n	n	
134	150e	1:34:22.20	30:32:39.4	$< 20.$		y	y	n	n	
135	112e	1:33:58.29	30:34:31.2	$< 20.$		n	n	y	y	
136	15e	1:33:10.68	30:35:50.6	$< 20.$		n	n	n	n	
137	133e	1:34:08.60	30:32:44.4	$< 20.$						
138	147e	1:34:16.13	30:33:44.7	$< 20.$		y	n	y	y	*
139	128e	1:34:04.89	30:45:03.1	$< 20.$		n	n	n	n	
140	125e	1:34:02.80	30:42:28.5	$< 20.$		n	n	n	n	
141	114e	1:33:58.72	30:35:26.1	$< 20.$		y	y	n	y	
142	148e	1:34:18.76	30:34:11.6	$< 20.$		n	n	y	y	
143	36e	1:33:19.58	30:35:29.9	$< 20.$		n	n	n	n	
144	129e	1:34:05.56	30:34:18.7	$< 20.$		y	n	n	n	
145	132e	1:34:08.22	30:34:04.9	$< 20.$		y	y	n	n	
146	122e	1:34:01.19	30:36:18.2	$< 20.$		y	y	y	y	*
147	131e	1:34:07.89	30:32:48.4	$< 20.$		y	n	n	n	
148	142e	1:34:15.07	30:40:36.0	$< 20.$		n	n	n	n	
149	52e	1:33:28.92	30:36:34.3	$< 20.$	20.38	n	y	n	y	
150	9e	1:33:10.07	30:38:40.0	$< 20.$	20.84	y	y	n	n	
151	11e	1:33:10.24	30:38:45.0	$< 20.$		y	y	n	n	
152	56e	1:33:33.32	30:31:47.0	$< 20.$		n	n	n	n	
153	1e	1:32:52.64	30:38:20.4	$< 20.$	19.98	y	y	n	n	

[a]Objects with an asterisk are included in Table 4.3.

Table A.2: Embedded Candidates

#	ID	R.A. (J2000)	Dec. (J2000)	V^b	Hβ	O_3	C_3/N_3	He_2	
1	162b	1:33:44.92	30:36:28.3	14.36	n	n	n	n	
2	177b	1:33:46.13	30:36:53.6	16.28	y	y	y	y	*
3	28b	1:33:12.09	30:38:52.2	16.55	y	y	y	y	*
4	137b	1:33:43.18	30:39:06.5	16.87	n	n	y	y	
5	221b	1:33:58.71	30:35:26.0	16.87	y	y	n	y	
6	165b	1:33:45.15	30:36:19.9	16.93	y	n	y	y	*
7	113b	1:33:37.05	30:36:37.5	17.13	y	n	y	y	*
8	207b	1:33:55.21	30:34:29.6	17.22	y	y	n	y	
9	16b	1:33:10.26	30:38:44.7	17.28	y	y	n	n	
10	150b	1:33:44.64	30:35:59.0	17.39	y	y	n	n	
11	153b	1:33:44.68	30:36:11.2	17.40	y	n	n	n	
12	182b	1:33:48.00	30:33:04.5	17.43	y	y	n	n	
13	92b	1:33:33.79	30:41:32.2	17.45	n	n	y	y	
14	25b	1:33:11.88	30:38:53.6	17.50	y	y	y	y	
15	157b	1:33:44.81	30:44:45.0	17.51	y	y	n	n	
16	196b	1:33:52.40	30:39:20.9	17.57	y	n	n	y	
17	65b	1:33:29.09	30:40:24.2	17.68	y	y	y	y	*
18	199b	1:33:53.23	30:38:53.7	17.76	y	y	n	n	*
19	206b	1:33:54.12	30:33:09.8	17.81	y	y	n	n	
20	197b	1:33:52.67	30:39:13.7	17.82	y	y	n	n	
21	139b	1:33:43.70	30:39:05.3	17.87	y	y	n	n	*
22	132b	1:33:42.53	30:32:58.3	17.93	y	y	n	n	
23	84b	1:33:33.50	30:41:33.0	18.02	n	n	y	y	
24	209b	1:33:55.86	30:34:07.5	18.17	n	n	y	y	
25	83b	1:33:33.49	30:41:31.8	18.23	n	y	y	y	
26	203b	1:33:53.80	30:35:27.7	18.23	y	y	n	y	
27	17b	1:33:10.43	30:38:49.4	18.31	y	n	n	n	
28	218b	1:33:57.84	30:35:31.7	18.43	y	y	n	n	
29	175b	1:33:45.71	30:36:09.6	18.47	y	y	n	n	
30	180b	1:33:47.53	30:38:39.8	18.51	y	y	n	n	
31	141b	1:33:43.73	30:40:56.6	18.59	y	y	n	n	
32	202b	1:33:53.61	30:38:51.6	18.65	y	n	y	y	
33	66b	1:33:29.78	30:40:23.4	18.65	y	y	n	n	
34	149b	1:33:44.56	30:44:32.6	18.76	y	y	n	n	
35	213b	1:33:56.42	30:34:20.6	18.84	y	y	n	y	
36	160b	1:33:44.83	30:44:32.6	18.84	y	y	n	n	
37	185b	1:33:49.72	30:37:30.3	18.93	y	y	n	n	
38	184b	1:33:48.81	30:39:47.1	18.94	y	y	n	y	
39	169b	1:33:45.18	30:44:49.1	18.97	y	y	n	y	

#	ID	R.A. (J2000)	Dec. (J2000)	V^b	Hβ	O_3	C_3/N_3	He_2	
40	142b	1:33:43.78	30:36:44.7	18.97	y	y	n	n	
41	60b	1:33:27.28	30:39:09.5	18.98	y	n	y	y	
42	226b	1:33:59.24	30:35:44.9	19.01	y	y	n	n	
43	159b	1:33:44.83	30:44:45.1	19.11	y	y	n	y	
44	126b	1:33:41.81	30:41:49.5	19.17	y	y	n	n	
45	74b	1:33:32.97	30:41:35.9	19.17	n	n	y	y	
46	251b	1:34:06.74	30:41:54.2	19.18	y	y	y	y	*
47	68b	1:33:30.05	30:31:45.3	19.23	y	y	n	y	
48	208b	1:33:55.63	30:37:41.1	19.29	y	n	n	n	
49	190b	1:33:50.86	30:39:45.8	19.30	y	y	n	n	
50	200b	1:33:53.28	30:39:18.7	19.36	n	y	n	n	
51	201b	1:33:53.58	30:35:19.7	19.36	y	y	n	n	
52	265b	1:34:14.21	30:33:43.1	19.36	y	y	n	n	
53	240b	1:34:02.47	30:38:41.5	19.38	y	y	n	n	
54	187b	1:33:50.68	30:41:20.6	19.38	y	y	n	n	
55	133b	1:33:42.56	30:33:14.5	19.39	n	n	y	y	
56	155b	1:33:44.72	30:44:37.0	19.41	y	y	y	y	*
57	36b	1:33:14.64	30:32:35.4	19.45	y	y	n	n	
58	195b	1:33:52.25	30:39:26.2	19.46	y	y	n	n	
59	18b	1:33:10.97	30:27:33.5	19.48					
60	227b	1:33:59.32	30:35:52.0	19.48	y	y	n	n	
61	238b	1:34:02.24	30:38:50.0	19.49	y	y	n	n	
62	19b	1:33:10.97	30:29:56.9	19.50	y	n	n	n	
63	99b	1:33:34.39	30:32:08.2	19.51	y	y	n	y	*
64	104b	1:33:34.89	30:36:30.3	19.51	y	y	n	n	
65	198b	1:33:53.22	30:39:02.8	19.52	y	y	n	n	
66	62b	1:33:27.50	30:31:53.6	19.54	y	y	y	y	*
67	191b	1:33:51.11	30:40:05.0	19.54	y	y	n	n	
68	117b	1:33:39.00	30:32:36.1	19.54	y	y	n	y	
69	89b	1:33:33.73	30:32:01.1	19.55	y	y	n	n	
70	130b	1:33:42.27	30:33:01.4	19.55	y	y	n	n	
71	59b	1:33:27.03	30:38:42.2	19.56	y	y	n	n	
72	172b	1:33:45.39	30:36:42.9	19.58	y	y	n	n	
73	179b	1:33:46.86	30:33:32.6	19.58	y	y	n	y	
74	236b	1:34:01.77	30:44:57.3	19.64	y	y	n	n	
75	38b	1:33:14.92	30:45:00.4	19.65	y	y	n	y	
76	98b	1:33:34.38	30:42:01.2	19.66	n	n	n	n	
77	210b	1:33:56.05	30:34:21.8	19.66	y	y	n	y	
78	264b	1:34:14.03	30:33:44.1	19.68	y	y	n	n	
79	267b	1:34:14.39	30:34:34.3	19.69	y	y	n	n	
80	131b	1:33:42.28	30:33:01.1	19.69	y	y	n	n	

#	ID	R.A. (J2000)	Dec. (J2000)	V[b]	Hβ	O_3	C_3/N_3	He_2	
81	119b	1:33:39.24	30:32:39.5	19.72	y	y	n	n	
82	189b	1:33:50.76	30:37:06.3	19.74	y	y	n	n	
83	138b	1:33:43.50	30:39:11.7	19.75	y	y	n	n	
84	222b	1:33:58.83	30:41:13.5	19.79	y	y	n	n	
85	205b	1:33:54.10	30:33:00.0	19.79	y	y	n	n	
86	186b	1:33:50.25	30:33:47.2	19.79	y	y	n	n	
87	116b	1:33:38.98	30:32:06.4	19.81	y	y	n	n	*
88	263b	1:34:13.96	30:33:39.5	19.82	y	y	n	n	
89	245b	1:34:06.37	30:41:43.8	19.85	y	y	n	n	
90	72b	1:33:30.43	30:31:58.4	19.87	y	y	n	n	
91	14b	1:33:09.92	30:38:55.5	19.89	n	y	n	n	
92	254b	1:34:11.20	30:36:10.7	19.96	y	y	n	n	
93	105b	1:33:34.90	30:37:05.5	19.97	y	y	n	n	
94	13b	1:33:09.87	30:38:46.4	19.97	y	y	n	n	
95	135b	1:33:43.07	30:44:40.9	20.02	y	y	n	n	
96	212b	1:33:56.12	30:41:15.8	20.03	y	y	n	n	
97	73b	1:33:32.72	30:36:55.1	20.04	y	y	n	n	
98	15b	1:33:09.96	30:27:27.5	20.05					
99	51b	1:33:20.75	30:32:04.8	20.06	y	n	n	n	
100	61b	1:33:27.33	30:38:42.2	20.07	y	y	n	n	
101	54b	1:33:26.24	30:39:02.8	20.07	y	y	n	n	
102	192b	1:33:51.79	30:40:54.4	20.08	y	y	n	n	
103	231b	1:34:00.27	30:40:47.6	20.09	y	y	n	n	
104	9b	1:33:02.95	30:41:07.3	20.11	y	y	n	n	
105	120b	1:33:40.21	30:37:22.3	20.12	y	y	n	n	
106	129b	1:33:42.25	30:32:57.9	20.13	y	y	n	n	
107	2b	1:32:55.75	30:39:30.9	20.14	y	n	n	n	
108	47b	1:33:19.06	30:39:32.3	20.15					
109	63b	1:33:27.76	30:31:50.8	20.17	y	y	n	y	
110	97b	1:33:34.30	30:41:30.1	20.19	y	y	n	n	
111	235b	1:34:01.66	30:44:58.1	20.19	y	y	n	n	
112	23b	1:33:11.26	30:39:14.5	20.20	n	n	n	n	
113	127b	1:33:41.84	30:41:49.3	20.22	y	y	n	n	
114	136b	1:33:43.10	30:33:26.2	20.26	y	y	n	n	
115	239b	1:34:02.42	30:38:50.7	20.27	y	y	n	n	
116	128b	1:33:42.21	30:33:06.0	20.28	y	y	n	n	
117	58b	1:33:26.96	30:39:11.2	20.30	y	y	y	y	*
118	21b	1:33:11.20	30:27:40.9	20.32					
119	103b	1:33:34.86	30:41:47.4	20.38	y	y	n	n	
120	55b	1:33:26.27	30:40:44.9	20.40	y	y	n	y	*
121	82b	1:33:33.49	30:41:38.0	20.41	y	y	n	n	

#	ID	R.A. (J2000)	Dec. (J2000)	V[b]	Hβ	O_3	C_3/N_3	He_2	
122	193b	1:33:51.92	30:40:21.2	20.42	y	y	y	y	
123	75b	1:33:33.08	30:32:10.1	20.45	y	y	n	n	
124	50b	1:33:20.64	30:31:59.3	20.45	y	y	n	n	
125	145b	1:33:44.10	30:44:38.1	20.48	y	y	n	n	
126	134b	1:33:42.73	30:32:59.9	20.49	y	y	n	n	
127	217b	1:33:57.69	30:35:27.7	20.50	y	y	n	n	
128	233b	1:34:01.05	30:43:52.8	20.51	y	y	n	n	
129	20b	1:33:11.09	30:27:36.6	20.52					
130	268b	1:34:14.56	30:42:28.3	20.57	y	n	n	n	
131	90b	1:33:33.74	30:41:36.2	20.58	n	y	y	y	
132	100b	1:33:34.48	30:36:28.4	20.58	y	n	n	n	
133	96b	1:33:34.04	30:41:16.9	20.61	n	n	y	y	
134	183b	1:33:48.18	30:39:18.5	20.62	y	y	n	n	
135	174b	1:33:45.54	30:36:39.7	20.63	y	y	n	n	
136	144b	1:33:44.09	30:44:38.1	20.63	y	y	n	n	
137	125b	1:33:41.46	30:41:51.8	20.64	y	y	n	n	
138	57b	1:33:26.81	30:39:00.6	20.66	y	y	n	n	
139	56b	1:33:26.65	30:39:03.9	20.67	y	y	n	n	
140	48b	1:33:20.41	30:32:48.6	20.68	y	y	n	n	
141	40b	1:33:15.12	30:32:28.2	20.69	y	y	n	n	
142	111b	1:33:36.06	30:42:33.2	20.70	y	y	n	n	
143	49b	1:33:20.53	30:32:01.5	20.71	y	y	n	n	*
144	107b	1:33:35.30	30:41:29.2	20.73	y	y	n	n	
145	242b	1:34:06.12	30:41:46.5	20.73	y	y	n	n	
146	53b	1:33:23.45	30:31:35.4	20.75	y	y	n	n	
147	112b	1:33:36.80	30:43:23.2	20.75	y	y	n	n	
148	143b	1:33:43.80	30:36:45.0	20.76	y	y	n	n	
149	115b	1:33:38.93	30:32:37.7	20.76	y	y	n	n	
150	178b	1:33:46.18	30:36:01.9	20.77	y	y	n	y	
151	34b	1:33:13.89	30:29:44.6	20.78	y	y	n	n	
152	274b	1:34:17.40	30:33:34.6	20.79	y	y	n	y	
153	140b	1:33:43.70	30:31:33.6	20.79	n	n	n	n	
154	273b	1:34:17.40	30:33:43.9	20.82	y	y	n	n	
155	106b	1:33:35.23	30:37:03.3	20.85	y	y	n	n	
156	32b	1:33:13.29	30:39:20.1	20.93	y	y	n	n	
157	244b	1:34:06.21	30:41:36.0	20.96	y	y	n	n	
158	269b	1:34:15.04	30:33:47.6	21.07	y	y	n	n	
159	39b	1:33:15.08	30:32:37.0	21.07	y	y	n	n	
160	194b	1:33:52.03	30:40:52.4	21.09	y	y	n	n	
161	279b	1:34:20.58	30:34:09.9	21.09	y	y	n	n	
162	6b	1:33:01.80	30:41:07.4	21.11	y	n	n	n	

#	ID	R.A. (J2000)	Dec. (J2000)	V^b	Hβ	O_3	C_3/N_3	He_2	
163	42b	1:33:17.11	30:31:10.9	21.12	y	y	n	n	
164	85b	1:33:33.56	30:41:27.0	21.13	y	y	y	y	*
165	69b	1:33:30.09	30:32:05.9	21.20	y	y	n	n	
166	76b	1:33:33.12	30:41:32.6	21.25	y	y	y	y	*
167	10b	1:33:03.84	30:39:55.0	21.26	y	y	n	n	
168	26b	1:33:11.94	30:30:15.6	21.28	y	y	n	n	
169	80b	1:33:33.37	30:41:41.7	21.29	y	y	n	n	
170	11b	1:33:03.87	30:40:00.8	21.29	y	y	n	n	
171	45b	1:33:18.24	30:41:15.4	21.30	y	y	n	n	
172	78b	1:33:33.24	30:33:43.1	21.33	y	y	n	n	
173	109b	1:33:35.58	30:41:23.5	21.38	y	y	n	n	
174	1b	1:32:55.48	30:39:33.7	21.40	y	n	n	n	
175	43b	1:33:17.18	30:31:13.4	21.42	y	y	n	n	
176	4b	1:33:00.26	30:39:01.8	21.51	y	y	n	n	
177	243b	1:34:06.18	30:41:40.0	21.55	y	y	n	n	
178	166b	1:33:45.15	30:33:08.6	21.55	y	y	n	n	
179	266b	1:34:14.22	30:33:45.8	21.60	y	y	n	n	
180	121b	1:33:40.41	30:41:34.8	21.63	y	y	n	n	
181	44b	1:33:18.23	30:41:15.5	21.67	y	y	n	n	
182	41b	1:33:15.16	30:32:32.9	21.73	y	y	n	n	
183	86b	1:33:33.59	30:41:35.1	21.73	n	n	y	y	
184	277b	1:34:19.54	30:33:43.8	21.76	y	y	n	y	
185	101b	1:33:34.53	30:41:50.8	21.76	y	y	n	n	
186	225b	1:33:59.12	30:34:36.8	21.79	y	y	n	n	
187	275b	1:34:17.46	30:33:38.0	21.88	y	y	n	n	
188	278b	1:34:19.73	30:33:44.0	21.89	y	y	n	y	
189	94b	1:33:34.00	30:41:35.6	21.97	y	y	y	y	*
190	102b	1:33:34.82	30:41:38.6	21.97	y	y	n	n	
191	262b	1:34:13.76	30:33:41.9	22.25	y	y	n	n	
192	230b	1:34:00.27	30:40:45.1	22.28	y	y	n	n	
193	37b	1:33:14.86	30:45:04.4	22.35	y	y	n	y	
194	3b	1:32:58.85	30:41:31.1	22.42	y	y	n	n	
195	249b	1:34:06.44	30:41:56.4	22.69	y	y	n	n	
196	8b	1:33:02.89	30:41:12.9	22.71	y	y	n	n	
197	7b	1:33:02.26	30:39:53.3	22.74	y	n	n	n	
198	5b	1:33:01.64	30:41:05.4	22.84	y	n	n	n	
199	250b	1:34:06.53	30:41:48.6	23.18	y	y	y	y	*
200	256b	1:34:12.77	30:45:07.4	23.24	y	y	n	y	
201	253b	1:34:11.05	30:42:19.9	23.30	y	y	n	n	
202	110b	1:33:35.73	30:36:28.9	23.70	y	y	n	y	
203	52b	1:33:22.20	30:32:20.4	24.11	y	y	n	n	

#	ID	R.A. (J2000)	Dec. (J2000)	V^b	Hβ	O_3	C_3/N_3	He_2	
204	152b	1:33:44.67	30:44:52.9	24.44	y	y	n	n	
205	46b	1:33:18.92	30:33:14.3	25.02	y	y	n	n	
206	259b	1:34:13.46	30:41:58.6		y	y	n	n	
207	95b	1:33:34.01	30:41:47.8		y	y	n	n	
208	276b	1:34:19.38	30:33:43.3		y	y	y	y	*
209	67b	1:33:29.89	30:31:47.2		y	y	y	y	*
210	272b	1:34:17.21	30:33:39.0		y	y	n	n	
211	124b	1:33:41.34	30:41:53.5		y	y	n	n	
212	123b	1:33:40.67	30:42:57.8		y	y	y	y	
213	223b	1:33:58.84	30:41:13.6		y	y	n	n	
214	224b	1:33:59.08	30:34:41.9		y	y	y	n	
215	33b	1:33:13.65	30:39:28.8		y	y	n	n	
216	71b	1:33:30.41	30:31:55.2		y	y	n	n	
217	252b	1:34:10.55	30:39:16.1		y	y	n	y	
218	122b	1:33:40.51	30:41:38.0		y	y	n	n	
219	81b	1:33:33.47	30:41:29.4		y	y	y	n	
220	64b	1:33:28.07	30:31:50.5		y	y	y	y	*
221	171b	1:33:45.26	30:36:26.4		y	n	n	n	*
222	93b	1:33:33.80	30:41:29.5		y	y	y	y	
223	164b	1:33:44.96	30:36:16.8		y	y	n	n	*
224	215b	1:33:57.51	30:42:17.6		y	y	y	n	
225	91b	1:33:33.74	30:41:33.8		y	y	y	y	
226	232b	1:34:00.49	30:38:07.7		y	y	n	y	
227	167b	1:33:45.16	30:33:15.5		y	n	n	n	
228	35b	1:33:14.31	30:27:10.9		y	y	n	n	
229	188b	1:33:50.70	30:41:20.6		y	y	n	n	
230	216b	1:33:57.55	30:42:14.3		y	y	n	n	
231	170b	1:33:45.21	30:44:38.1		y	y	n	n	
232	27b	1:33:11.95	30:30:27.8		y	y	n	n	
233	204b	1:33:54.09	30:33:04.5		y	y	n	n	
234	214b	1:33:57.47	30:42:11.1		y	y	n	n	
235	148b	1:33:44.55	30:44:32.5		y	y	n	n	*
236	220b	1:33:58.47	30:42:26.9		y	y	n	n	
237	146b	1:33:44.42	30:44:35.1		y	y	y	y	*
238	154b	1:33:44.70	30:44:36.9		y	y	y	y	*
239	173b	1:33:45.47	30:36:47.8		y	y	n	n	
240	158b	1:33:44.82	30:44:32.5		y	y	n	n	
241	211b	1:33:56.12	30:41:15.8		y	y	n	n	
242	271b	1:34:16.38	30:37:12.3		y	y	y	y	
243	30b	1:33:12.73	30:38:40.9		y	y	y	y	*
244	168b	1:33:45.16	30:44:47.2		y	y	y	y	*

#	ID	R.A. (J2000)	Dec. (J2000)	V[b]	Hβ	O_3	C_3/N_3	He_2	
245	229b	1:33:59.90	30:34:26.9		y	y	n	n	
246	31b	1:33:13.18	30:34:07.5		y	n	n	n	
247	248b	1:34:06.44	30:41:46.5		y	y	n	n	
248	79b	1:33:33.35	30:41:39.0		y	y	n	n	
249	87b	1:33:33.63	30:41:31.8		y	y	y	y	
250	151b	1:33:44.65	30:36:31.5		n	n	n	n	
251	237b	1:34:01.94	30:43:55.9		y	y	n	n	
252	24b	1:33:11.64	30:34:36.1		y	n	n	n	
253	147b	1:33:44.43	30:44:35.0		y	y	y	y	*
254	255b	1:34:12.59	30:45:07.9		y	y	y	y	
255	88b	1:33:33.65	30:41:29.6		y	y	y	y	
256	246b	1:34:06.39	30:41:44.7		y	y	n	n	
257	247b	1:34:06.42	30:37:49.7		y	y	n	n	
258	163b	1:33:44.92	30:44:48.9		y	y	y	y	*
259	29b	1:33:12.61	30:34:10.1		y	y	n	n	
260	161b	1:33:44.90	30:44:48.8		y	y	y	y	*
261	258b	1:34:12.99	30:40:17.1		y	n	n	n	
262	22b	1:33:11.23	30:39:17.0		n	n	n	y	
263	118b	1:33:39.16	30:32:32.5		y	y	n	n	
264	114b	1:33:37.59	30:32:02.3		y	n	n	n	
265	77b	1:33:33.13	30:32:12.3		y	y	n	n	
266	156b	1:33:44.76	30:44:46.7		y	y	n	y	
267	241b	1:34:02.52	30:38:39.7		y	y	n	n	
268	261b	1:34:13.73	30:33:45.0		y	y	n	n	
269	257b	1:34:12.90	30:45:09.5		y	y	n	n	
270	70b	1:33:30.12	30:31:47.9		y	y	n	n	
271	234b	1:34:01.08	30:43:53.3		y	y	n	n	
272	176b	1:33:46.13	30:42:47.9		y	y	n	n	
273	260b	1:34:13.61	30:34:48.6		y	y	n	n	
274	219b	1:33:58.15	30:35:22.9		y	y	n	n	
275	181b	1:33:47.86	30:44:42.0		y	y	n	n	
276	228b	1:33:59.65	30:34:35.0		y	y	n	y	
277	108b	1:33:35.33	30:41:51.3		y	y	n	n	
278	270b	1:34:15.54	30:37:12.0		y	y	n	n	
279	12b	1:33:09.30	30:34:51.1		y	y	n	n	

[a]Objects with an asterisk are included in Table 4.3.

Appendix B

Candidate Diagrams

B.1 Objects Near Wolf-Rayet Stars

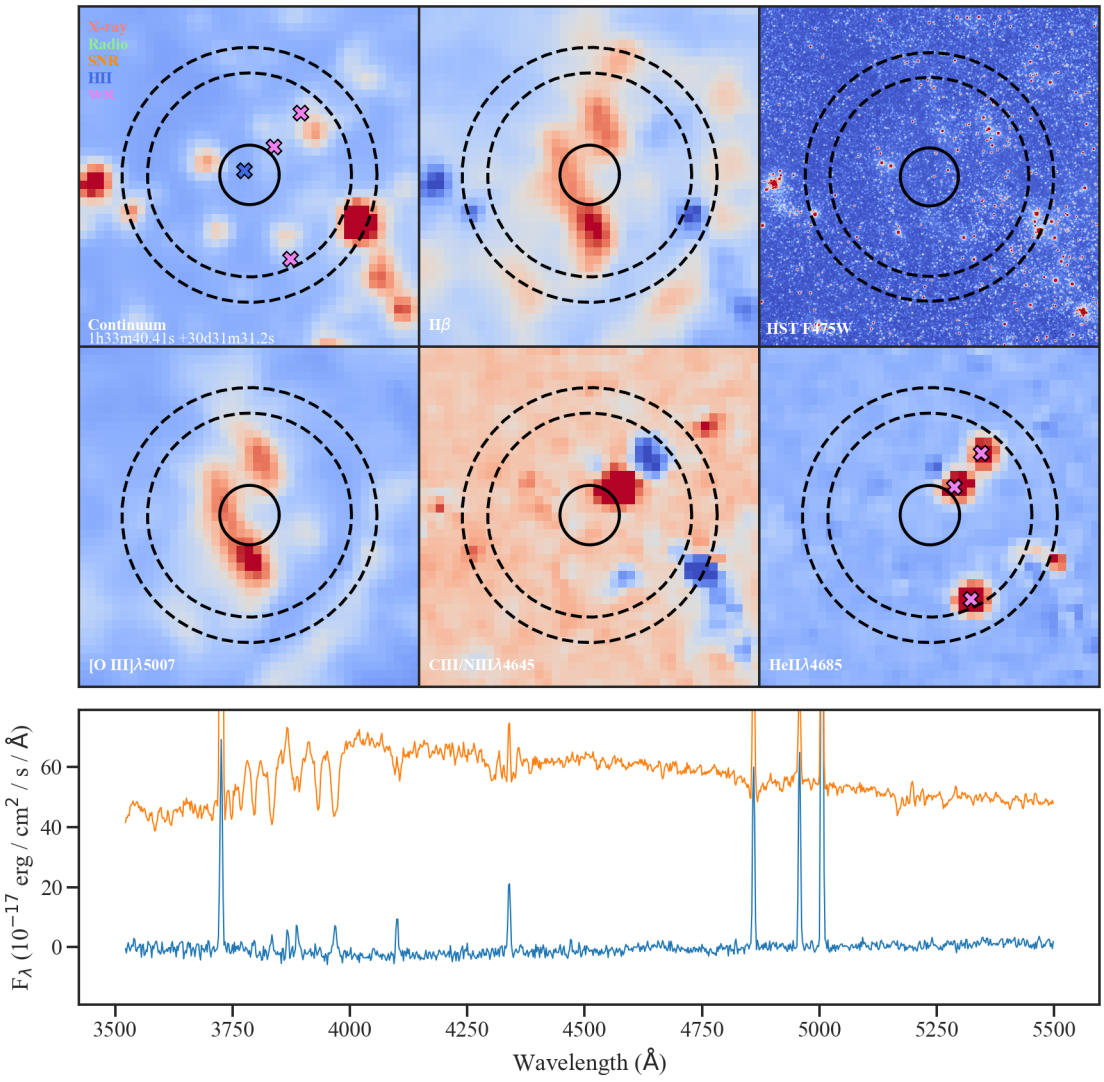

Figure B.1: Object 80e Inspection Diagram

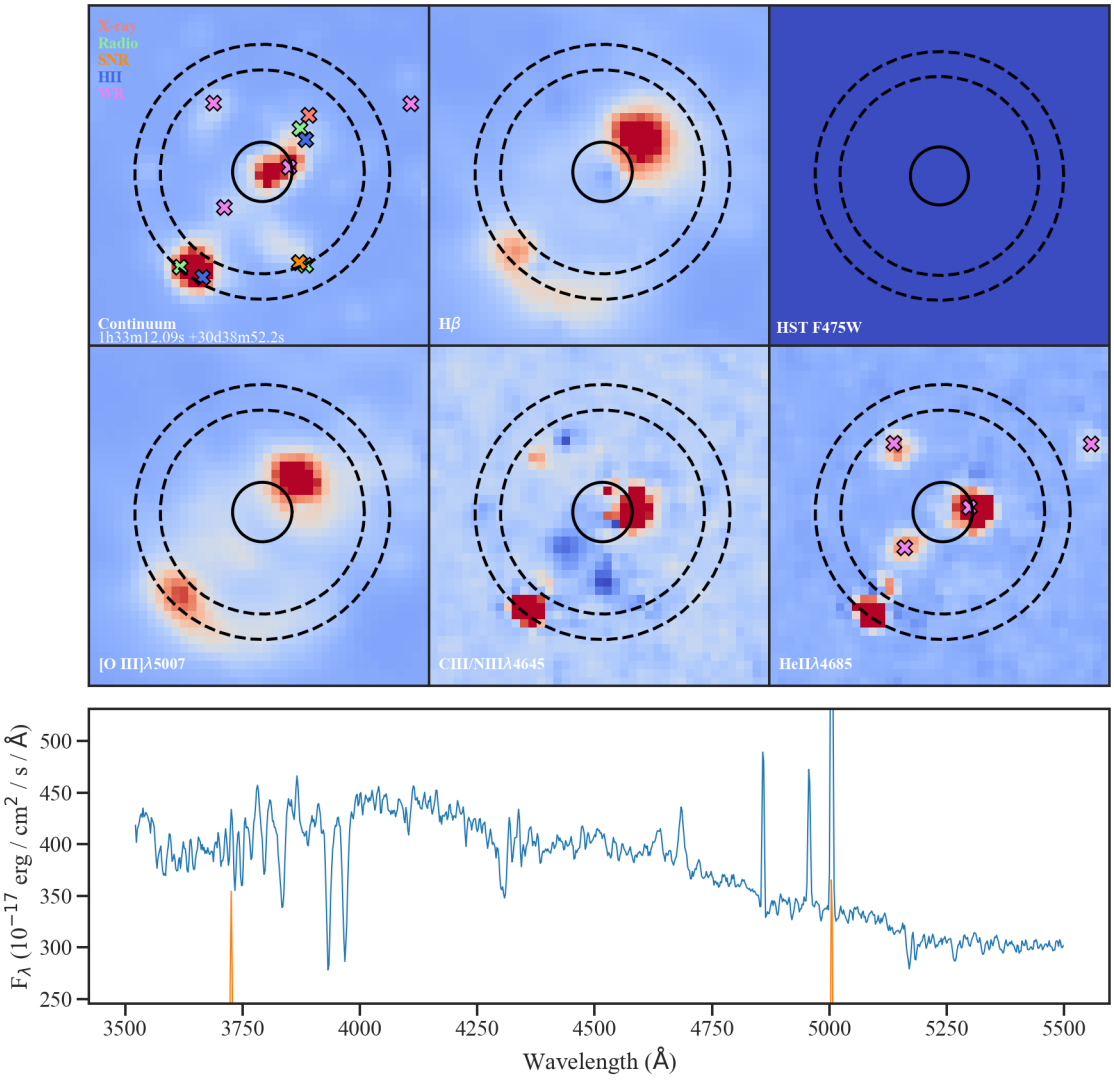

Figure B.2: Object 28b Inspection Diagram

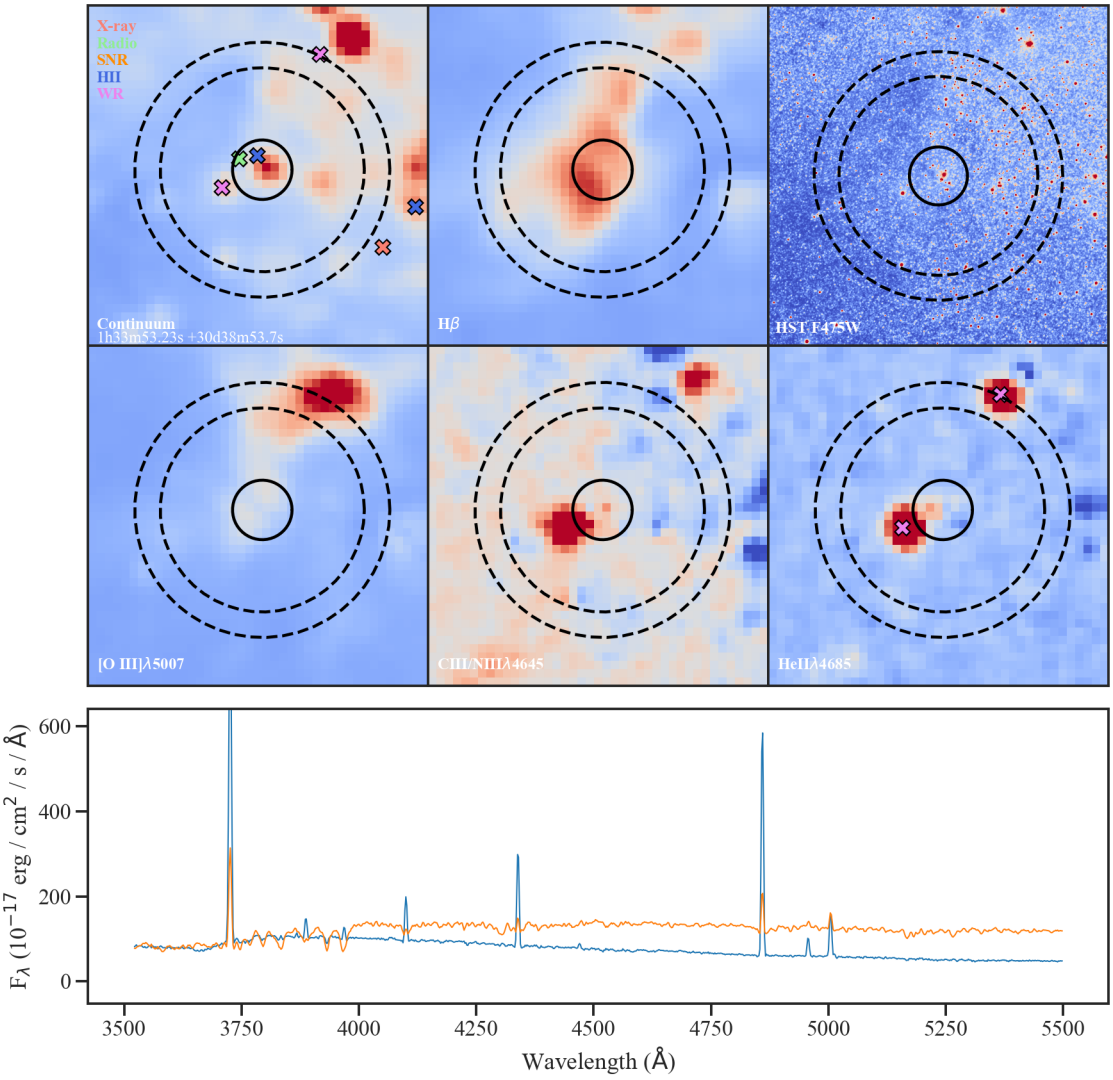

Figure B.3: Object 199b Inspection Diagram

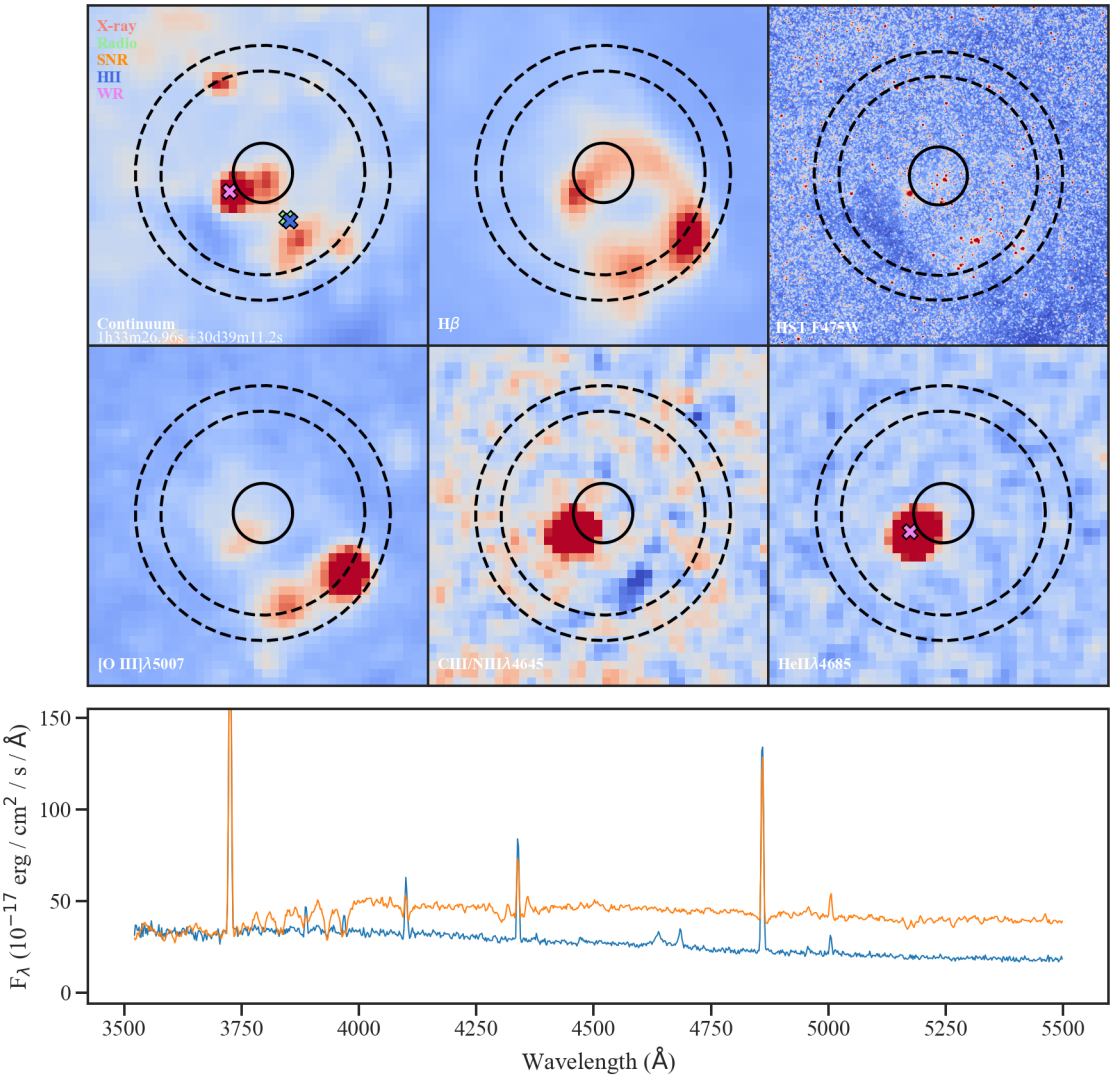

Figure B.4: Object 58b Inspection Diagram

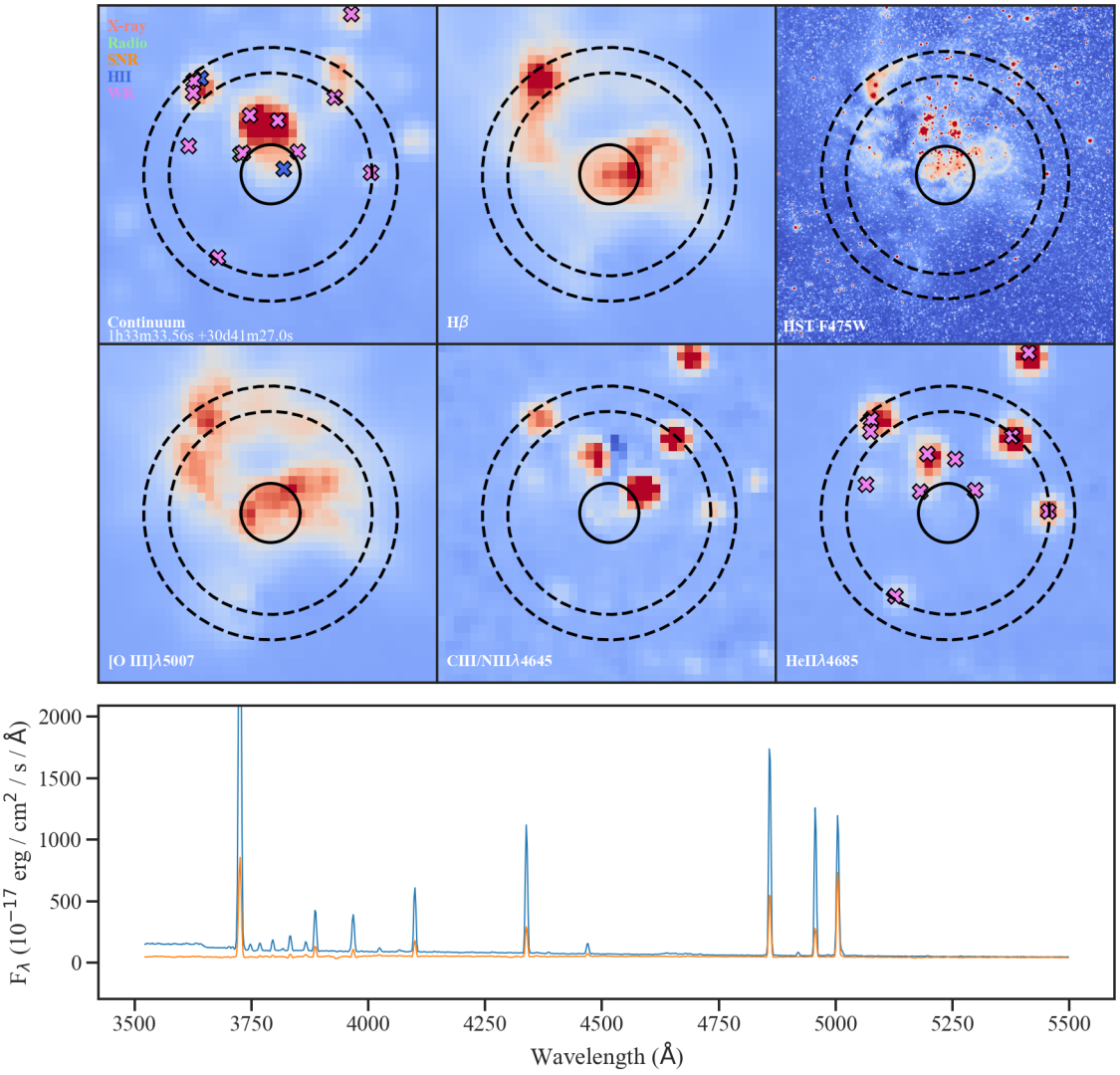

Figure B.5: Object 85b Inspection Diagram

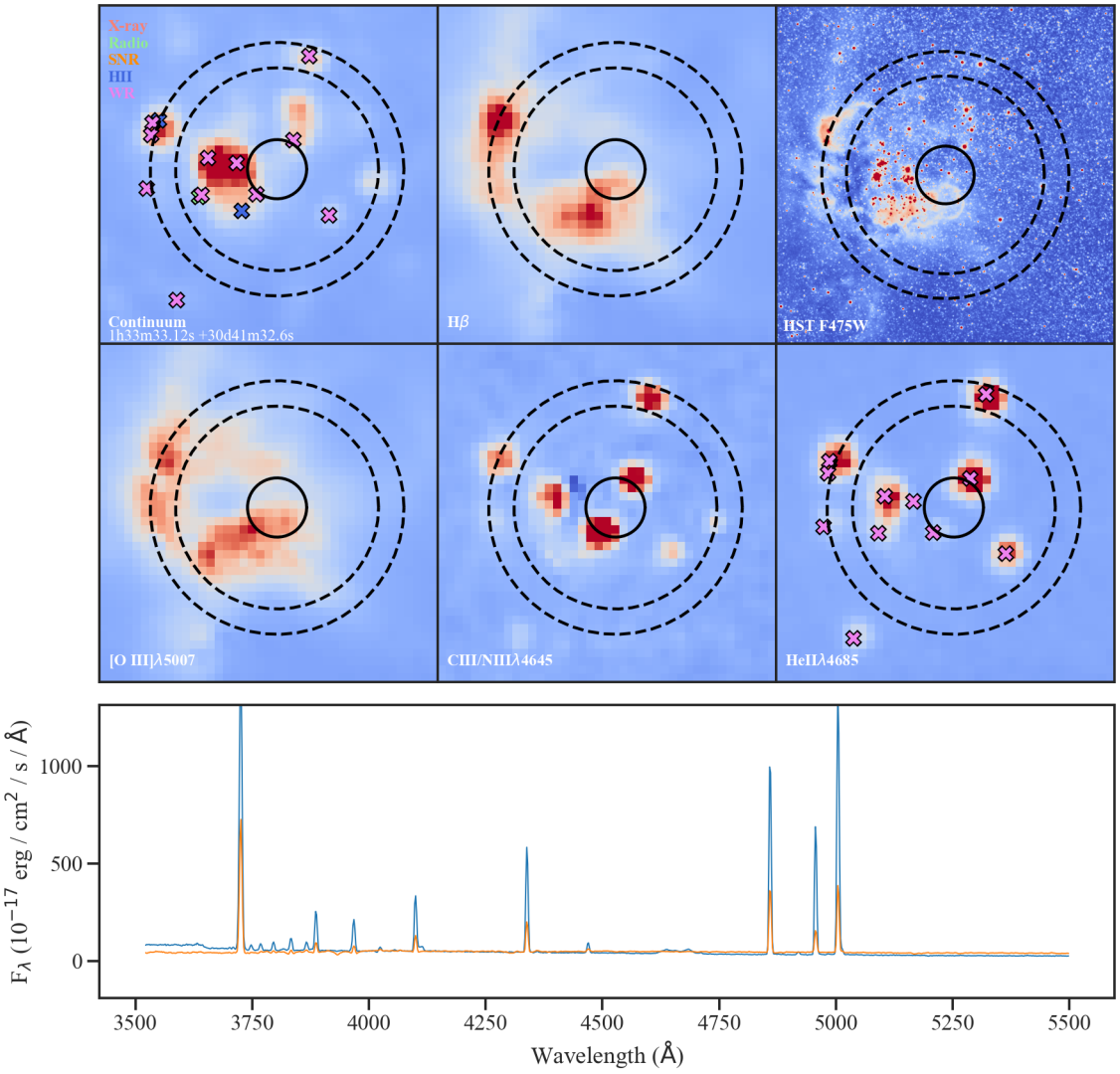

Figure B.6: Object 76b Inspection Diagram

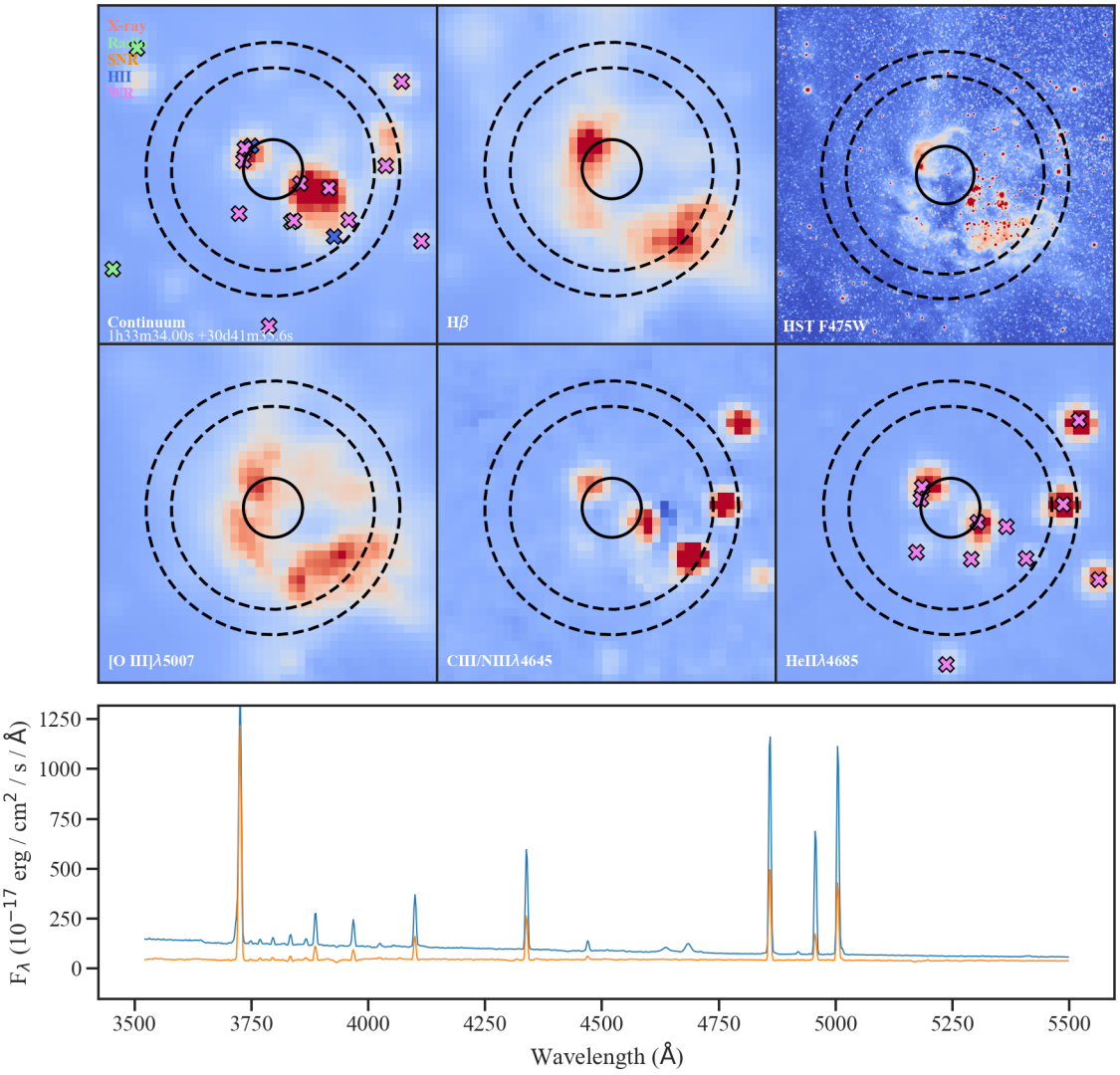

Figure B.7: Object 94b Inspection Diagram

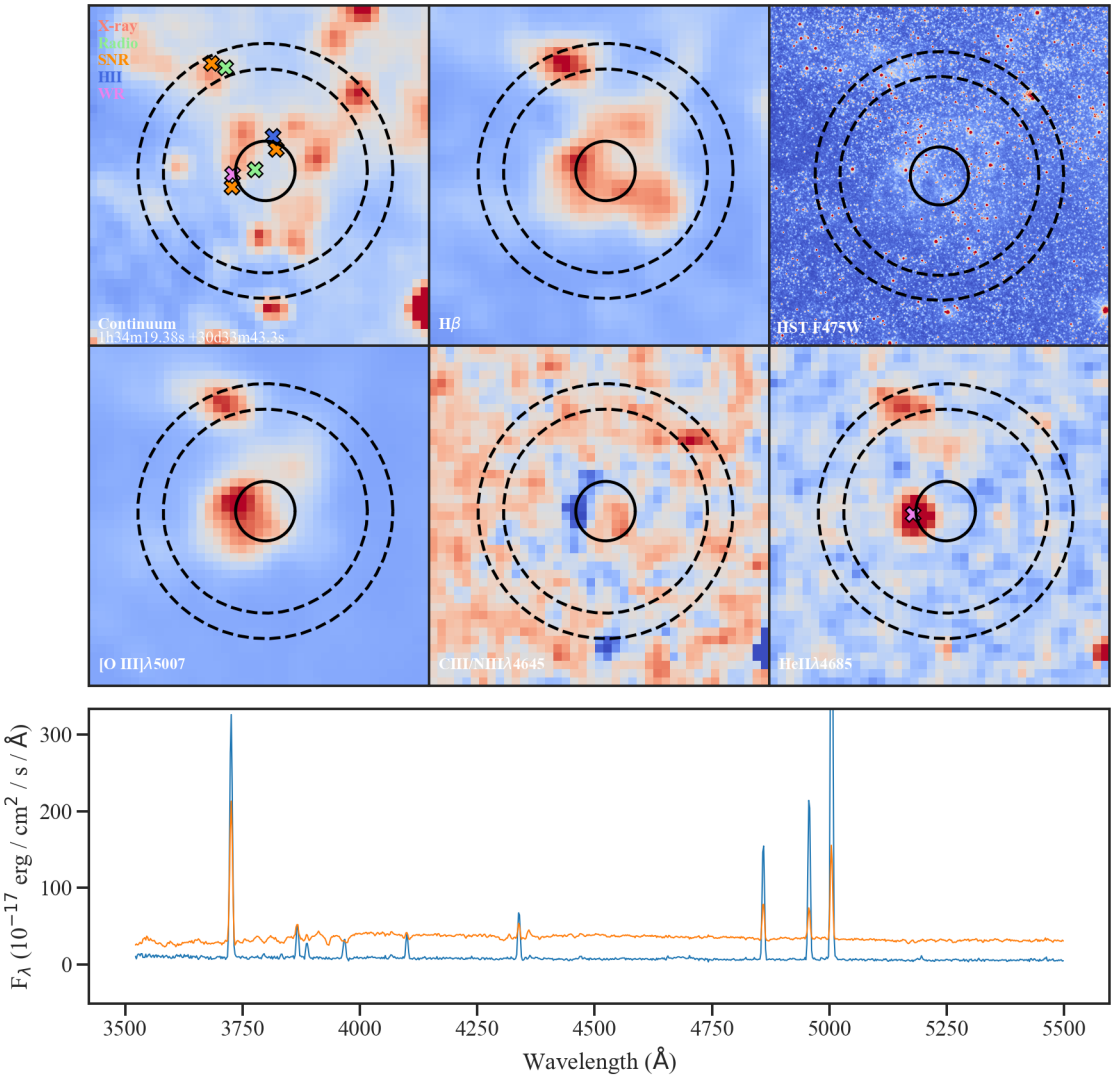

Figure B.8: Object 276b Inspection Diagram

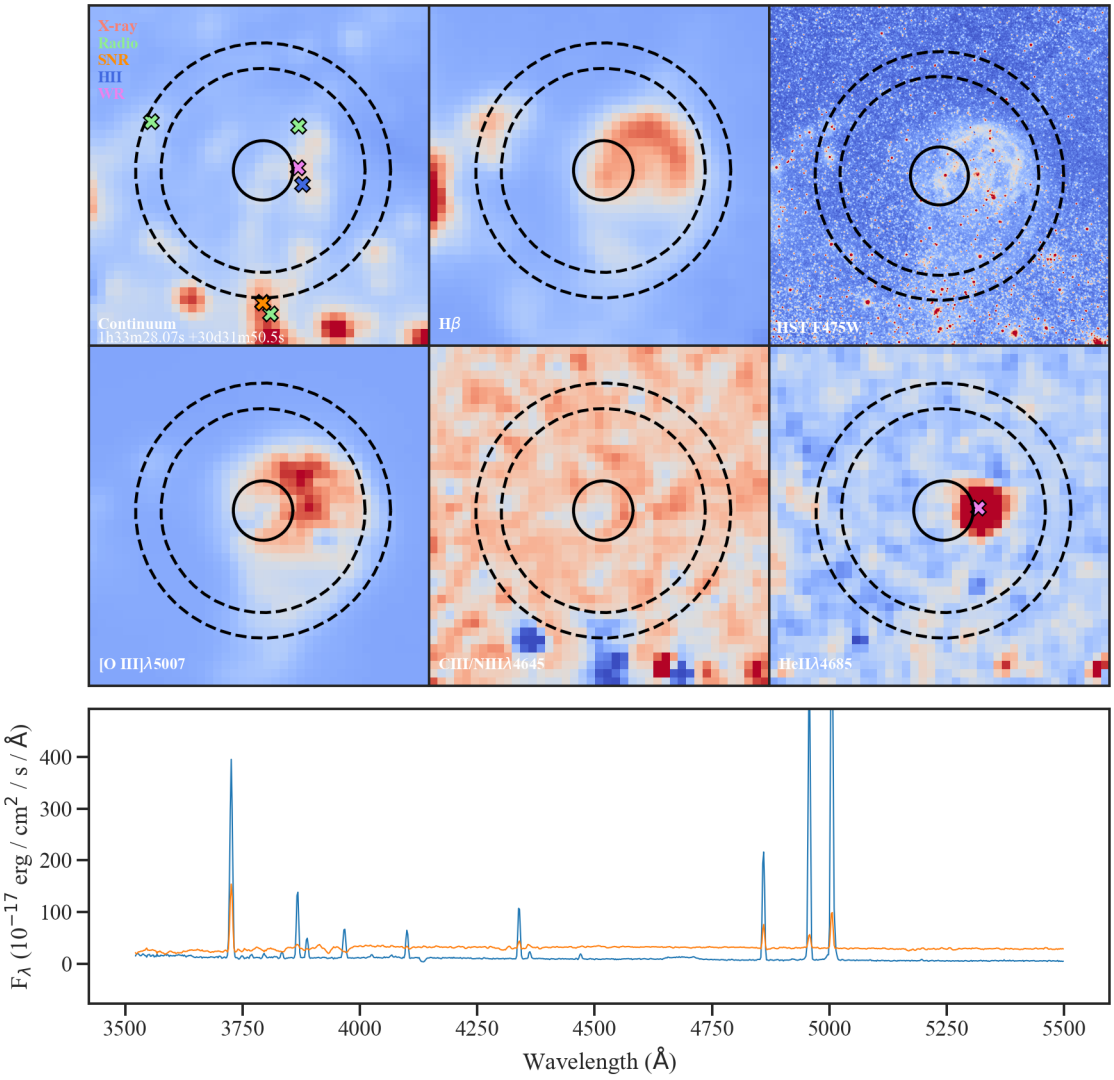

Figure B.9: Object 34b Inspection Diagram

B.2 New Wolf-Rayet Stars

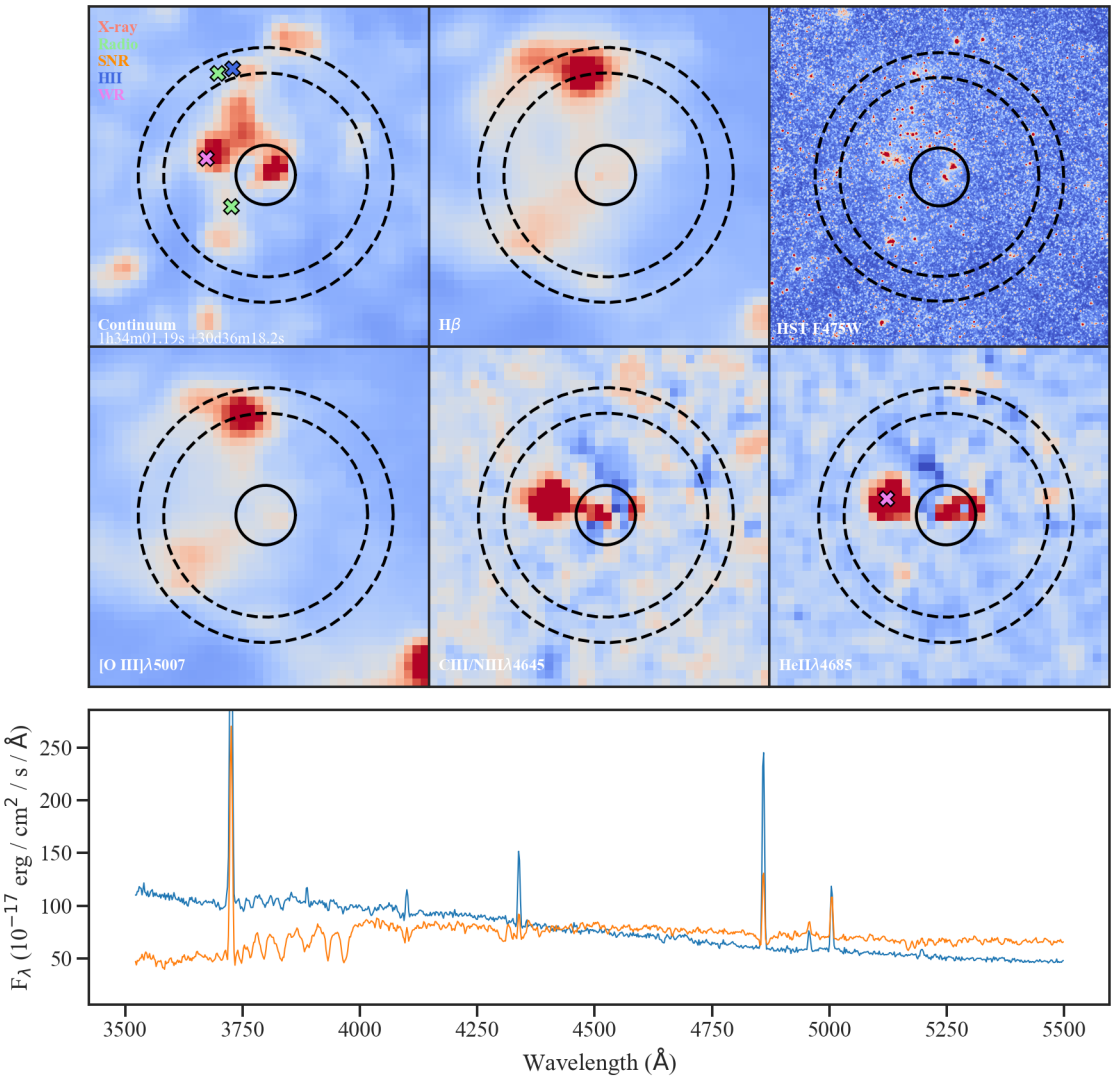

Figure B.10: Object 122e Inspection Diagram

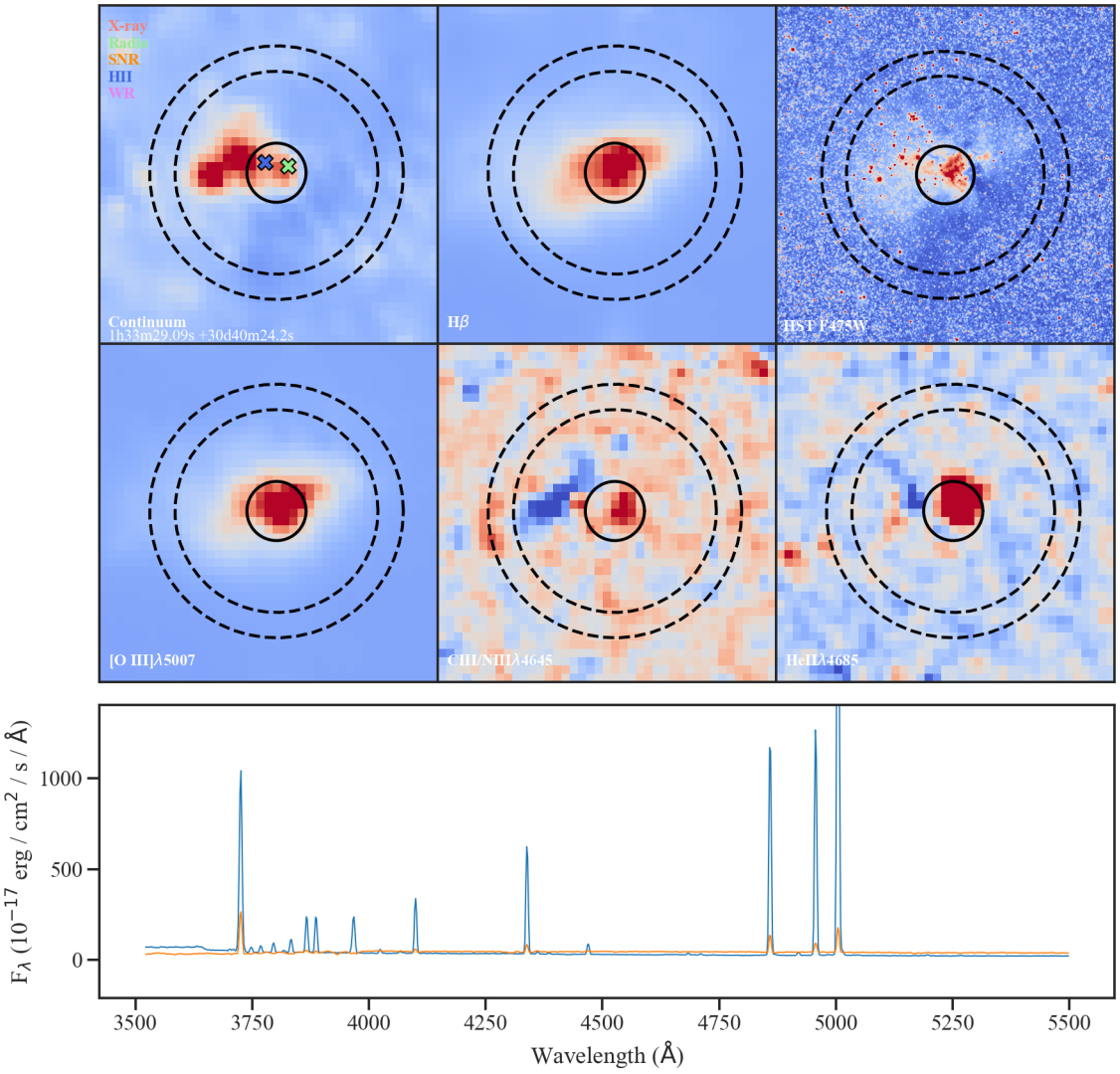

Figure B.11: Object 65b Inspection Diagram

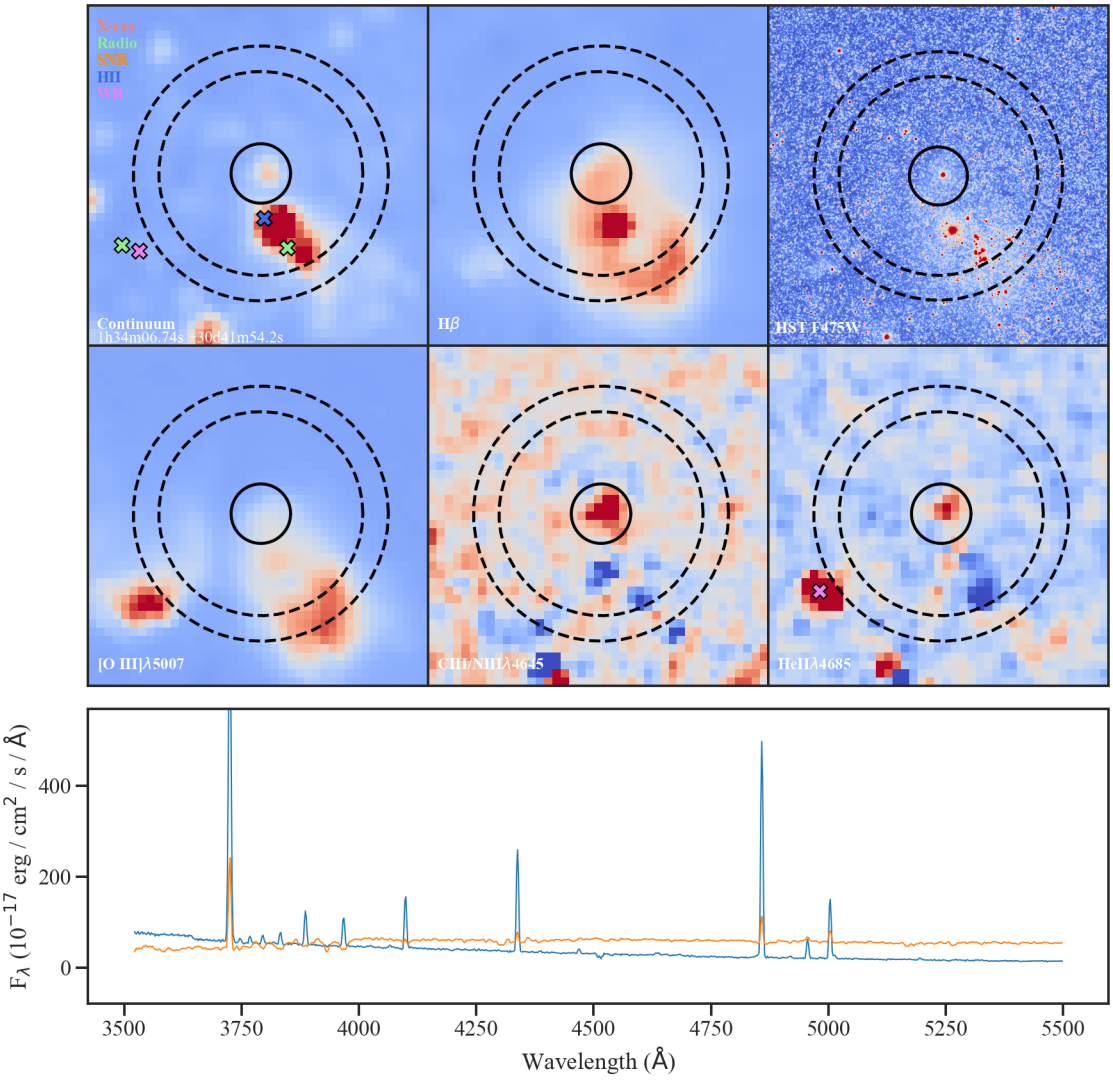

Figure B.12: Object 251b Inspection Diagram

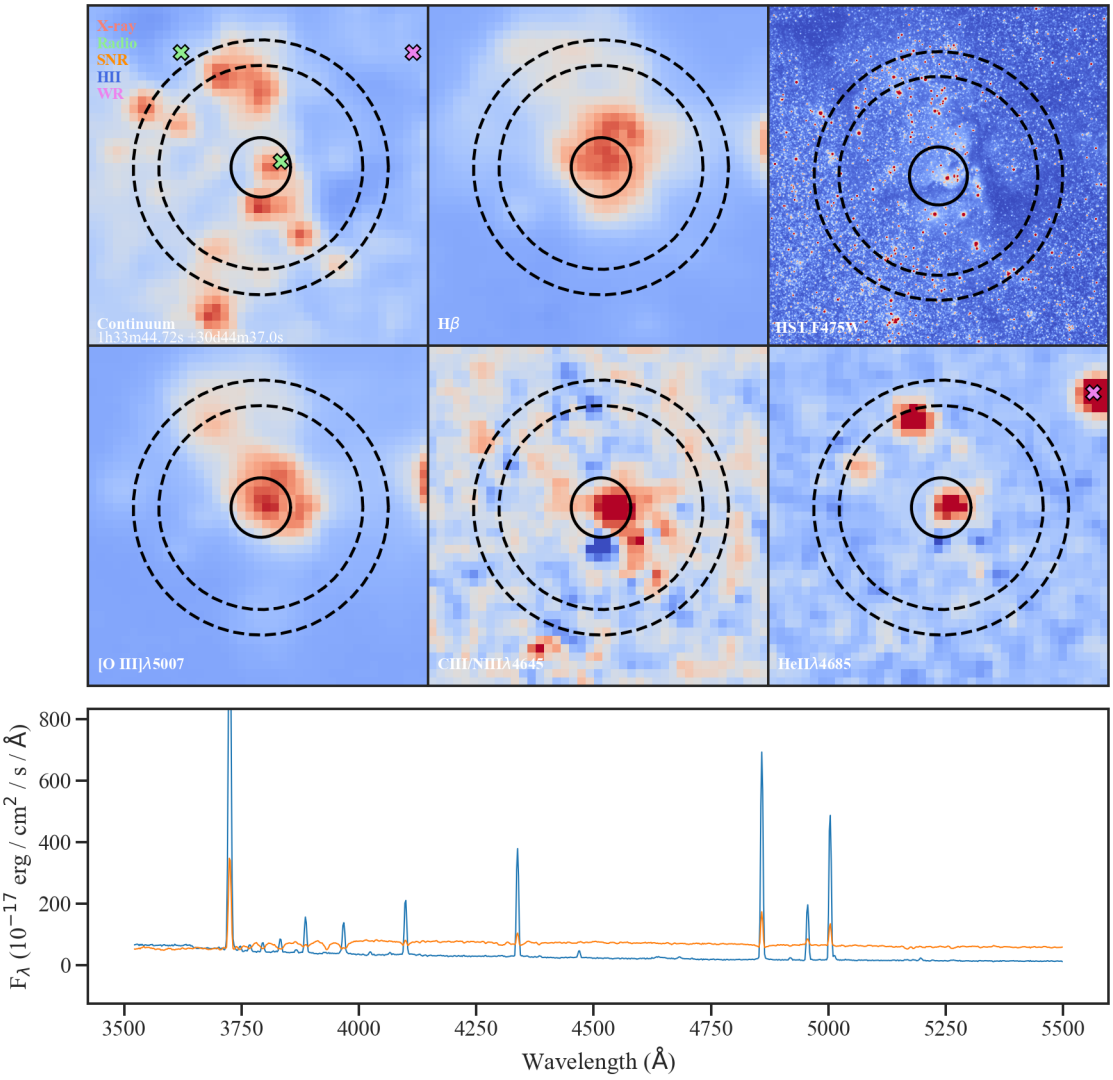

Figure B.13: Object 155b Inspection Diagram

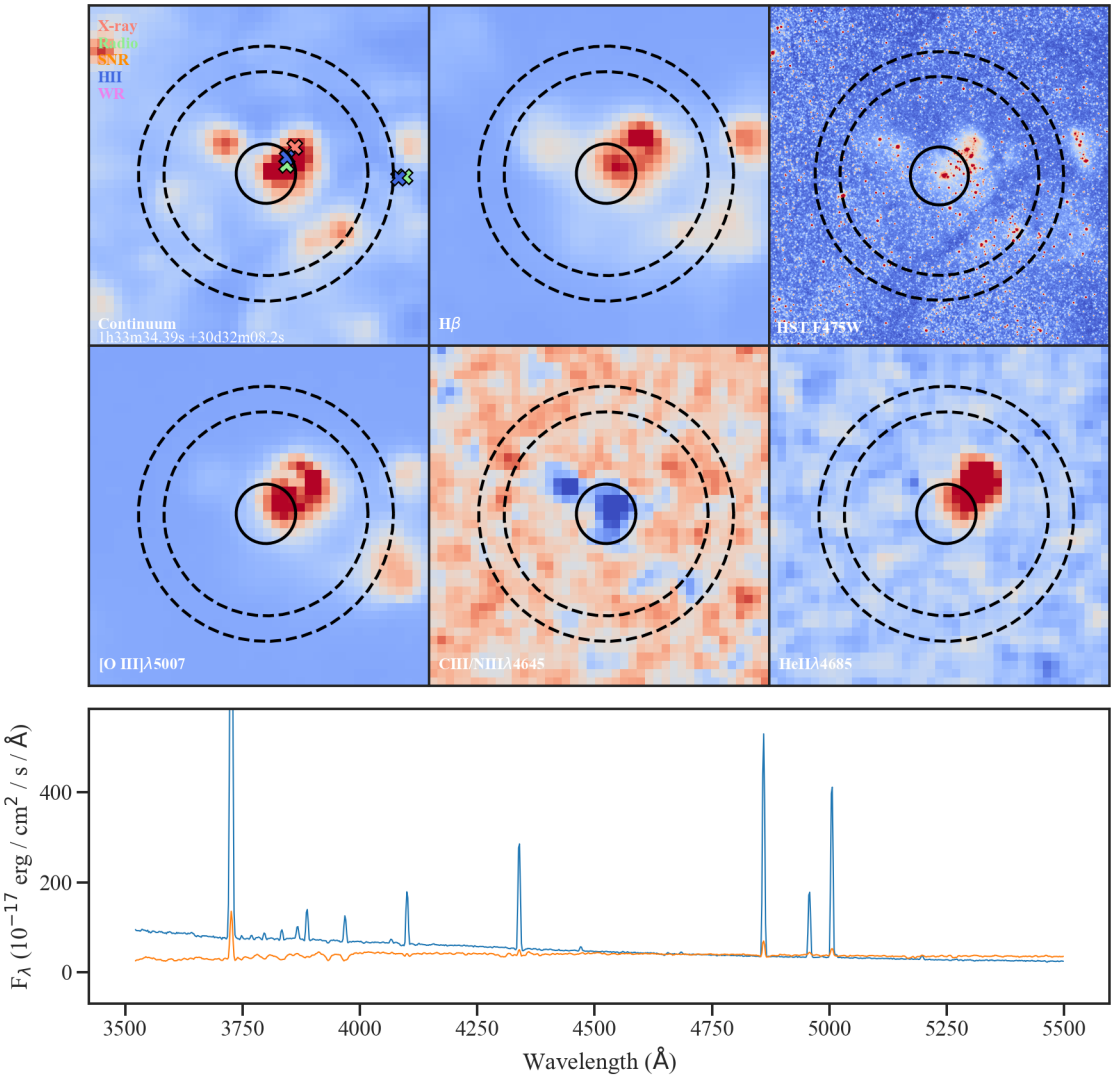

Figure B.14: Object 99b Inspection Diagram

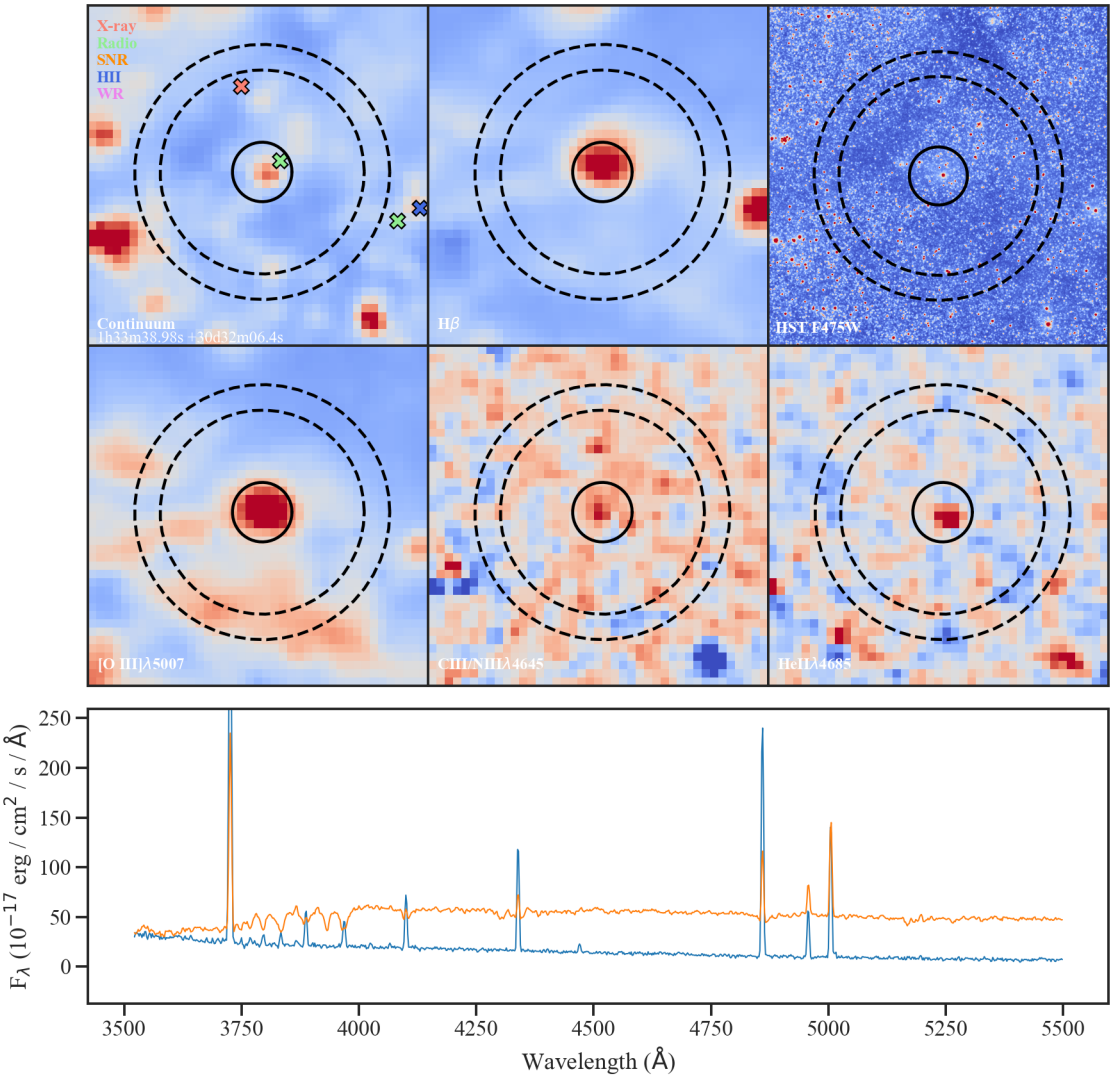

Figure B.15: Object 116b Inspection Diagram

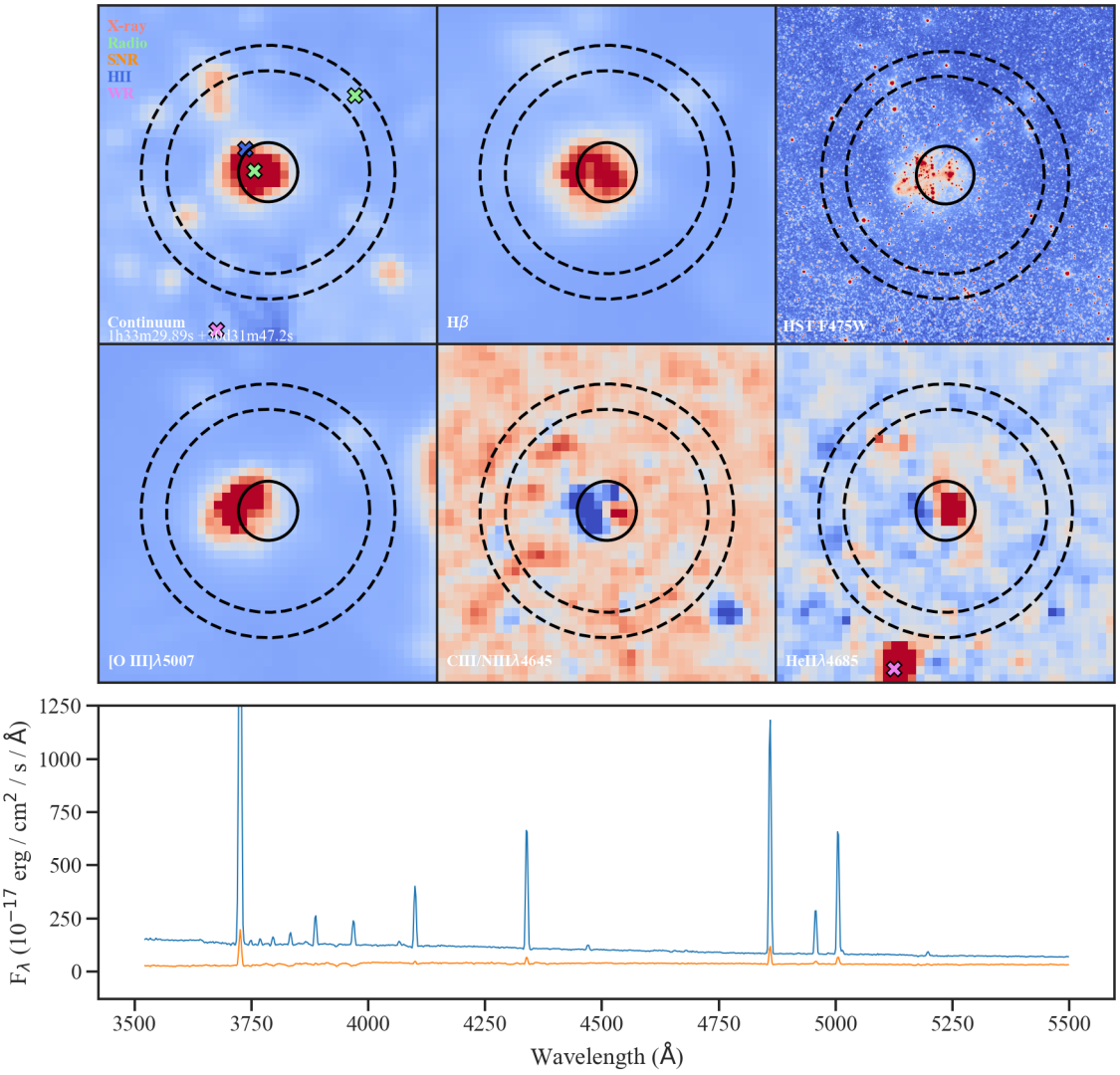

Figure B.16: Object 67b Inspection Diagram

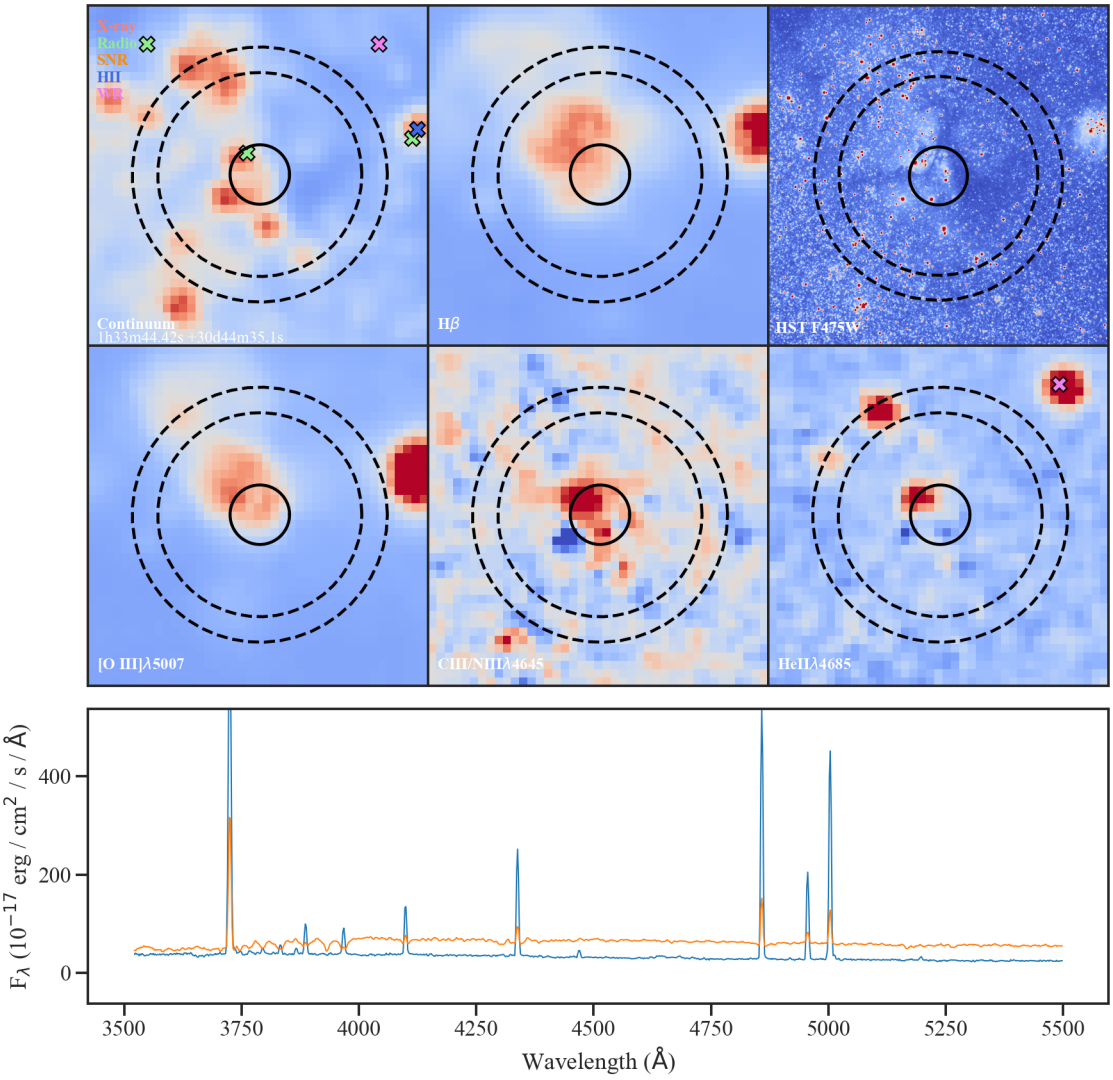

Figure B.17: Object 146b Inspection Diagram

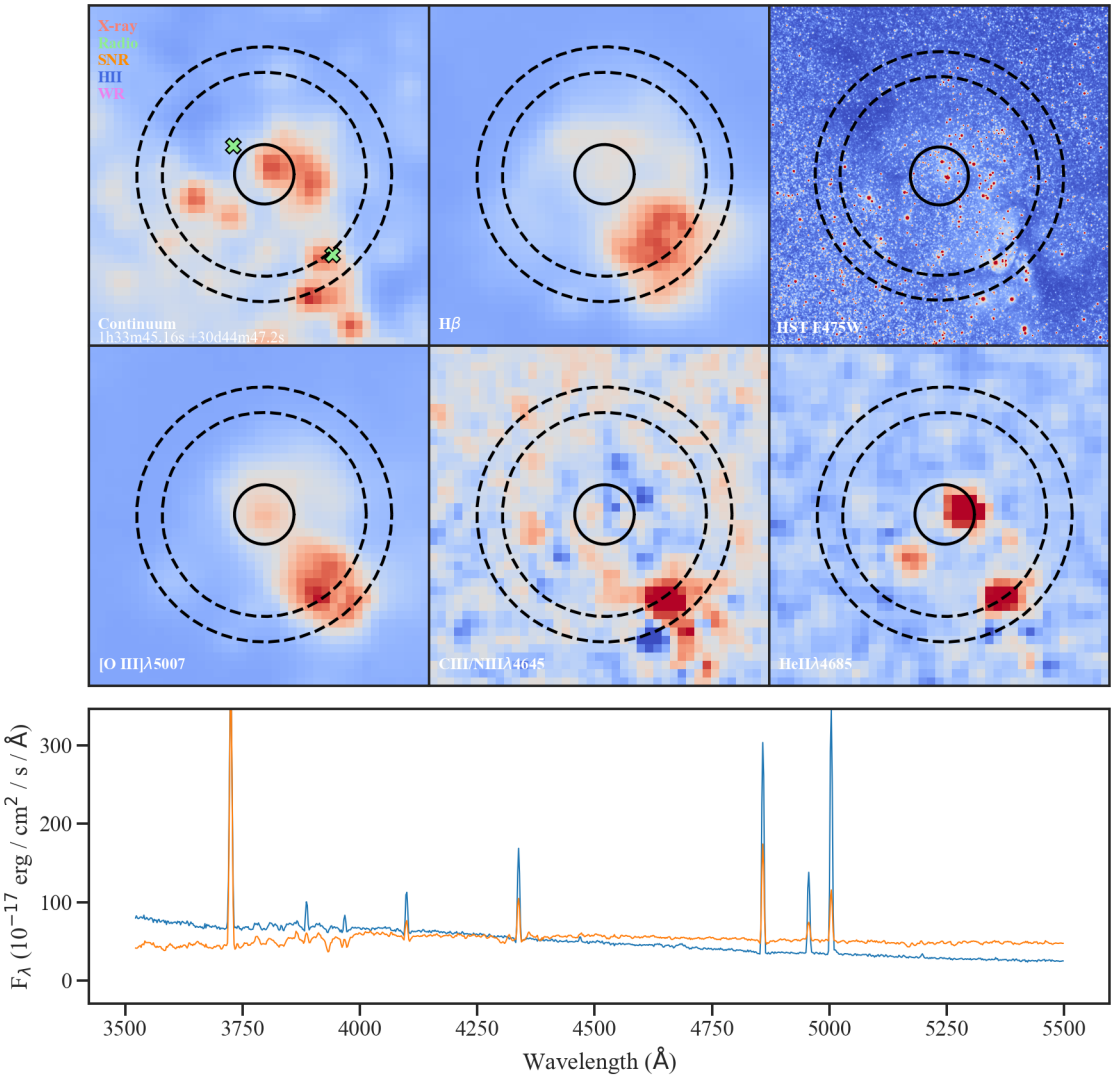

Figure B.18: Object 168b Inspection Diagram

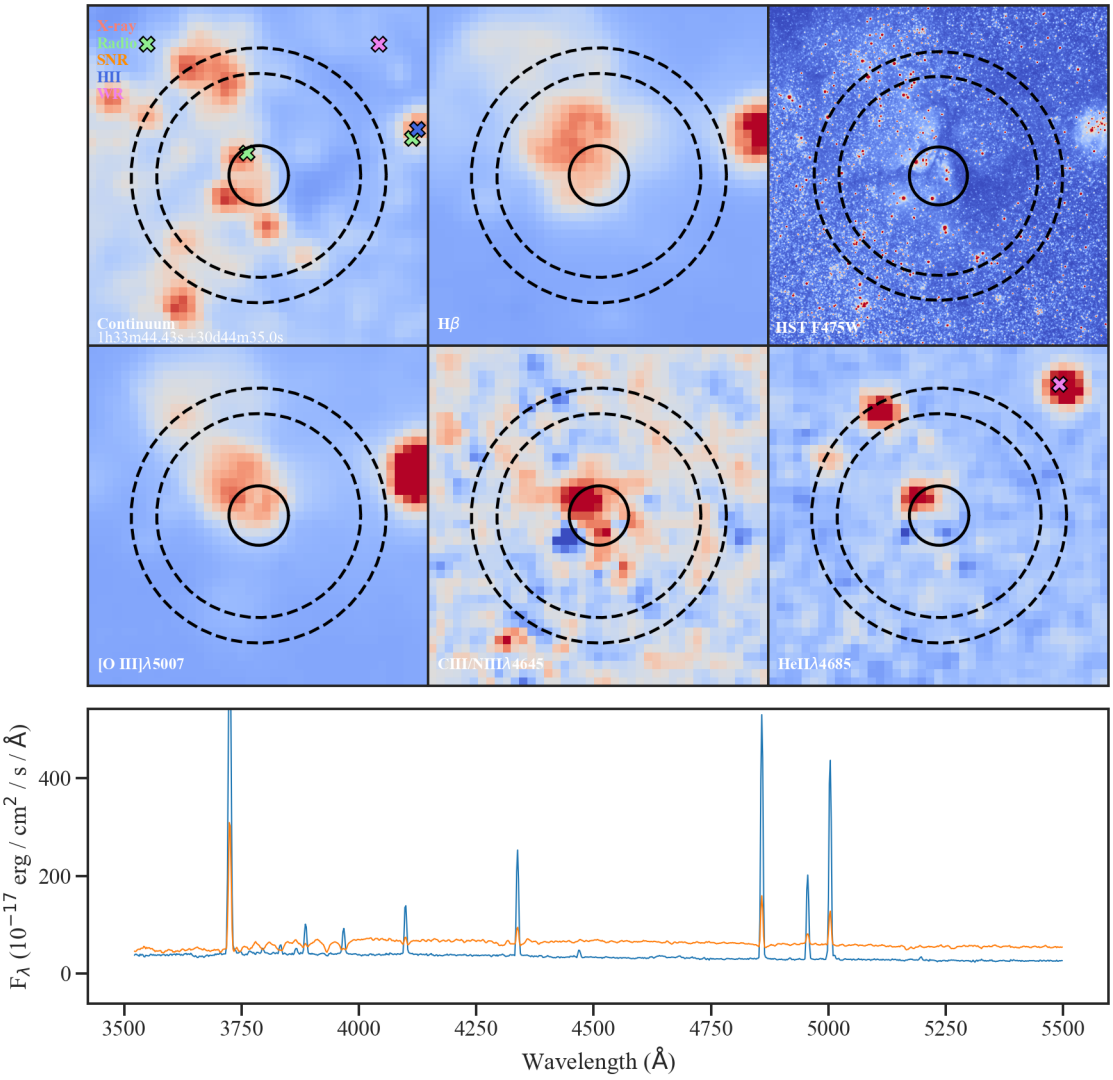

Figure B.19: Object 147b Inspection Diagram

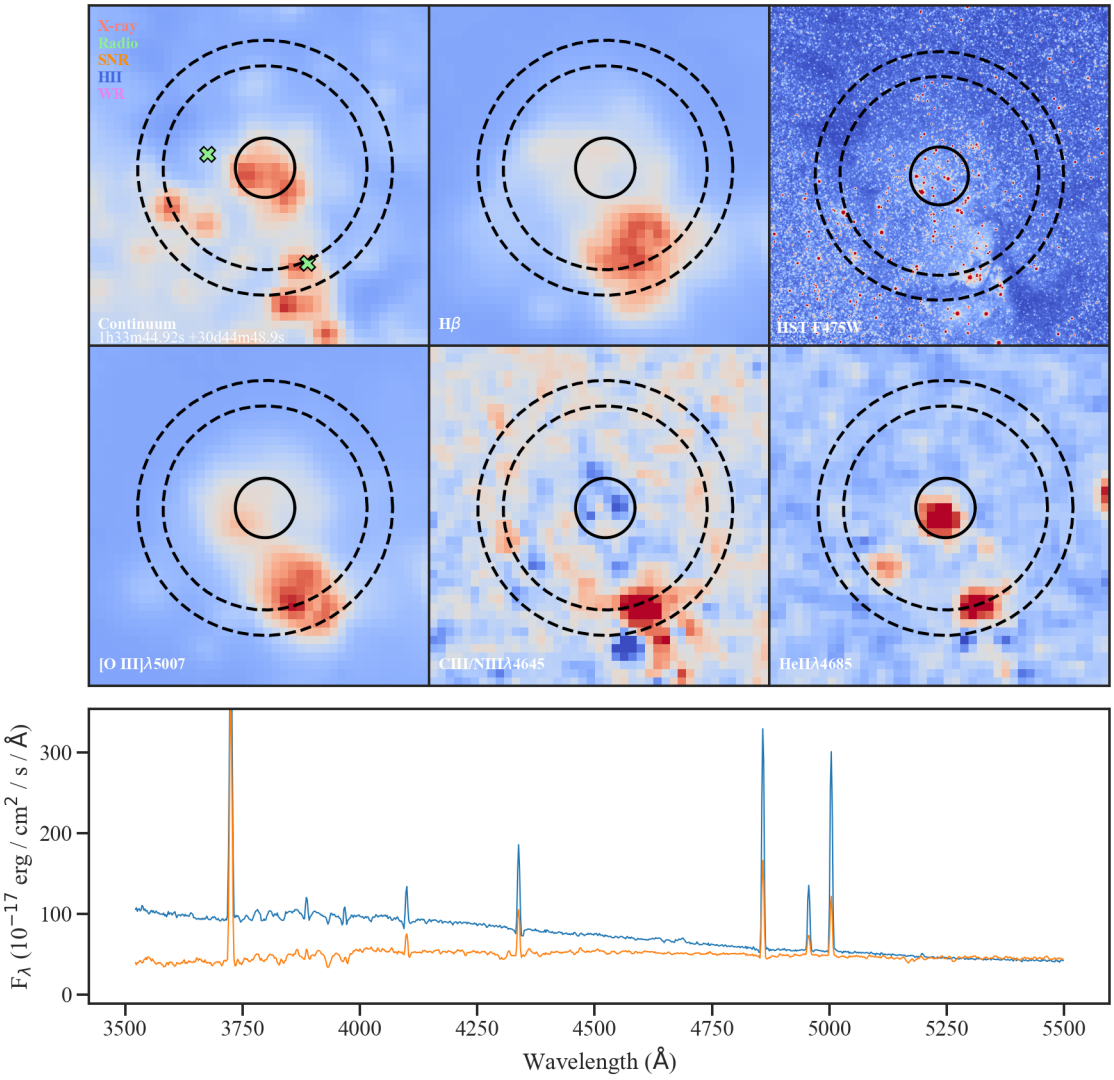

Figure B.20: Object 163b Inspection Diagram

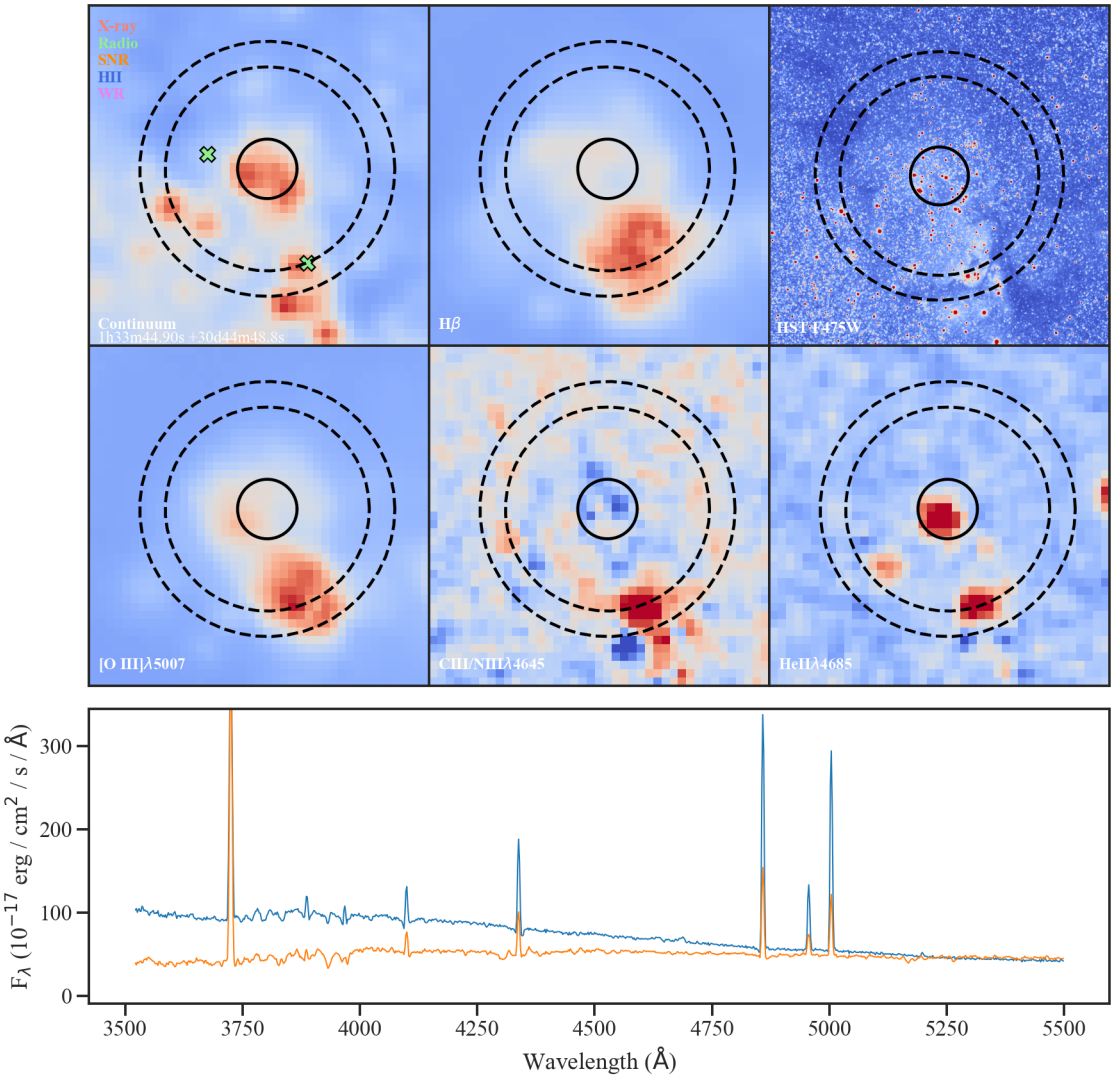

Figure B.21: Object 161b Inspection Diagram

B.3 Supergiant Stars

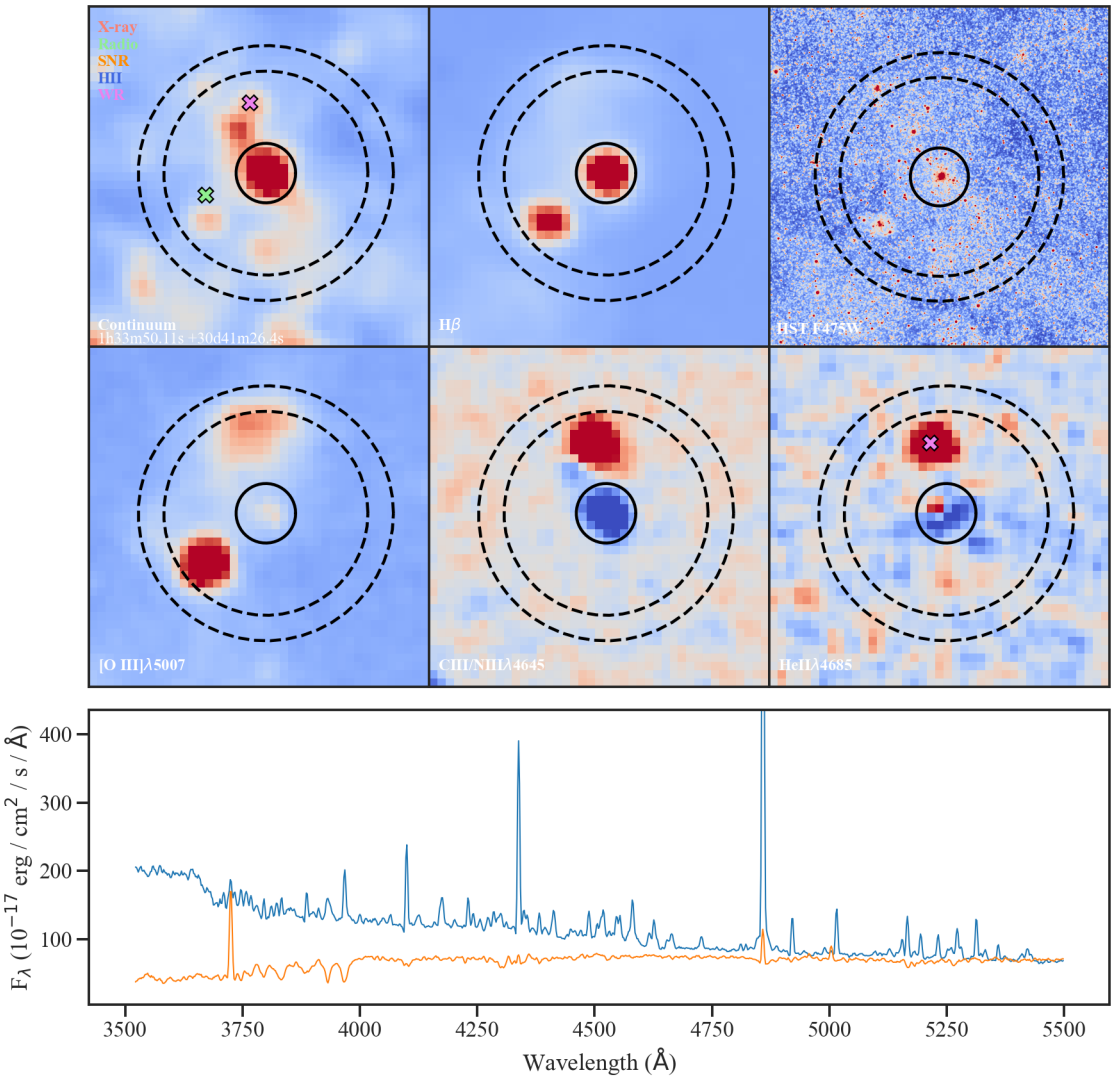

Figure B.22: Object 100e Inspection Diagram

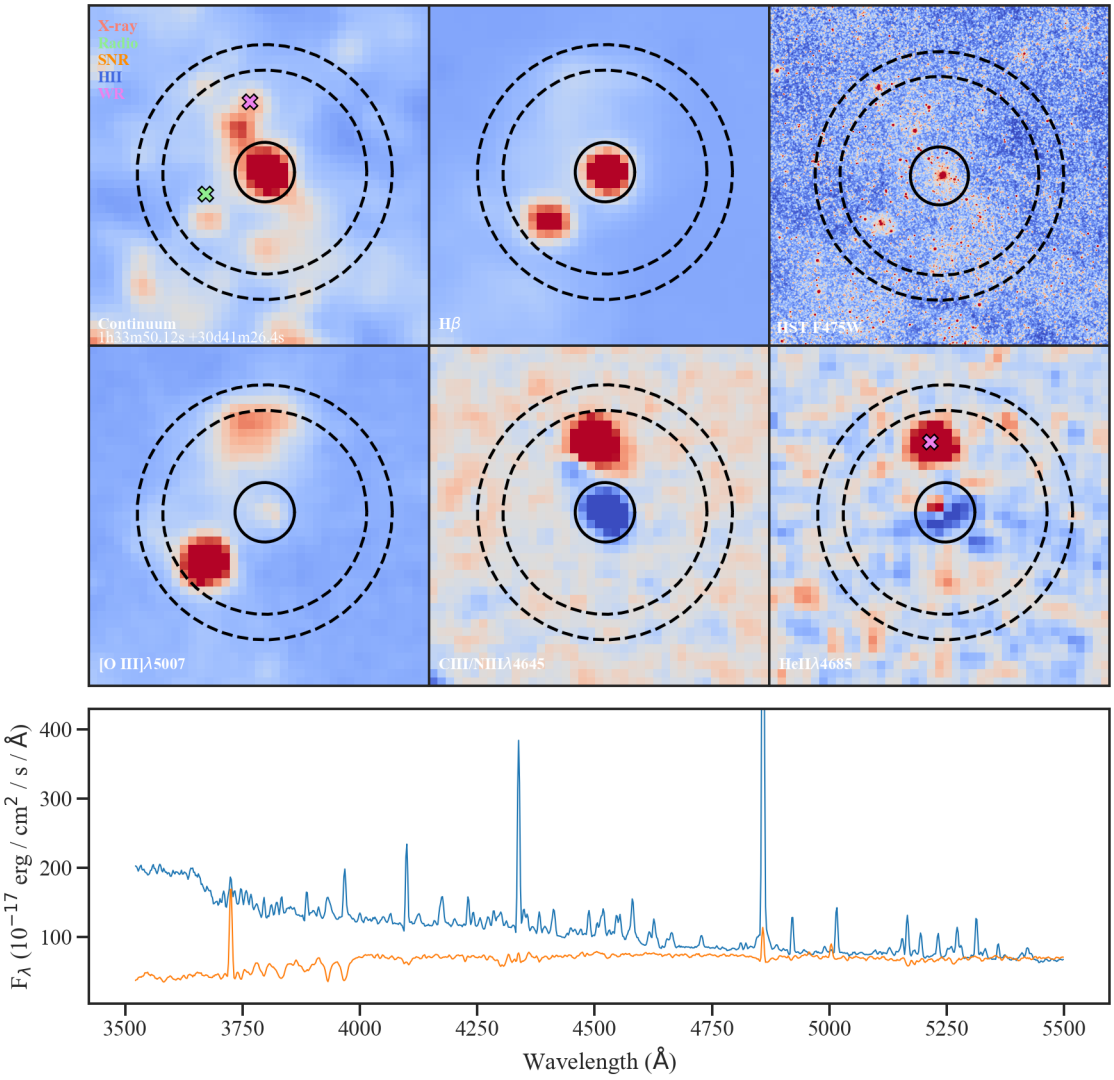

Figure B.23: Object 101e Inspection Diagram

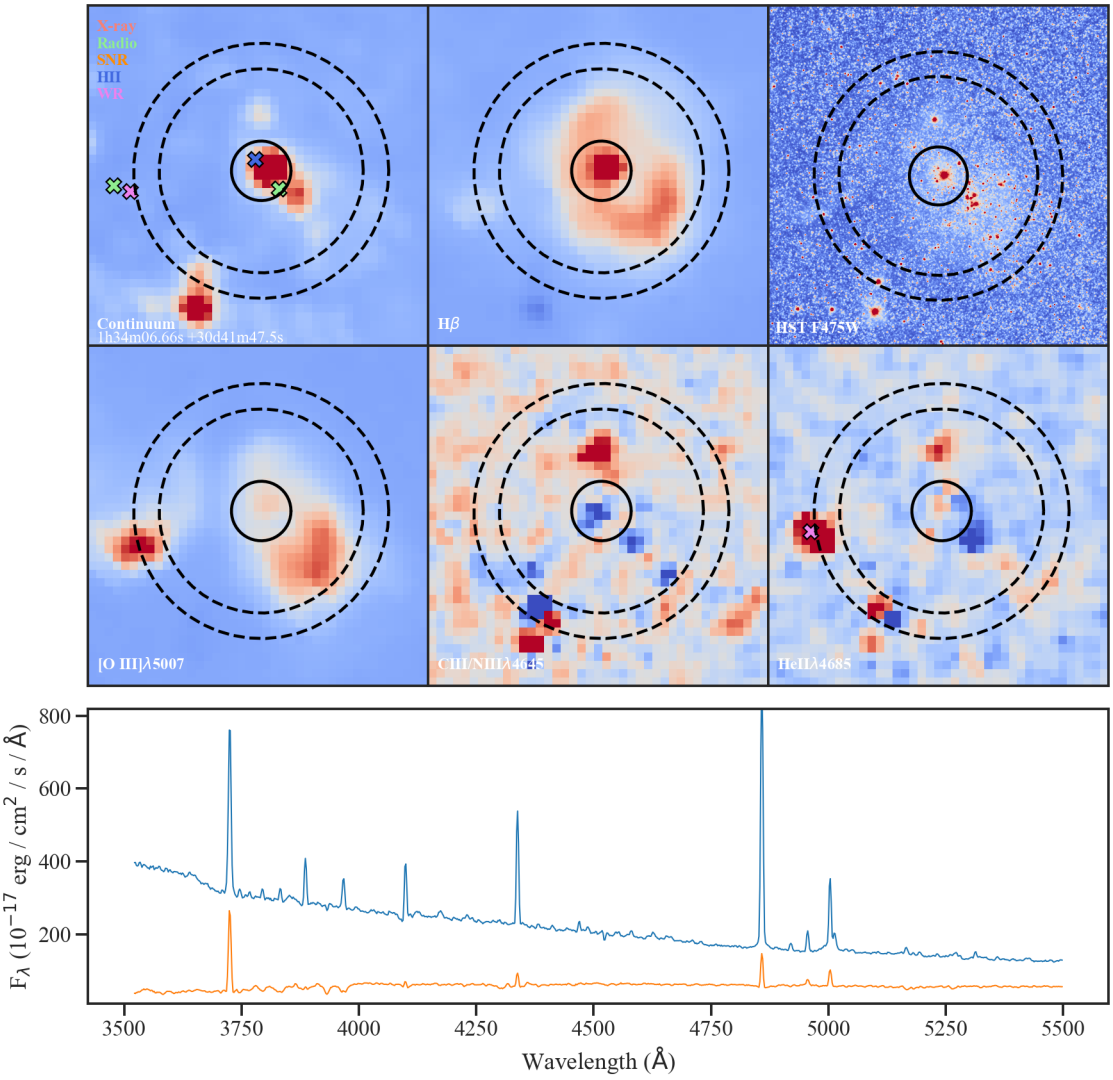

Figure B.24: Object 130e Inspection Diagram

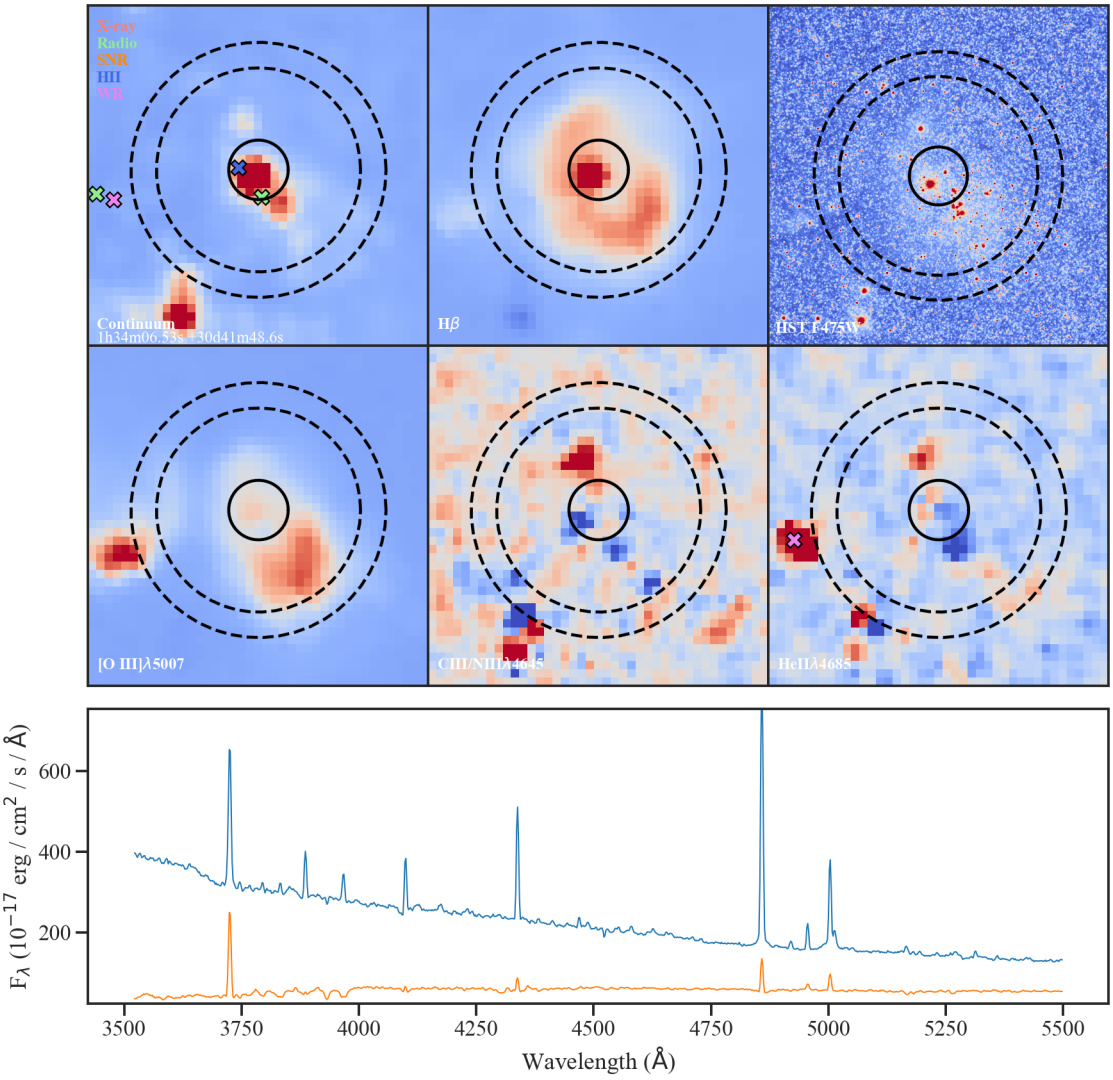

Figure B.25: Object 250b Inspection Diagram

B.4 Bright Star Spectra

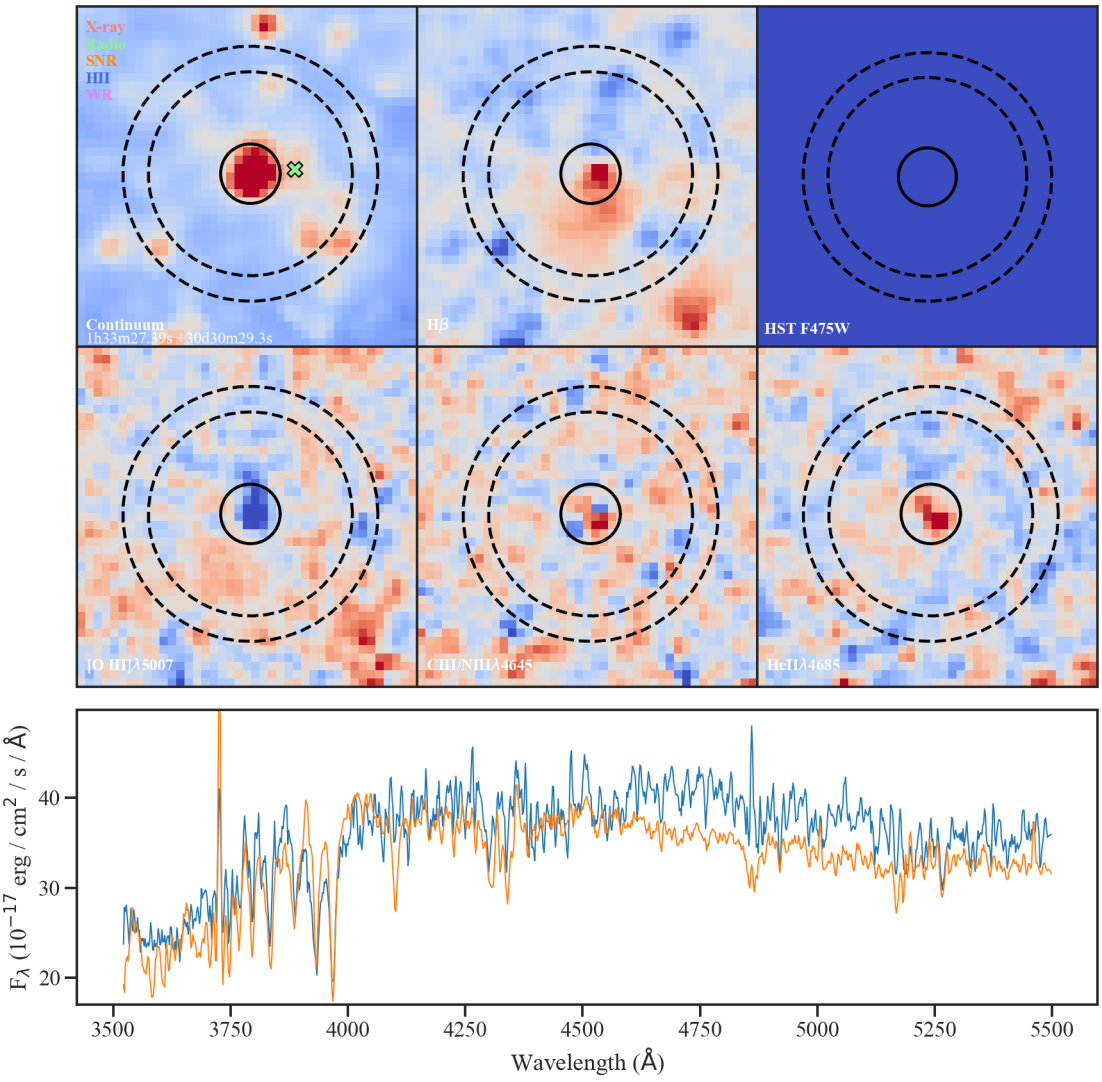

Figure B.26: Object 48e Inspection Diagram

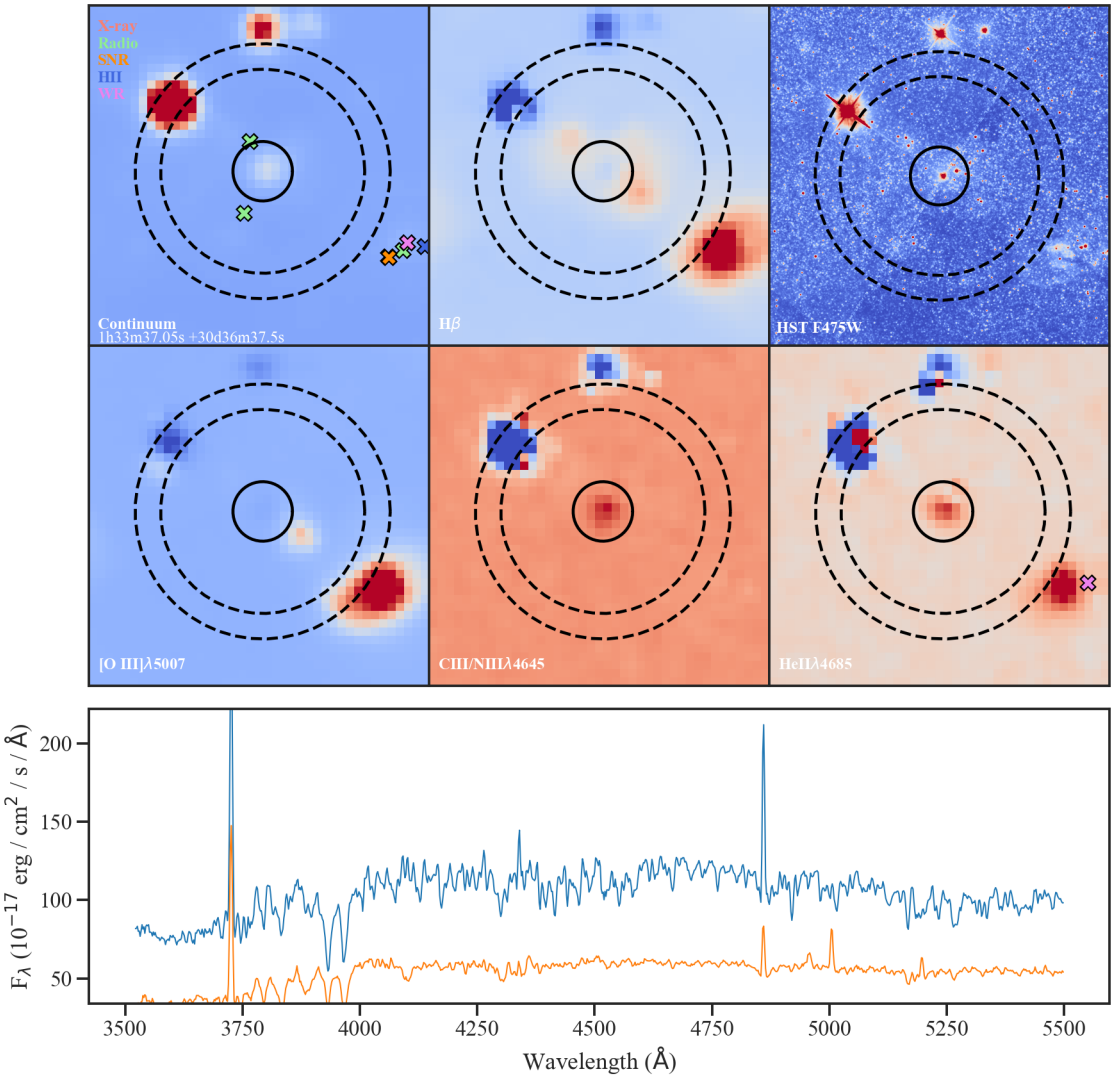

Figure B.27: Object 113b Inspection Diagram

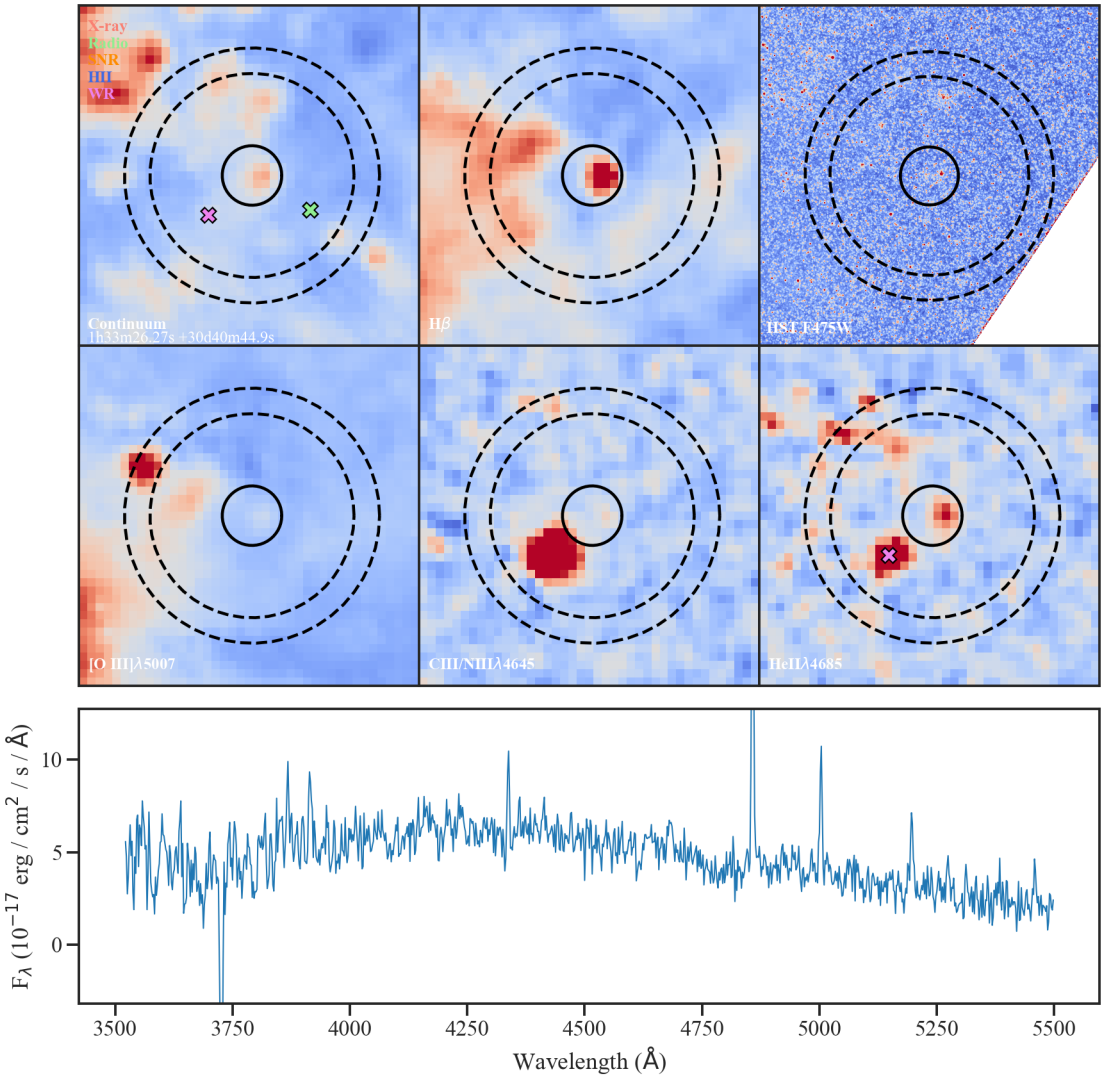

Figure B.28: Object 55b Inspection Diagram

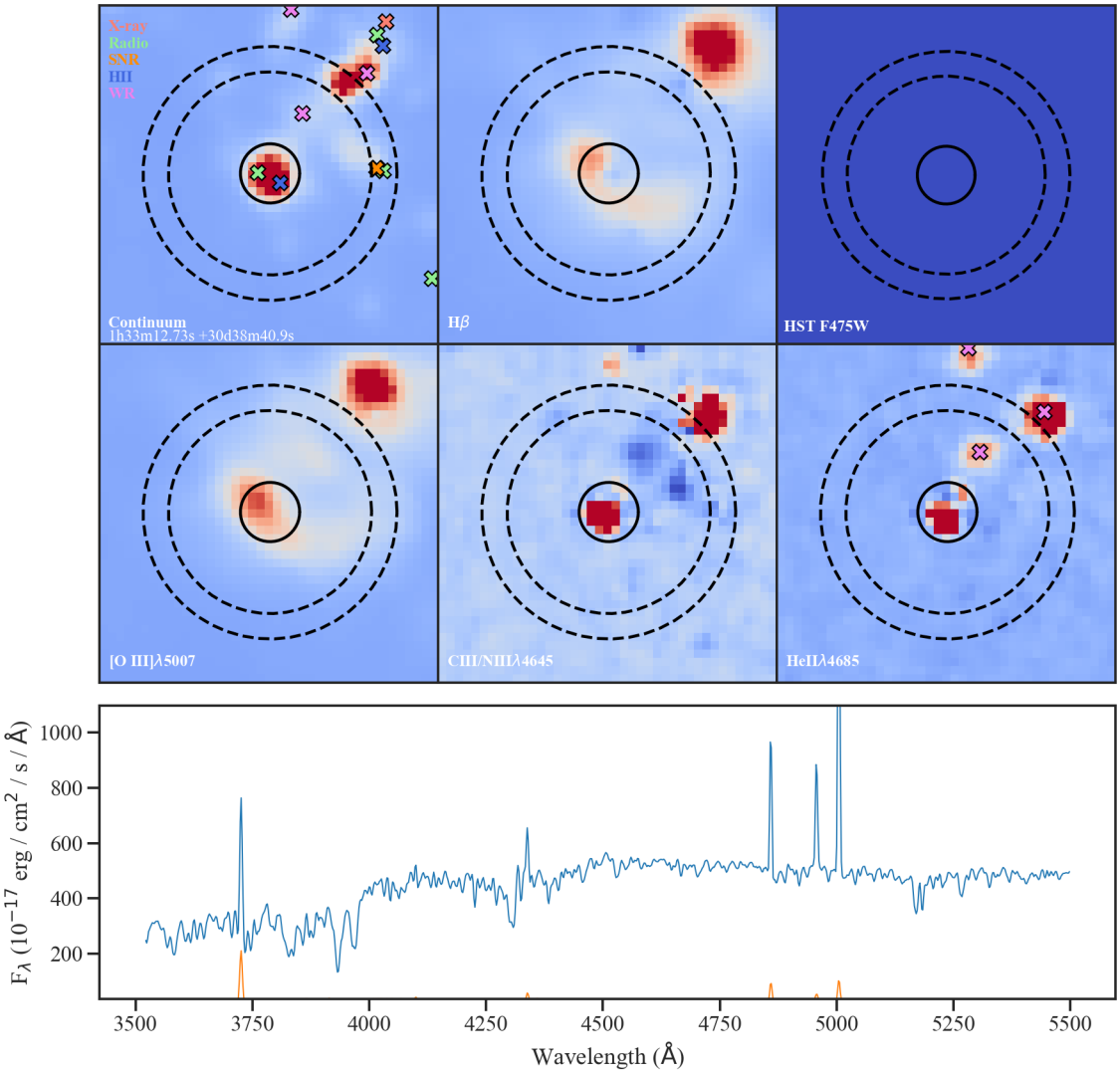

Figure B.29: Object 30b Inspection Diagram

B.5 Narrow Emission Spectra

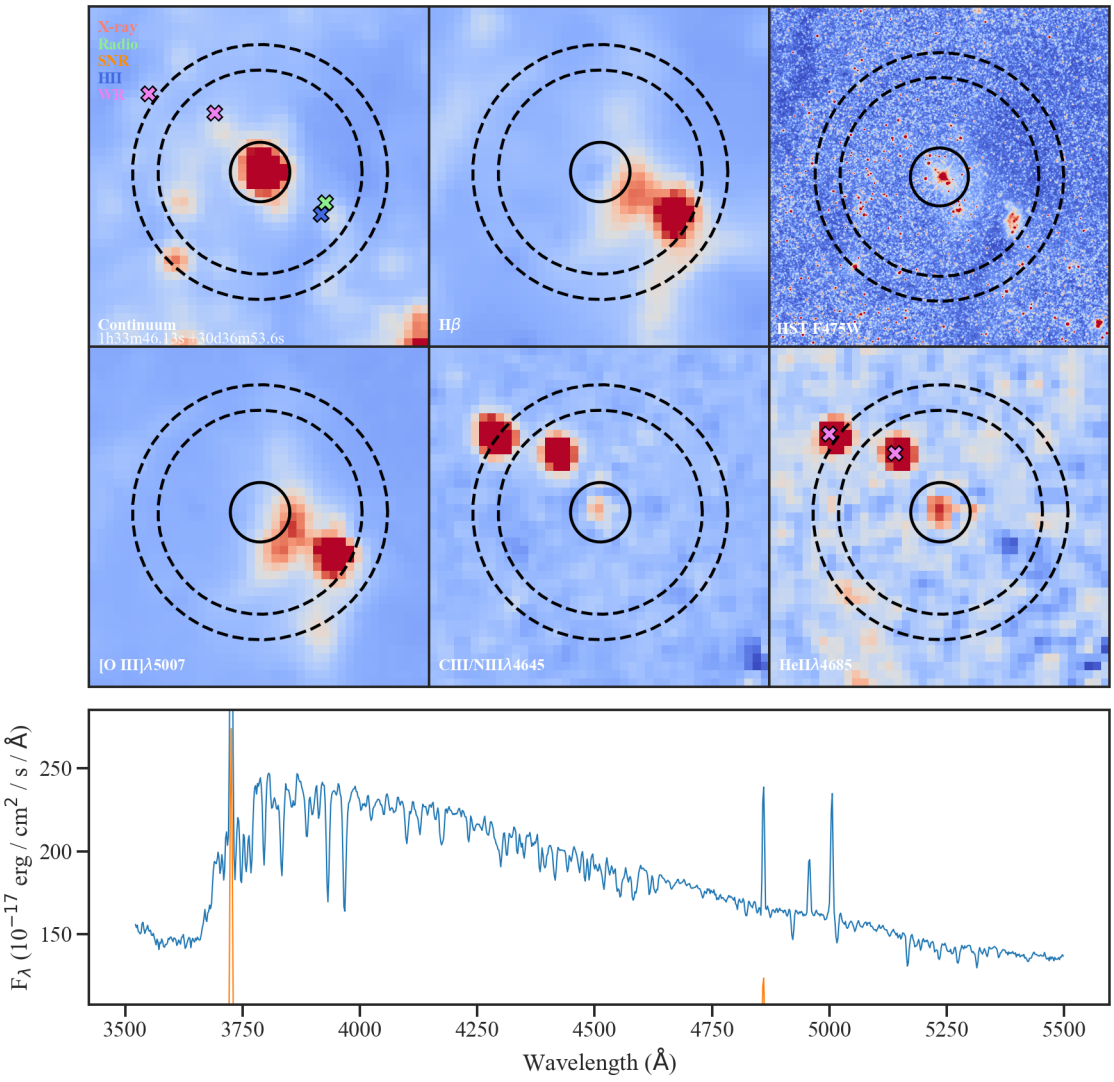

Figure B.30: Object 177b Inspection Diagram

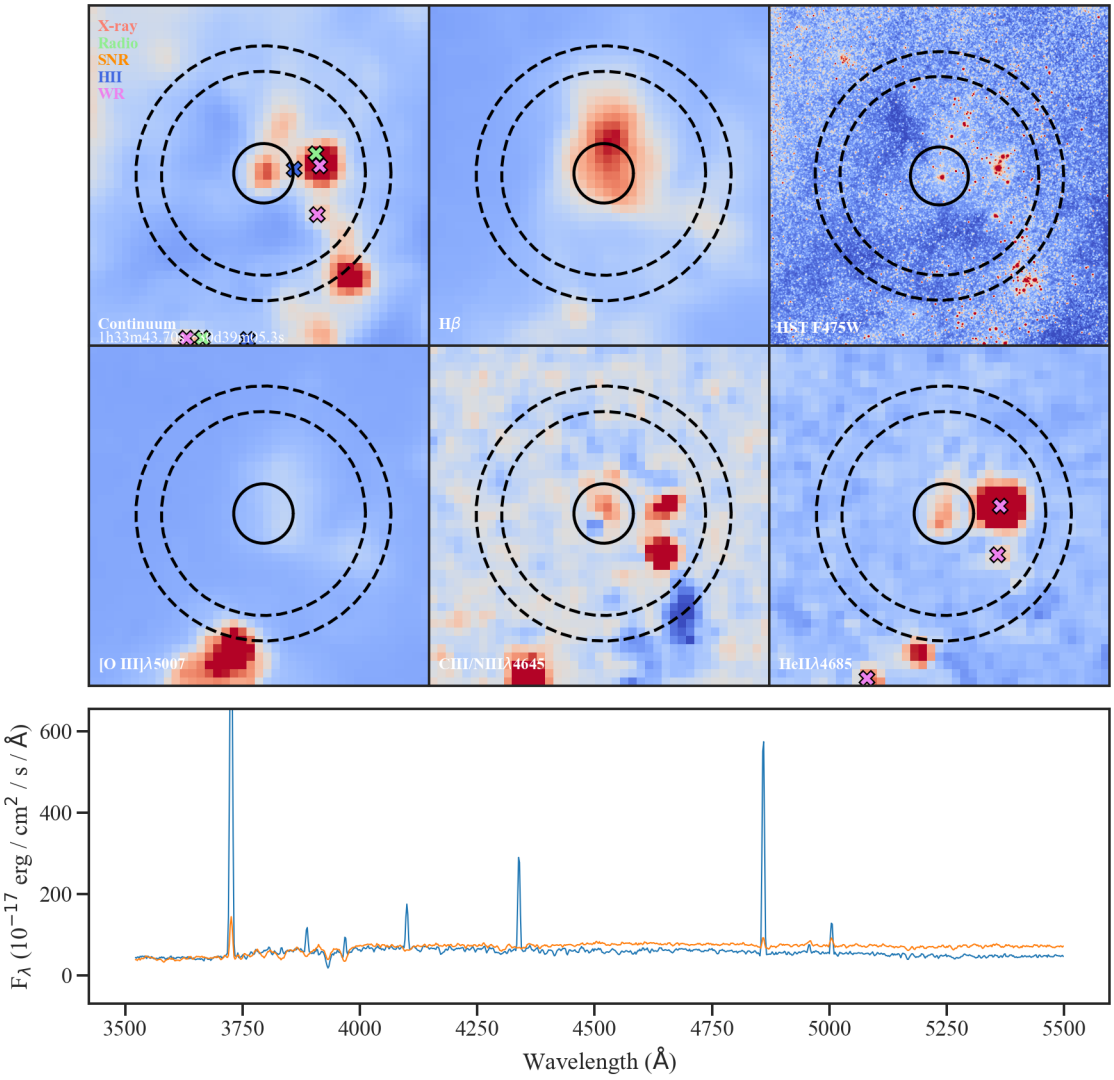

Figure B.31: Object 139b Inspection Diagram

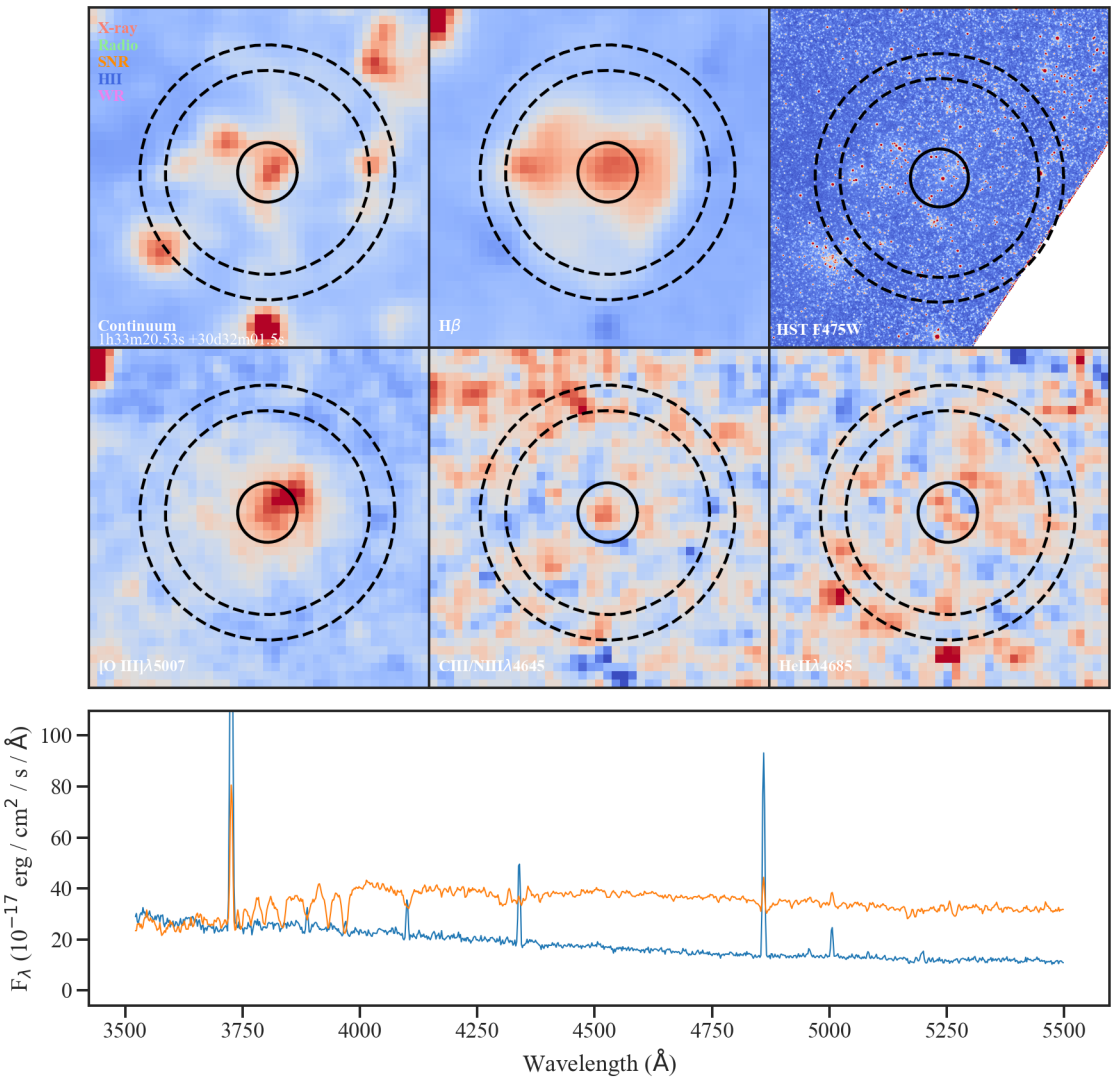

Figure B.32: Object 49b Inspection Diagram

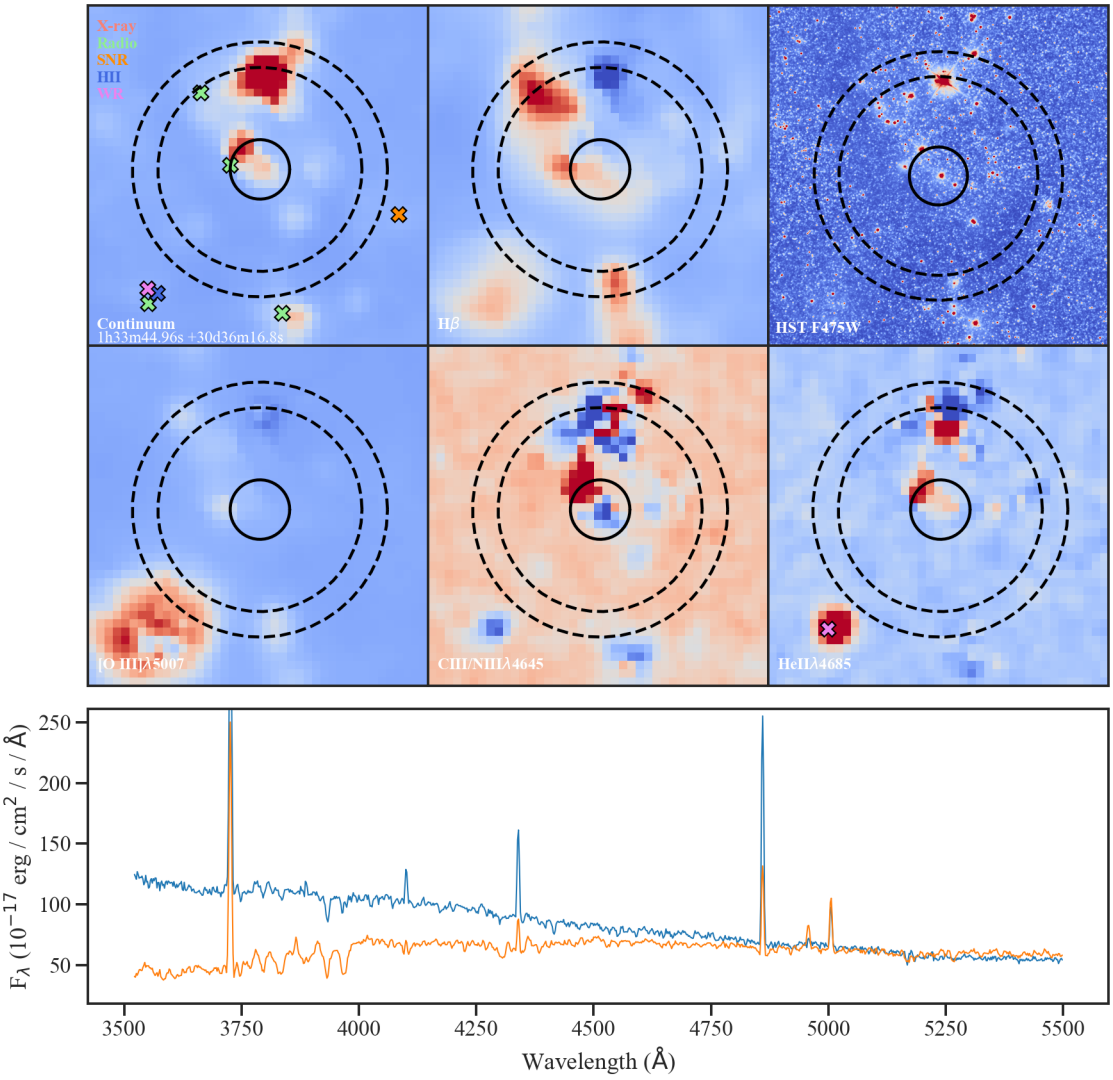

Figure B.33: Object 164b Inspection Diagram